PROCESS CONTROL DESIGN AND ANALYSIS FOR WASTEWATER DISINFECTION, STREAM NEUTRALIZATION, AND RUN-TO-RUN STRATEGIES

By

CHRISTOPHER EDWARD MEREDITH

A DISSERTATION PRESENTED TO THE GRADUATE SCHOOL
OF THE UNIVERSITY OF FLORIDA IN PARTIAL FULFILLMENT
OF THE REQUIREMENTS FOR THE DEGREE OF
DOCTOR OF PHILOSOPHY

UNIVERSITY OF FLORIDA

2003

To Becky and Ruby

ACKNOWLEDGMENTS

I would like to express my sincere appreciation to my advisor, Oscar Crisalle, without whose support this dissertation would not have been possible. I am also grateful for the opportunity he has given me to obtain a minor in electrical engineering.

I wish to thank Professors Haniph Latchman, Spyros Svoronos, and Jason Weaver for serving on my supervisory committee. Dr. Svoronos was particularly helpful in the development of the wastewater chlorination project, as were Chuck Fender and Profs. Paul Chadik and Robert Thieke.

I thank H. Mike Mahon, Varadharajan Basker, Giovani Nunes, Jon Engelstad, Serkan Kincal, and Chuck Baab, who came before and Brian Remark who will follow. They all have not only contributed greatly to my research but have been good friends.

Finally, I wish to thank my mother, Sheila, and my brother, Doug, for their unending support.

TABLE OF CONTENTS

page

Abstract of Dissertation Presented to the Graduate School
of the University of Florida in Partial Fulfillment of the
Requirements for the Degree of Doctor of Philosophy

PROCESS CONTROL DESIGN AND ANALYSIS FOR WASTEWATER DISINFECTION, STREAM NEUTRALIZATION, AND RUN-TO-RUN STRATEGIES

By

Christopher Edward Meredith

December 2003

Chairman: Oscar D. Crisalle
Major Department: Chemical Engineering

The wastewater chlorination process in fixed-size open-channel reactors is a challenging control problem because of the presence of a variable dead time caused by changes in the inlet flow rate. The approach proposed here involves the utilization of a moving weir as an actuator in a novel residence time control scheme, designed to ensure that fluid passing through the reactor experiences a constant residence time independent of flow rate. The dynamic weir control loop is conceived to supplement existing control structures that are charged with manipulating the dosage of chlorine. Simulations studies show that both feedforward and feedback manifestations of the residence time controller are highly effective at improving chlorine dosage control and are highly robust with respect to weir-flow modeling and measurement errors. In fact, these controllers have the potential to improve the control performance dramatically while saving as much as 45% of the chlorine used for treatment.

An automatic control system described as run-to-run is one in which a discrete controller is applied to an inherently discrete process, and where the performance measurements are made only after all processing is completed. A complete theoretical analysis is developed for the case of a static plant under proportional-integral control, resulting in quantitative descriptions of the nominal and robust stability regions, and recommended tuning heuristics. The analysis for the case of a Smith Predictor design shows that very small modeling errors in the estimated measurement delay may cause closed-loop instability. Therefore, the use of a Smith Predictor for run-to-run systems suffering from uncertainty in the delay is not recommended.

A weak-acid/strong-base neutralization control system utilizing two alternative pH sensors is modeled and analyzed. The first sensor is a traditional pH electrode whose output signal is proportional to pH, and the second sensor is a fiber-optic optrode that produces a signal that is proportional to hydrogen ion concentration. Systematic simulation studies show that no inherent performance improvement is observed when using the optrode instead of the electrode sensor in the feedback loop.

CHAPTER 1
INTRODUCTION

There are three types of process control studies addressed in this dissertation, namely, a design project, a theoretical project, and an experimental project. The design project examines wastewater chlorination control, a distributed-parameter system that is typically difficult to control with standard strategies due to the presence of high variations in flow rate. It is shown that a novel design modification based on an automatically adjusted moving weir can lead to dramatically improved performance. In the theoretical study, single-input single-output run-to-run unit operations are investigated for the case of a static plant. The run-to-run controller form is contrasted with a standard discrete controller form, exposing subtle differences in behavioral characteristics under closed-loop control. Finally, the experimental project seeks to improve the performance of pH control systems that use traditional pH electrodes. Known to be highly non-linear, the electrode may have limited performance potential as a result. A novel linear optical sensor is introduced as an alternative.

Chapter 2 presents a design study involving a standard wastewater chlorination basin. It is shown that traditional control schemes have difficulty maintaining the outlet concentration at a specified value. The difficulty is caused by the effect that the varying flow rate of wastewater has on the deadtime (residence time) of the system. Because the volume of the reactor is constant, residence time is inversely proportional to flow rate, and the latter can vary by as much as an order of magnitude. Specifically, the variable residence time causes poor closed-loop performance. The system is modified by

installation of a moving weir, which allows a controller to manipulate the volume of the reaction chamber. When matched to the flow rate of wastewater, the residence time can be held approximately constant.

To validate the effectiveness of the design modification, a comprehensive simulation of the system is used. The first step of the process is the development of a realistic representation of the flow through a basin. Next, traditional control schemes are considered, and their performance is evaluated. Finally, the basin model basin is modified to allow for the automatic adjustment of the volume through use of a moving weir, and controller performance is again tested. It is at this point that the merit of the design modification is clear, as it effectively rejects the given disturbance. Because the total chlorine consumption is highly influenced by residence time, the movable weir facilitates significant reduction in chlorine usage while attaining highly improved outlet concentration control by the existing control scheme.

A theoretical project that is the subject of Chapter 3 addresses the analysis of run-to-run systems where significant measurement delay is observed. A run-to-run system is one in which a unit operation processes batches of material in succession, with the constraint that each batch must be completed before the relevant end-product properties may be determined. Examples include a wide range of processes, such as industrial peanut roasting and compact disc sputtering operations. In each case, the unit operation that imparts some physical characteristic on each batch is only one of many in succession. Consequently, there is significant delay observed by the time said characteristic can be measured, and only then can adjustments be made to the system. An important finding of the work is that, although run-to-run systems have characteristics in

common with traditional discrete systems, they behave markedly different under closed-loop conditions, and care must be taken by the control designer to guarantee that the system will remain stable under realistic conditions.

The mathematical description is developed using standard techniques, primarily, the Jury Array, which provides necessary and sufficient conditions to guarantee that the roots of a polynomial are inside the unit circle. Discrete systems are necessarily unstable if at least one (uncancelled) pole lies outside the unit circle, making the Jury Array an appropriate stability test for this type of system. Next, because significant measurement delay is typical of many run-to-run systems, the performance of a deadtime compensator is analyzed. It is shown that such a compensator is ineffective, primarily because a run-to-run system is fundamentally different from the traditional discrete system for which compensators are designed.

Chapter 4 presents a thorough investigation of the properties of linear optical pH sensors. In contrast, traditional pH electrodes are logarithmic with respect to the measured variable, namely, the hydrogen ion concentration. Consequently, the two types of sensors behave differently in closed-loop feedback control loops. Generally, the linear sensor is expected to perform better than a non-linear one, and the primary result of the study is to quantify the design specifications in terms of how much the physical properties of the optical sensor can degrade while maintaining equivalent or better performance than the electrode. Similarly, it is also shown how much improvement can be expected by using the optical sensor assuming a realistic set of physical characteristics.

Both computer simulations and bench-scale experiments are used in the pH sensing study. Initially, the important chemical reactions that take place in an acid-base neutralization process are modeled and simulated. Next, the bench-scale pH control system is utilized for the purpose of verifying the validity of the simulation behavior. Simulations are used for the final phase of the project, which quantifies the performance of the optical sensor with respect to standard electrodes.

CHAPTER 2
WASTEWATER CHLORINATION USING A NOVEL CONTROL SCHEME

2.1 Introduction

A major requirement of wastewater treatment plants is that the treated water must be effectively disinfected before it is discharged. Although this can be done in several ways, the most common approach is through chemical reaction with chlorine (Metcalf & Eddy, 1979). Chlorine is consumed in the process, but regulations stipulate that a residual chlorine concentration must be present at or above a minimum level upon discharge from the reactor. The restriction ensures that enough chlorine is present in the water for a long enough time to guarantee satisfactory cleansing (Hammer and Hammer, 1996). However, excessively high chlorine levels are problematic for three reasons. First, the purchase of chlorine is a significant operating cost. Second, unnecessary addition of chlorine means that greater volumes must be stored on-site, which can be both costly and dangerous. Third, under high chlorine concentrations the formation of trihalomethane (THM) contaminants is favored (Jolley *et al.,* 1990), and accordingly, the process must satisfy regulations restricting their maximum level. It is therefore desirable to maintain the outlet chlorine concentration as closely as possible to a predetermined value.

The goal of this research is to develop an effective, automatic, chlorine-dosage control scheme for a wastewater treatment plant. With relatively little storage capacity, many plants must process incoming water as it arrives, and are therefore subjected to the daily cyclical nature of water usage (Hammer and Hammer, 1996). Because a reactor's

size is fixed, the varying rate of the flowing water poses the most significant technical challenge to automatic control—it introduces a time-varying system delay, which significantly degrades treated wastewater quality (Smith, 1971). In addition, other disturbances such as intense solar radiation (causing increases in volatilization of chlorine, evaporation of water, and chemical reaction rates) and rainfall (causing dilution) can affect the dynamics of these outdoor reactors.

A number of feedback control designs can be considered as candidates to ensure optimal outlet chlorine concentration levels. The least complex strategy is simple proportional-integral (PI) feedback, but this approach is usually inadequate for processes with large input disturbances and deadtime (Seborg, Edgar, and Mellichamp, 1989). At the price of increased complexity, a cascade regime helps minimize the effects of input disturbances. Furthermore, adding a Smith Predictor (which requires an accurate model of the reactor) can counter the adverse effects of deadtime, provided the deadtime has limited variability (Ogunnaike and Ray, 1994). While many of these attributes are promising, it is unlikely that they are fully adequate, even in combination, to control a system with such a highly varying deadtime. It is proposed that a process modification may prove effective in aiding the control of residual chlorine concentration. If the end of the reactor is fitted with a dynamic weir, the volume of the reactor could be varied; this would allow the operator to manipulate the residence time of the fluid in the reactor and, hence, potentially ensure that the time-delay of the system remains approximately constant.

An accurate model of a wastewater treatment plant can be used to quantify the relative effectiveness of each candidate control approach. The sections contained in this

chapter identify issues pertinent to the formulation of a viable model, as well as the results of applying various control schemes. More specifically, Section 2.2 describes all the major aspects of reactor modeling. Critical parameters of the derived reactor model are then identified in Section 2.3 using experimental plant data. Next, the design and performance assessment is presented in Section 2.4 for several possible control schemes. Then, Section 2.5 details the potential of a novel process modification—a dynamic weir—as an alternative design, and finally, conclusions for the most effective strategy to control residual chlorine concentration in wastewater are outlined in Section 2.6.

2.2 Process Model of a Typical Wastewater Disinfection Plant

An abstract representation of a disinfection system is depicted in Figure 2-1. The rectangle at the left of the figure represents the dosing area, where chlorine is mixed into the system. The chlorine reacts with ammonia nitrogen (and other trace species) present in the incoming water, consuming a portion of the chlorine very quickly. The amount consumed by this process is referred to as the ammonia nitrogen *chlorine demand* (the effect of the trace species is included in this term in this study for brevity). The dosing area is designed to eliminate ammonia nitrogen from the water and to promote an outlet flow with a uniform *free-plus-combined* (FPC) residual chlorine concentration (Metcalf & Eddy, 1979). The outlet flow immediately enters the next stage, or contact area, where the bulk of disinfection takes place. There are four important values associated with determining the chlorine concentration in the dosage area: namely, Q(t), the influent volumetric flowrate measured in cubic meters per second (m^3/s); $\delta(t)$, the ammonia nitrogen chlorine demand of the incoming water measured in parts per million (ppm) (where ppm is g/m^3); V_{da}, the volume of liquid in the dosage area measured in cubic

meters (m^3); and u(t), the chlorine dosage input rate measured in grams per second (g/s). Water leaving the dosage area has a concentration $C_0(t)$ measured in parts per million (ppm). The dosing area is distinguished from the contact area at a point where uniform chlorine concentration $C_0(t)$ and plug-flow can be guaranteed. Physically, the dosing and contact areas are parts of the same basin; there may or may not be some partition (such as a gate) between the two areas, depending upon the design of the plant.

The rectangle on the right of the figure represents the contact area, where the FPC residual chlorine disinfects the water. Disinfecting chlorine species are slowly consumed by chemical reactions during the time the liquid resides in the contact area, as well as lost through volatilization to the surrounding air. In contrast to the dosage area, minimal mixing is desired in the contact area, thus ensuring that all fluid that passes through it is retained for a length of time sufficient for disinfection. The contact area features two relevant variables: namely, Q(t), as defined before; and V_{ca}, the volume of the liquid in the contact area measured in cubic meters (m^3). In addition, a z-coordinate is introduced to represent the longitudinal direction of fluid travel. This facilitates reporting the value of variables at various spacial locations. Water passing through the contact area enters with a concentration $C_0(t)$, moves in the direction of increasing z while chemical reactions and volatilization take place, and exits the contact basin at the coordinate point $z = L$ with a concentration $C_L(t)$. The reactor is normally operated at constant volume by matching the inlet and outlet flowrates. Hence, the liquid volumes V_{da} and V_{ca} are

constants. The total volume of the liquid in the contact area is given by $V_{ca} = AL$, where A is the cross-sectional area of the liquid volume.

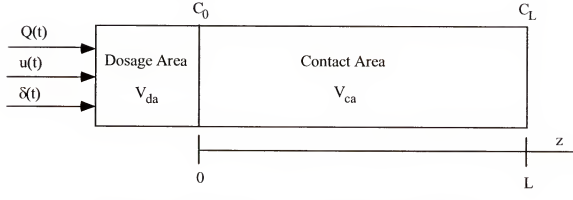

Figure 2-1. Schematic of a wastewater treatment plant, operated at constant volume.

Water disinfection plants implement the abstract design of Figure 2-1 in various forms. For example, space considerations often dictate that the contact basin is serpentine with a baffle-style arrangement. However, as long as uniform, plug-flow is preserved, such variations are conceptually equivalent to the abstract linear model proposed. The Kanapaha water treatment facility in Gainesville, Florida, is the basis for the process model adopted in this study, and Table 2-1 lists various physical quantities of the plant, used for both modeling and model validation purposes.

Table 2-1. Physical quantities that describe the reactor at Kanapaha water treatment facility in Gainesville, Florida.

V	2880 m^3
V_{da}	57.6 m^3 (0.02 V)
V_{ca}	2822.4 m^3 (0.98 V)
L	120 m (average)
A	24 m^2 (average)

In addition, Table 2-2 lists various typical operating conditions for the same facility. The first three quantities are the typical chlorine concentration at the entrance of the reactor $\bar{u}'$, the dosing-area/contact-area boundary concentration $\bar{C}_0$, and the exit concentration of the reactor $\bar{C}_L$, measured in parts per million (ppm). The final quantity is the typical flowrate $\bar{Q}$ through the plant measured in cubic meters per second (m^3/s). Note that the dosing rate u (measured in g/s) is fundamentally different from the dosage concentration u' (measured in ppm); this is an important distinction that is discussed in Section 2.2.1.

Table 2-2. Typical operating conditions for the reactor at Kanapaha water treatment facility in Gainesville, Florida.

$\bar{u}'$	8.5 ppm
$\bar{C}_0$	5.5 ppm
$\bar{C}_L$	2.5 ppm
$\bar{Q}$	0.4 m^3/s
$\bar{\delta}$	3.0 ppm

2.2.1 Kinetic Model of Chlorine Reaction in a Wastewater Treatment Plant

Using chlorine to eliminate ammonia and disinfect water is complicated in terms of chemistry. There is an initial series of reactions involving chlorine, ammonia nitrogen, and their products in the dosing area. Some of those products then act as disinfecting agents, and are slowly consumed as the water moves down the length of the contact basin. The ammonia reactions are described by the following Morris-Wei model (Morris and Wei, 1969):

$$NH_3 + HOCl \rightarrow NH_2Cl + H_2O \quad (2\text{-}1)$$

$$NH_2Cl + HOCl \rightarrow NHCl_2 + H_2O \quad (2\text{-}2)$$

$$NHCl_2 + HOCl \rightarrow NCl_3 + H_2O \quad (2\text{-}3)$$

$$NCl_3 + H_2O \rightarrow NHCl_2 + HOCl \quad (2\text{-}4)$$

$$NHCl_2 + H_2O \rightarrow NOH + 2H^+ + 2Cl^- \quad (2\text{-}5)$$

$$NOH + NH_2Cl \rightarrow N_2 + H_2O + H^+ + Cl^- \quad (2\text{-}6)$$

$$NOH + NHCl_2 \rightarrow N_2 + HOCl + H^+ + Cl^- \quad (2\text{-}7)$$

$$NOH + 2HOCl \rightarrow NO_3^- + 3H^+ + 2Cl^- \quad (2\text{-}8)$$

These reactions proceed rapidly to steady-state, with some reactions going to completion, and others reaching equilibrium. It is unclear why some reverse reactions (such as (2-4)) are not noted in the model, but it is certain that at least nine different chemical species are involved. In addition, the reaction-rate constants are also either temperature or pH dependent, or both. For example, pH and temperature strongly influence the point of equilibrium for the chloramine reactions (2-1) to (2-4) (Hammer and Hammer, 1996). While the Morris-Wei model is a well-founded proposal of what chemical reactions take place during ammonia destruction, it introduces numerous differential and algebraic relationships, hence complicating the theoretical analysis and increasing the computational burden significantly. Furthermore, concentrations of some of the nine species described are additionally influenced by organic nitrogen, metal ion, and other gas-forming reactions not represented in the Morris-Wei model.

It is therefore desirable to find a simplified though realistic model. The knowledge that the ammonia is almost completely consumed very rapidly may be exploited in deriving a simplified model. One possible approach is to treat the dosing area as a CSTR within which the ammonia reactions take place. The resulting model is described in Section 2.2.2. Although the dosing area is not always physically similar to a CSTR (for example, it can include a diffuser, or a line source of chlorine being injected into the influent), it is argued that the relevant behavior of the dosing area is adequately reflected by this model, with the added benefit that the model is conceptually quite simple.

The disinfection reactions in the contact area, however, are not intended to proceed to completion and do not necessarily reach equilibrium. The regulations that require minimum residual chlorine refer specifically to free-plus-combined (FPC) chlorine, which are the four species that promote disinfection. They include monochloramine (NH_2Cl), dichloramine ($NHCl_2$), hypochlorous acid (HOCl), and hypochlorite ion (OCl^-). The four are collectively referred to as "chlorine" with regard to the contact area, and are generically represented by the symbol Cl^-. Because disinfection chemistry is even more complicated than ammonia destruction chemistry, it is again desirable to find a simplified description of chlorine concentration. It is proposed that the chlorine consumption in the contact area can be modeled through the lumped chemical reaction

$$Cl^- \rightarrow \text{Products} \qquad (2\text{-}9)$$

with a phenomenological first-order overall rate of reaction (Fogler, 1992)

$$r_{rxn} = -k_{rxn}C \tag{2-10}$$

where k_{rxn} is the overall reaction rate constant of chlorine measured in reciprocal seconds (1/s), and C is the concentration of chlorine measured in parts per million (ppm). In addition, FPC chlorine disappears from the reactor through volatilization and undesired chemical reactions dependent upon UV radiation exposure; these phenomena occur at rates that are also concentration-dependent. Therefore, it is plausible to account for these effects within the lumped parameter approach of (2-10). It is initially assumed that a first-order model is appropriate, since most chemical species that are present in any appreciable quantity over the operating range of the system are monatomic in chlorine (Snoeyink and Jenkins, 1980). The suitability of the overall kinetic expression (2-10) is assessed using experimental data in Section 3.

2.2.2 Dosage Area Model

A first-principles model for the dosage area is based upon the constant-volume continuously-stirred tank reactor (CSTR) formulation (Ogunnaike and Ray, 1994)

$$V_{da}\frac{dC_0(t)}{dt} = Q_d(t)C_d - Q(t)C_0(t) + rV_{da} \tag{2-11}$$

$$V_{da}\frac{dAN(t)}{dt} = Q(t)AN_{IN}(t) - Q(t)AN(t) + r_{AN}V_{da} \tag{2-12}$$

where $Q_d(t)$ is the flowrate of the manipulated dosage stream (m^3/s), C_d is the constant chlorine concentration in the dosage stream (g/m^3), r is the rate of reaction of chlorine (g/s), AN_{IN} is the effective incoming ammonia-nitrogen concentration (g/m^3), AN is the effective ammonia-nitrogen concentration exiting the reactor (g/m^3), and r_{AN} is the rate

of reaction of ammonia nitrogen (g/s). The term "effective" indicates that the bulk of the reactant is ammonia nitrogen, with the remainder comprised of trace reactants such as metal ions.

A series of assumptions and observations allows the two equations to be combined into one. First, although the slow reactions begin in the dosing area, the residence time is low enough that they are considered negligible, so they are ignored. Second, note that $r = R(t)r_{AN}$, where R is the ratio of the stoichiometric coefficients for the effective ammonia and chlorine reactions (after appropriate conversion from molar units to mass units). Note that this term is time dependent, since the trace reactant concentration, pH, and temperature may cause the demand for chlorine for each unit of ammonia to fluctuate. In other words, every gram of ammonia reacts quickly to equilibrium with R grams of chlorine, and R is dynamic. Also, $AN \cong 0$, because it has already been assumed that virtually all of the ammonia is consumed in the CSTR. Next, $\frac{dAN}{dt} \cong 0$, since it is assumed that the ammonia-nitrogen quickly reaches its steady-state. Finally, it should be noted that the assumption $r = 0$ *cannot* be made, because although $r_{C_0} = kC_0^{\,n}AN^m$ and $AN \cong 0$, the value of k is very large, and therefore prevents the term from being effectively zero. The steady-state and zero ammonia-nitrogen concentration assumptions reduce (2-12) to $r_{AN}V_{da} = Q(t)AN(t)$, and then using $r = Rr_{AN}$ to substitute into (2-11) yields

$$V_{da}\frac{dC_0(t)}{dt} = Q_d(t)C_d - Q(t)C_0(t) - Q(t)R(t)AN(t) \qquad (2\text{-}13)$$

Recognizing that both R(t) and AN(t) are unmeasured disturbances, let

$$R(t)AN(t) = \delta(t) \tag{2-14}$$

where $\delta(t)$ is referred to as the *chlorine demand*, is measured in ppm (g/s), and defines how many ppm of chlorine are consumed by fast reactions per unit of flow. When this demand is satisfied, the system is said to have reached *breakpoint* (Bierck *et al.,* 1996). Therefore, the final CSTR model is cast in the form

$$V_{da}\frac{dC_0(t)}{dt} = Q_d(t)C_d - Q(t)C_0(t) - Q(t)\delta(t) \tag{2-15}$$

The model maintains a high level of simplicity while capturing the important characteristics of a dosing area. First, it reflects that two streams are being combined to a uniform concentration. In addition, it captures the fact that some chemical reactions quickly proceed to completion and/or equilibrium; the resulting behavior can be viewed as a load on the system. Finally, it is assumed that any differences in the dynamic behavior of a CSTR and an actual dosing area are negligible on the time scale of the contact area, since its volume, and therefore its residence time, typically comprises only a small fraction (perhaps 1 or 2 percent) of the total volume of the plant.

A standard linearization (Seborg, Edgar, and Mellichamp, 1989) of the model (2-15) yields

$$\frac{d\tilde{C}_0(t)}{dt} = -\frac{\overline{Q}}{V_{da}}\tilde{C}_0(t) + \frac{C_d}{V_{da}}\tilde{Q}_d(t) - \frac{\overline{Q}}{V_{da}}\tilde{\delta}(t) - \frac{(\overline{C}_0 + \overline{\delta})}{V_{da}}\tilde{Q}(t) \tag{2-16}$$

where the deviation variables

$$\tilde{C}_0 := C_0(t) - \overline{C}_0 \tag{2-17}$$

$$\tilde{Q}_d := Q_d(t) - \overline{Q}_d \tag{2-18}$$

$$\tilde{\delta} := \delta(t) - \overline{\delta} \tag{2-19}$$

$$\tilde{Q} := Q(t) - \bar{Q} \tag{2-20}$$

are defined as a function of the steady state values $\bar{C}_0, \bar{Q}_d, \bar{\delta}$, and $\bar{Q}$ that make the right-hand side of (2-16) identically zero. The Laplace transform of (2-16) yields the transfer-function model

$$\tilde{C}_0(s) = \frac{\frac{C_d}{\bar{Q}}}{\frac{V_{da}}{\bar{Q}}s+1}\tilde{Q}_d(s) - \frac{1}{\frac{V_{da}}{\bar{Q}}s+1}\tilde{\delta}(s) - \frac{\frac{\bar{C}_0+\bar{\delta}}{\bar{Q}}}{\frac{V_{da}}{\bar{Q}}s+1}\tilde{Q}(s) \tag{2-21}$$

Note that since the manipulated variable is

$$u(s) := Q_d(s)C_d \tag{2-22}$$

then

$$\tilde{u}(s) := \tilde{Q}_d(s)C_d \tag{2-23}$$

where

$$\tilde{u}(s) := u(s) - \bar{u} \tag{2-24}$$

and (2-21) becomes

$$\tilde{C}_0(s) = \frac{\frac{1}{\bar{Q}}}{\frac{V_{da}}{\bar{Q}}s+1}\tilde{u}(s) - \frac{1}{\frac{V_{da}}{\bar{Q}}s+1}\tilde{\delta}(s) - \frac{\frac{\bar{C}_0+\bar{\delta}}{\bar{Q}}}{\frac{V_{da}}{\bar{Q}}s+1}\tilde{Q}(s) \tag{2-25}$$

Values of the constants appearing in (2-25) are given in Table 2-2.

It is common practice in industry to report the chlorine dosage in ppm (as in Table 2-2), which is calculated by dividing the flowrate Q(t) into the dosing rate $Q_d(t)C_d$. The goal is to report u(t), $C_0(t)$, and $C_L(t)$ all in units of ppm. The result introduces the alternate dosage variable

$$u'(t) := \frac{Q_d(t)C_d}{Q(t)} \tag{2-26}$$

where $u'(t)$ is measured in ppm (*i.e.,* g/m^3). The product $Q_d(t)C_d$ is the equivalent of $u(t)$, the mass dosing rate of chlorine, and (2-26) remains valid provided that $Q_d(t) << Q(t)$, which is the case at all typical operating conditions. This is because, strictly speaking, the chlorine dosing rate, $Q_d(t)C_d$, should be divided by the *sum* of the flowrates, $Q(t) + Q_d(t)$, to calculate the concentration; it is assumed that the flowrate $Q_d(t)$ is negligible compared to $Q(t)$. However, using (2-26) would introduce a bilinear term to (2-15) and (2-25), which would result in a more complex model, and so $u'(t)$ is used throughout the study strictly for reporting purposes, while $u(t)$ remains as the actual control variable. Of course, using the sum of the flowrates in the denominator of (2-26) would be even more non-linear, and is also therefore eliminated from consideration as a choice of control variable.

2.2.3 Contact Area Model

The most important component of the system is the contact basin, and its model is therefore critical. As a distributed-parameter system (Seborg, Edgar, and Mellichamp, 1989), the contact area can be modeled as a plug flow reactor (PFR) with chemical reaction through the standard equation

$$\frac{\partial C}{\partial t} = -v(t)\frac{\partial C}{\partial z} + r_{rxn} + D\frac{\partial^2 C}{\partial z^2} \tag{2-27}$$

where $C = C(t,z)$ is the chlorine concentration measured in parts per million (ppm), $v(t) = Q(t) / A$ is the linear flow velocity measured in meters per second (m/s), t is the time measured in seconds (s), r_{rnx} is the rate of chemical reaction measured in parts per

million per second (ppm/s), z is the horizontal length coordinate of the reactor measured in meters (m), and D is the effective dispersion coefficient measured in meters squared per second (m^2/s). A complete derivation of Equation (2-27) is given in Appendix A. The boundary condition is $C(t,0) = C_0(t)$, and the initial condition is $C(0,z) = C^0(t,z)$, where $C^0(t,z)$ is a known initial spatial concentration profile.

Three primary modeling issues arise. First, the rate of chemical reaction r_{rnx} must be adequately described; this matter is investigated in Section 2.2.3. Second, Equation (2-27) is a partial differential equation (PDE), which is not directly useful for the purposes of control design; Sections 2.2.4 and 2.2.5 outline one approach to a solution. Third, since an ideal PFR passes any input proportionally after a delay, and the delay is defined as the residence time $\theta_{ca}(t) = V_{ca} / Q(t)$, the model predicts that this system features a delay that is inversely proportional to the flowrate. Because the flowrate is time-varying, it is critical to select a control design that can perform effectively even if the delay changes. The performance for different schemes is explored in Section 2.4.

2.2.4 Simplified Model of a Plug Flow Reactor

Substituting the kinetic rate model (2-10) and the linear velocity expression $v(t)= Q(t)/A$ into Equation (2-27) yields the PDE

$$\frac{\partial C}{\partial t} = -\frac{Q(t)}{A}\frac{\partial C}{\partial z} - k_{rxn}C + D\frac{\partial^2 C}{\partial z^2} \qquad (2\text{-}28)$$

The design of feedback controllers for PDEs of the form (2-28) is particularly challenging. It is therefore desirable to approximate (2-28) by a set of ordinary differential equations (ODEs). One possible approach is to divide the volume of the

contact area into N smaller volumes, $\Delta V_{ca} = V_{ca}/N$, as shown in Figure 2-2, where each volume is considered a chemical reactor.

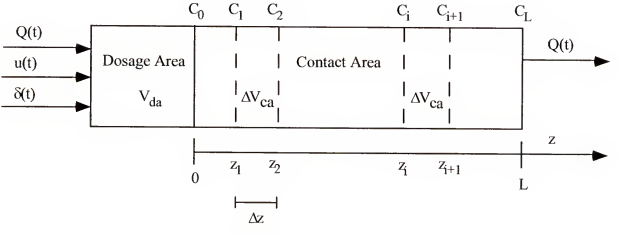

Figure 2-2. Schematic of the wastewater treatment plant when divided into N small volumes $\Delta V_{ca} = V_{ca}/N$.

The notation $C_i(t) = C(t,z_i)$ represents the chlorine concentration of the i^{th} volume section, z_i is the horizontal coordinate that denotes the end of the i^{th} volume-section, $\Delta z = z_i - z_{i-1}$ is the length of the i^{th} reactor, and $\Delta V_{ca} = V_{ca} / N$ is the volume of each reactor. All other quantities are as given in Figure 2-1.

Assuming that N is large, the difference equations

$$\frac{\partial C_i(t)}{\partial z} = \frac{C_i(t) - C_{i-1}(t)}{z_i - z_{i-1}}, \qquad i = 1,2,\ldots N \tag{2-29}$$

can be used to approximate the spatial partial derivatives. Combining Equations (2-28) and (2-29) yields the set of ordinary differential equations

$$\frac{dC_i(t)}{dt} = -\frac{Q(t)}{A(z_i - z_{i-1})}\left(C_i(t) - C_{i-1}(t)\right) - k_{rxn}C_i(t), \qquad i = 1,2,\ldots,N \tag{2-30}$$

Recognizing that

$$A(z_i - z_{i-1}) = \Delta V_{ca} \tag{2-31}$$

produces the system of equations

$$\frac{dC_1(t)}{dt} = -\left(\frac{Q(t)}{\Delta V_{ca}}\right)C_1(t) + \left(\frac{Q(t)}{\Delta V_{ca}}\right)C_0(t) - k_{rxn}C_1(t) \tag{2-32}$$

$$\frac{dC_2(t)}{dt} = -\left(\frac{Q(t)}{\Delta V_{ca}}\right)C_2(t) + \left(\frac{Q(t)}{\Delta V_{ca}}\right)C_1(t) - k_{rxn}C_2(t) \tag{2-33}$$

$$\vdots$$

$$\frac{dC_N(t)}{dt} = -\left(\frac{Q(t)}{\Delta V_{ca}}\right)C_N(t) + \left(\frac{Q(t)}{\Delta V_{ca}}\right)C_{N-1}(t) - k_{rxn}C_N(t) \tag{2-34}$$

which can be written in a more compact notation as

$$\frac{dC_i(t)}{dt} = -\left(\frac{Q(t)}{\Delta V_{ca}} + k_{rxn}\right)C_i(t) + \left(\frac{Q(t)}{\Delta V_{ca}}\right)C_{i-1}(t), \qquad i = 1,2,\ldots,N \tag{2-35}$$

Finally, the outlet chlorine concentration in the contact area is found as

$$C_L(t) = C_N(t) \tag{2-36}$$

Equation (2-35) can interpreted as a cascade of continuously-stirred tank reactors (CSTRs) where C_0 is the input, $Q(t)$ is a disturbance, C_i are the states for $i = 1,2,\ldots,N$, and C_L is the output. Although simplification is gained because the system is now composed of N ODEs instead of one PDE, it is important to note that each equation is nonlinear because of the presence of bilinear terms of the form $Q(t)C_i(t)$ and $Q(t)C_{i-1}(t)$. Finally, just how large N needs to be in order to accurately describe a wastewater treatment plant is investigated in Section 2.3. Note that the behavior described by the dispersion term of (2-28) is approximated when N is a finite number. Therefore, it is ignored in (2-35).

2.2.5 Linearized State-Space Model of a Plug Flow Reactor

With the PDE (2-27) cast as a series of ODEs (2-35), the final step in creating a linear state-space description of the contact basin is linearization about a steady state. A standard linearization process applied to (2-35) yields

$$\frac{d\tilde{C}_i(t)}{dt} = -\left(\frac{\bar{Q}}{\Delta V_{ca}} + k_{rxn}\right)\tilde{C}_i(t) + \left(\frac{\bar{Q}}{\Delta V_{ca}}\right)\tilde{C}_{i-1}(t) - \left(\frac{\bar{C}_i}{\Delta V_{ca}} - \frac{\bar{C}_{i-1}}{\Delta V_{ca}}\right)\tilde{Q}(t), \qquad (2\text{-}37)$$

$$i = 1,2,\ldots,N$$

where the deviation variables

$$\tilde{C}_i := C_i - \bar{C}_i, \qquad i = 0,1,2,\ldots,N \qquad (2\text{-}38)$$

$$\tilde{Q} := Q(t) - \bar{Q} \qquad (2\text{-}39)$$

are defined as a function of the steady state values $\bar{C}_0, \bar{C}_1, \bar{C}_2, \ldots \bar{C}_N$, and $\bar{Q}$ that make the right-hand side of (2-37) identically zero. The model (2-37) can now be cast into the Nx2 linear state-space form (Kailath, 1980)

$$\mathbf{x} = \mathbf{A}\mathbf{x} + \mathbf{B}\mathbf{d} \qquad (2\text{-}40)$$

$$y = \mathbf{C}\mathbf{x} + \mathbf{D}\mathbf{d} \qquad (2\text{-}41)$$

where

$$\mathbf{x}^T = \begin{bmatrix} C_1 & C_2 & \cdots & C_N \end{bmatrix} \qquad (2\text{-}42)$$

$$\mathbf{d}^T = \begin{bmatrix} C_o & Q \end{bmatrix} \qquad (2\text{-}43)$$

and

$$\mathbf{A}=\begin{bmatrix} -(\frac{\overline{Q}}{\Delta V}+k_{rxn}) & 0 & 0 & \cdots & 0 & 0 \\ \frac{\overline{Q}}{\Delta V} & -(\frac{\overline{Q}}{\Delta V}+k_{rxn}) & 0 & \cdots & 0 & 0 \\ 0 & \frac{\overline{Q}}{\Delta V} & -(\frac{\overline{Q}}{\Delta V}+k_{rxn}) & \cdots & 0 & 0 \\ \vdots & \vdots & \ddots & \ddots & 0 & 0 \\ 0 & 0 & 0 & \frac{\overline{Q}}{\Delta V} & -(\frac{\overline{Q}}{\Delta V}+k_{rxn}) & 0 \\ 0 & 0 & 0 & 0 & \frac{\overline{Q}}{\Delta V} & -(\frac{\overline{Q}}{\Delta V}+k_{rxn}) \end{bmatrix} \qquad (2\text{-}44)$$

$$\mathbf{B}=\begin{bmatrix} \frac{\overline{Q}}{\Delta V} & -\frac{\overline{C}_1-\overline{C}_o}{\Delta V} \\ 0 & -\frac{\overline{C}_2-\overline{C}_1}{\Delta V} \\ 0 & -\frac{\overline{C}_3-\overline{C}_2}{\Delta V} \\ \vdots & \vdots \\ \vdots & \vdots \\ 0 & -\frac{\overline{C}_N-\overline{C}_{N-1}}{\Delta V} \end{bmatrix} \quad , \quad \mathbf{C}=\begin{bmatrix} 0 & \cdots & 0 & 1 \end{bmatrix} \quad , \quad \mathbf{D}=\begin{bmatrix} 0 & 0 \end{bmatrix} \qquad (2\text{-}45,2\text{-}46,2\text{-}47)$$

where $\mathbf{x}\in\Re^N, y\in\Re, \mathbf{d}\in\Re^2, \mathbf{A}\in\Re^{NxN}, \mathbf{B}\in\Re^{Nx2}, \mathbf{C}\in\Re^{1xN}$, and $\mathbf{D}\in\Re^{2x2}$.

2.3 Plant Data Fitting and Parameter Estimation

In order to have confidence that a simulation including simplifying assumptions is an accurate approximation of a real plant, it is appropriate to validate it with real plant data. Based upon the model developed in Section 2.2, two parameters remain to be investigated thoroughly against experimental data: namely, the reaction rate constant, k_{rxn}; and the number N of CSTRs needed to adequately match the experimental data. Since only two parameters are unknown, they can be easily identified through a computationally inexpensive exhaustive numerical search. Consider the cost function

$$J_N(k_{rxn})=\frac{1}{n}\sum_{i=1}^{n}[C_L(t_i;N,k_{rxn})-C_L^{exp}(t_i)]^2 \qquad (2\text{-}48)$$

where $C_L^{exp}(t_i)$ represents the experimental concentration values measured at the plant outlet point $z = L$ at time t_i for $i = 1,2,\ldots,n$, and $C_L(t_i;N,k_{rxn})$ is the output concentration predicted by the model (2-35) if the nonlinear model is used or by (2-37) if the linear model is used. Note that $C_L(t_i;N,k_{rxn})$ is a function of k_{rxn}—the greater k_{rxn}, the lower the resulting outlet concentration for any arbitrarily chosen value of N. The functional (2-48) can be minimized to find the optimum value of k_{rxn} for a given model of order N, *i.e.*

$$k_{rxn}^{opt}(N) = \text{argmin } J_N(k_{rxn}) \tag{2-49}$$

Figure 2-3 plots (2-48) as a function of candidate values of k_{rxn}, with each curve representing a different value of N. The figure shows that for $N \geq 50$, the value $k_{rxn}^{opt} = 1.09\text{x}10^{-4}\ s^{-1}$ is a component of the optimizing solution of (2-49). Furthermore, close inspection reveals that the minimum over N is realized at roughly $N = 100$. In other words, as N is increased from to 25 toward 100, J_N becomes increasingly smaller, but then it begins to increase after N becomes greater than 100. This is in reasonable agreement with tracer tests performed at the facility (Barrios *et al.,* 2002).

It should be noted that it is assumed throughout the simulation study that these values are constants. In practice they are disturbances, as they are not controlled, and may or may not change value. The additional complexity introduced into the model by allowing them to vary is not necessary to show that traditional control configurations are inadequate to control this type of system.

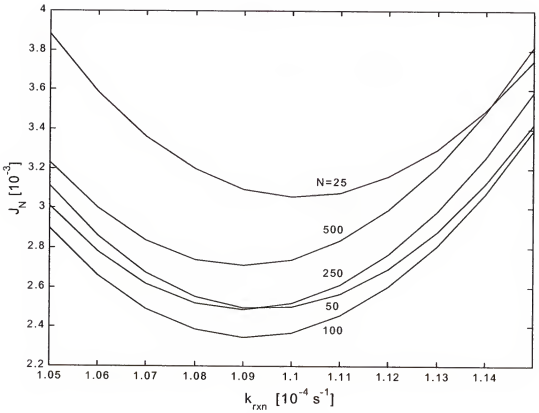

Figure 2-3. Map of the cost function for candidate values of k_{rxn}, with each line representing a different number of reactors N. A minimum is realized for N=100 and $k_{rxn}^{opt}(100) = 1.09 \times 10^{-4}$ s^{-1}.

Figure 2-4 shows the result of a simulation using a portion of experimental plant data gathered at the Kanapaha Wastewater Treatment Plant (Demir, 2001). The bottom graph shows the value of the disturbance Q(t) versus time. Initially, the flow is held nearly equal to 0.5 m^3/s, but is suddenly decreased to slightly more than 0.4 m^3/s after approximately 5.25 hours. The data is noise free because the available flowrate values are simply the setpoint of a flowrate controller, as the flowrate is not actually measured on-line. The top graph plots three chlorine concentrations versus time. The first plot, depicted by a dashed line, is the concentration $C_0(t)$ measured at the beginning of the contact basin. The experiment involves intentionally increasing C_0 at approximately t =

5 hours, and then decreasing its original value at approximately t = 5.7 hours. The second concentration plotted, shown as a dashed-dot line, is the measured value of chlorine at the outlet, $C_L^{exp}(t)$. Finally, the third line is solid, and corresponds to the output concentration $C_L(t, N)$ predicted by passing the values of $C_0(t)$ and Q(t) through the nonlinear model (2-35)-(2-36) for the special case of $N = 100$ and $k_{rxn}^{opt}(100) = 1.09 \times 10^{-4}\ s^{-1}$.

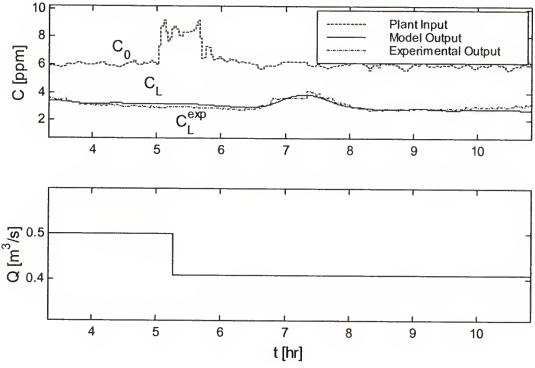

Figure 2-4. Fit of plant data using value of k_{rxn} that minimizes the Equation (2-49) for N=100; it is $k_{rxn}^{opt}(100) = 1.09 \times 10^{-4}\ s^{-1}$.

Figure 2-4 suggests that the proposed model parameters $N = 100$ and $k_{rxn}^{opt}(100) = 1.09 \times 10^{-4}\ s^{-1}$ provide an acceptable fit. However, a few characteristics may require further explanation. If a linear model is used, its predictions are most accurate near the steady state about which the nonlinear model has been linearized. The further it strays

from that point, the larger the errors. Therefore, at the expense of additional computation time, the nonlinear model was used for fitting the data. Also, the model output appears much smoother than the plant input; this is because the series of CSTRs acts as a low-pass filter, and because the model does not include the measurement noise associated with the observation of $C_L(t)$.

In fact, the real plant output (dashed-dot line in Figure 2-4) seems to be a delayed, scaled, and smoothed copy of the true plant input (dashed line in Figure 2-4), indicating that the plant does not exhibit truly ideal PFR behavior. Rather, it suffers from a small degree of mixing, which tends to better mimic the output of a large series of CSTRs. In light of this, instead of using as many reactors as possible to minimize k_{rxn}^{opt} in an attempt to approximate a PFR, Figures 2-3 and 2-4 imply that there is a finite number of reactors N that best describes plant data. Figure 2-5 is constructed to determine the optimal number of reactors N that minimizes the minima of the curves in Figure 2-3. It plots the number of reactors N versus $J_N = (k_{rxn}^{opt})$, where J_N is given in (2-48), k_{rxn}^{opt} is given in (2-49), and focuses on a neighborhood of N = 100.

It is clear that the function is minimized very near to N = 100. In fact, N = 102 does minimize the cost function to a resolution of two CSTRs. As with any data fitting exercise, higher degrees of precision can be found with ever more exhaustive searches. However, there is a limit to their validity beyond a couple of decimal places. Therefore, the values N = 100 and $k_{rxn}^{opt}(100) = 1.09 \times 10^{-4}\ s^{-1}$ are chosen as sufficient for the purposes of modeling both open-loop and closed-loop performance.

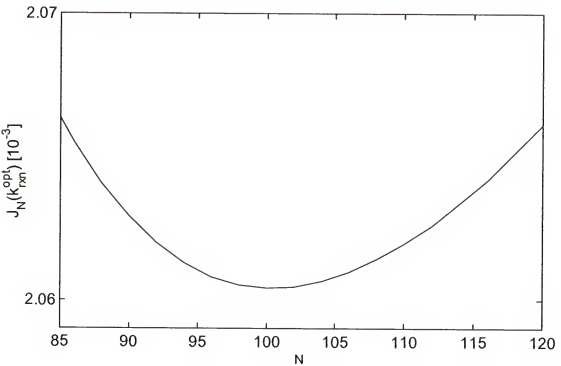

Figure 2-5. Optimization of N to minimize the error between the nonlinear model and the true plant output.

2.4 Control Design and Assessment of Performance

With a viable model of a wastewater chlorination system, including values for its parameters, characteristics of the particular system must be considered in selecting an appropriate control scheme. For example, the system is affected by two primary disturbances, ammonia chlorine demand and flowrate. Also, there is a large time delay associated with the disinfection process, implying that deadtime compensation of some type could be beneficial.

Unlike more complicated disturbances such as flowrate through a fixed volume (discussion to follow), a cascade control system is a common strategy employed to reject load-type input disturbances such as ammonia chlorine demand. Therefore, a cascade control scheme is considered in addition to standard feedback design. As stated

previously, the dosing area portion of the reactor does not suffer from large time delay; it is the contact area that has a large deadtime. Therefore, a proportional-integral (PI) controller should be sufficient to achieve satisfactory control in the slave loop, when it is utilized. However, the extremely large delay of the contact basin suggests that a deadtime compensation strategy, in addition to a standard PI controller, should be considered for the master controller. (Note: while the lone controller in a standard feedback system is generally referred to as a "feedback" controller, it is also referred to as a "master" controller in this study for brevity.) A Smith Predictor is chosen as the deadtime compensator. Thus, there are three variables pertinent to control design, and each has two possible values; they are summarized in Table 2-3.

Table 2-3. Summary of the total variations to consider in choosing a control design.

Control Scheme	1. Standard Feedback
	2. Cascade Feedback
Master Controller	1. PI
	2. PI with a Smith Predictor
Disturbances	1. Ammonia Chlorine Demand
	2. Flowrate

Because the effect of the ammonia chlorine demand on the system is fully realized in the dosing area (fast reactions consume chlorine before leaving the dosing area), it follows that a secondary loop (cascade control) should be effective in the rejection of this disturbance. Consequently, cascade control is anticipated to be more effective than standard feedback control, regardless of which master controller is chosen;

results verifying this assertion are given in Appendix B. The block diagram and process used for obtaining open-loop responses, controller tunings, and simulation results in standard feedback configuration is analogous to that discussed in detail in Section 2.4.2 for a cascade configuration. Therefore, cascade control is assumed to solve the problem of chlorine demand as a control design issue.

In addition, flowrate can easily be measured, and input concentration is often maintained with a (feedforward) ratio controller, as is always the case in this study. When such a strategy is employed, the ratio controller can be inserted into the control loop independent of all other design choices. For the purposes of modeling, the valve dynamics are assumed to be much faster than the transport delays associated with a reactor of this size. As a result, the model of a ratio controller is omitted within the simulations for simplicity, and it is assumed that the desired input concentration u(t) can be achieved instantaneously (*i.e.,* the ratio controller has no dynamics; rather, it is simply a ratio station that performs a calculation). In practice, any error introduced by using a feedforward controller is automatically corrected by the slave controller that is being used to reject the ammonia chlorine demand disturbance, thus reinforcing the argument for using cascade control rather than standard feedback control.

However, input concentration is only one of two ways in which flowrate effects the system; residence time is the other. Residence time is an effect seen throughout the reactor, so it is a characteristic that cannot be compensated for solely by a secondary (slave) loop. The control design problem is now to select the proper master controller (to be used in a cascade control scheme) based upon the closed-loop performance of the

system when subject to realistic flowrate patterns. In other words, the pertinent control design issues presented in Table 2-3 are reduced to those given in Table 2-4.

Table 2-4. Summary of the simplified total variations to consider in choosing a control design.

Control Scheme	Cascade Feedback
Master Controller	1. PI
	2. PI with a Smith Predictor
Disturbances	Flowrate

A block diagram of the cascade control scheme is shown in Figure 2-6, where G_{sc}, G_{mc}, and RC are the slave, master, and ratio controllers, respectively. In addition, G_{da} is the dosage-area model, G_{ca} is the contact-area model, r_{sc} and r_{mc} are the slave and master setpoints, respectively, and e_{sc} and e_{mc} are the slave and master error signals, respectively. Finally, $R_d(t) = Q_d(t)/Q(t)$ is the flowrate ratio required of the ratio controller. All other quantities are the same as defined in Section 2.2.

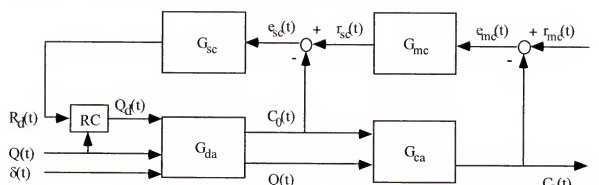

Figure 2-6. Block diagram of a wastewater treatment plant under cascade control.

An input of chlorine dosing stream flowrate $Q_d(t)$ (and with constant chlorine concentration C_d) is received in the dosing area from the ratio controller RC. The chlorine is mixed with the incoming untreated water arriving at a flowrate Q(t), and chlorine consumption due to reaction with ammonia occurs to a significant extent. Then, the chlorinated stream passes from the dosing area into the contact area transported at the same flowrate Q(t) and with an established initial concentration $C_0(t)$.

It is during the extended period of time that the liquid is in the contact area that the disinfecting and slow reactions take place, as well as volatilization and UV reactions. The inlet concentration $C_0(t)$ is reduced to the outlet concentration value $C_L(t)$ during the time the flow traverses the length of the reactor. The exit concentration $C_L(t)$ is measured and compared to the master setpoint r_{mc}. This signal is processed in the master controller G_{mc} which prescribes an appropriate slave setpoint r_{sc}. The latter is compared to the measurement $C_0(t)$ to produce the feedback error e_{sc}, which in turn is processed by the slave controller G_{sc} producing the prescription $R_d(t)$, which is sent to the ratio controller. The ratio controller uses the information, along with a measurement of Q(t), to produce $Q_d(t)$, thereby completing the loop.

2.4.1 Description and Tuning of the Slave PI Controller

The slave proportional-integral controller (Ogunnaike and Ray, 1994) is of the standard form

$$G_{sc}(s) = K_{sc}(1 + \frac{1}{\tau_{sc}s}) \tag{2-50}$$

where K_{sc} is the gain of the controller, and τ_{sc} is the integral time constant of the controller.

2.4.1.1 Open-loop response of the dosing area model to step changes in dosing rate and tuning parameters of a slave PI controller

In cascade systems, the inner loop (slave loop) is normally more aggressive, and must be tuned first (Ogunnaike and Ray, 1994). The outer loop is left open during this procedure (*i.e.* the gain of the master controller is set equal to zero). The range of typical (as opposed to extreme) flowrates Q(t) for the Kanapaha facility is 0.2 m^3/s to 0.6 m^3/s

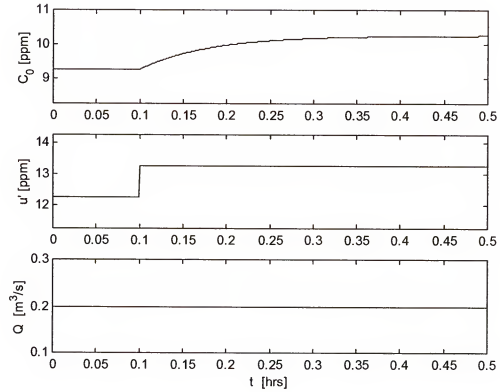

Figure 2-7. Open-loop response of the dosing area for a step in dosage $u(t) = Q_d(t)C_d$ from 2.451 to 2.651 g/s at disturbance value of Q(t) = 0.2 m^3/s.

(recall that the nominal value is 0.4 m^3/s). Accordingly, 0.6, 0.4, and 0.2 m^3/s are designated as high, middle, and low values of the disturbance Q(t). Figure 2-7 shows the open-loop response of the dosing area to a step change in input concentration u(t) from 12.25 ppm to 13.25 ppm at time 0.1 hr as predicted by the model (2-15). The top plot shows the output concentration $C_0(t)$ as a function of time, the center plot shows the input concentration u(t) as a function of time, and the bottom plot shows that the flowrate is held constant at the value Q = 0.2 m^3/s (the ammonia chlorine demand δ is also held constant at 3 ppm, but not depicted).

The first-order plus deadtime (FODT) fit (Seborg, Edgar, and Mellichamp, 1989)

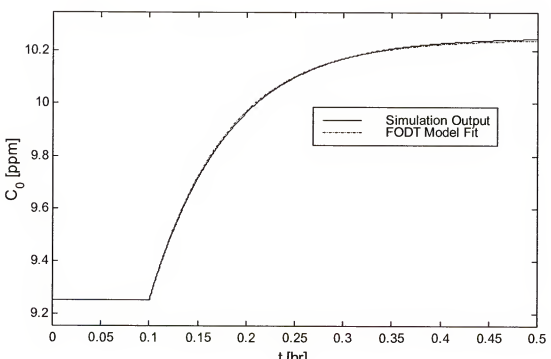

Figure 2-8. FODT fit of the dosing area for a step in $Q_d(t)C_d$ from 2.451 to 2.651 g/s; the observed parameters are K_{da} = 5.0 ppm-s/g, τ_{da} = 280 s, and θ_{da} = 0 s.

of the concentration output $C_0(t)$ of the dosing area for the open-loop step change in dosage input u(t) from 2.451 g/s to 2.651 g/s (the top plot in Figure 2-7) is shown in Figure 2-8. Output from the simulation is represented with a solid line, and the FODT model is represented with a dashed-dot line. The criterion used to decide which curve yields the best fit is minimization of the sum of the squared error (SSE).

The procedure is repeated with a step down in input, and at middle and high flow conditions, resulting in a total of six sets of FODT parameters. They are then averaged, and the averages are used to tune the slave controller. Table 2-5 lists the inputs and outputs for each trial, the observed FODT transfer function parameters for each case, and the averages of the values. The first two columns report the value of the input u(t) in g/s before and after the step change, respectively. The next two columns give the value of the output $C_0(t)$ in ppm both before the step and after the system has been allowed to

Table 2-5. Dosing area transfer function parameters for various steps in control variable $u(t) = Q_d(t)C_d$ for various values of disturbance Q(t).

Initial S.S. DA Input $Q_d(t)C_d$ [g/s]	Final S.S. DA Input $Q_d(t)C_d$ [g/s]	Initial S.S. DA Output $C_0(t)$ [ppm]	Final S.S. DA Output $C_0(t)$ [ppm]	Plant Flowrate Q(t) [m^3/s]	K_{da} [ppm-s/g]	τ_{da} [s]	θ_{da} [s]
2.451	2.651	9.25	10.25	0.2	5.0	280	0
2.451	2.251	9.25	8.26	0.2	5.0	280	0
2.926	3.326	4.31	5.31	0.4	2.5	140	0
2.926	2.526	4.31	3.31	0.4	2.5	140	0
3.805	4.405	3.34	4.34	0.6	1.7	100	0
3.805	3.205	3.34	2.34	0.6	1.7	100	0
				Average	3.1	170	0

reach its new steady-state, respectively. The fifth column gives the value of the flowrate disturbance Q(t) for each particular trial, and the final three columns report the observed FODT parameters, K_{da}, τ_{da}, and θ_{da}. Finally, average vales for each of the parameters are listed across the bottom row.

Table 2-6 repeats the average values, and reports the resulting values of slave controller gain K_{sc} and integral time constant τ_{sc}. In this case, they are found by the trial-and-error method, since the ratio of θ / τ does not fall into the suggested range of $0.1 \leq \theta / \tau \leq 1.0$ set forth by standard tuning rules such the ITAE and ISE methods (Ogunnaike and Ray, 1994), primarily because the FODT fit of an ideal CSTR model results in a zero delay value.

Table 2-6. Estimated dosing area transfer function parameters and resulting slave controller parameters found by trial-and-error tuning.

Transfer Function Parameters	Numerical Value	Controller Parameters	Numerical Value
K_{da}^{*}	3.1 ppm-s/g	K_{sc}	0.025 g/ppm-s
τ_{da}^{*}	170 s	τ_{sc}	50 s
θ_{da}^{*}	0 s		

2.4.1.2 Closed-loop response of the dosing area model for step changes in concentration setpoint

Figure 2-9 shows three closed-loop responses of the dosing area model (2-15) for a setpoint change in r_{sc} from 2 to 3 ppm at time 0.1 hr, which is depicted as a dotted line. The top plot shows the output concentration $C_0(t)$ as a function of time, the center plot is the input to the dosing area u(t) administered by the slave controller as a function of time,

and the bottom plot is the water flowrate Q(t) through the dosing area as a function of time. The dashed-dot line represents the result for a low-flow disturbance (0.2 m^3/s), the solid line represents the calculation for a medium-flow disturbance (0.4 m^3/s), and the dashed line represents the response for a high-flow disturbance value (0.6 m^3/s).

The controller accomplishes a setpoint tracking change for each disturbance value almost instantly; in addition, overshoot is minimal, and oscillations are almost non-existent. The primary reason is that the dosing area is based upon an ideal CSTR, which has no time delay from the input to the output. In reality, a dosing area is likely to have some small delay. However, note that the slave controller accomplishes the setpoint change within a very small fraction of an hour. Even with a small delay and the associated dynamics, the closed-loop response would resemble a step when viewed on the time scale of the contact area. Therefore, the model provides an acceptable representation of a slave controller implemented around a real dosing area.

In addition to setpoint tracking, the slave loop is required to reject disturbances in ammonia chlorine demand. The simulation studies show that here again, the performance is comparatively fast, and the closed-loop response essentially appears to be a flat line when viewed on the time scale of the contact area. These responses are not shown for brevity. Note also that the simulations are performed with the slow reactions included, yet the steady-state behavior of the dosing area is virtually identical at all flowrates, thereby confirming the assumption that only the fast reactions are important in this part of the reactor.

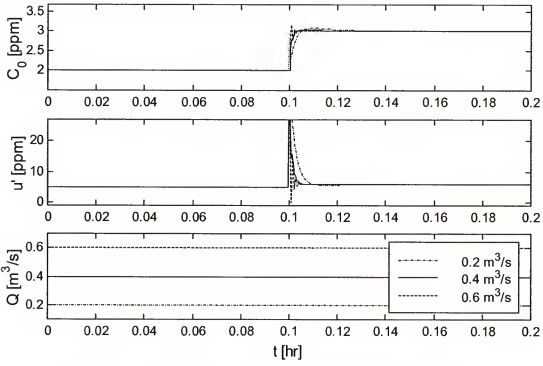

Figure 2-9. Closed-loop response of the dosing area using a PI controller with K_{sc} = 0.025 g/ppm-s and τ_{sc} =50 s for disturbance values Q(t) = 0.2 m^3/s, 0.4 m^3/s, and 0.6 m^3/s.

2.4.2 Description and Tuning of the Master PI Controller

With the inner loop tuned, the outer master loop must be tuned next. A PI controller is selected for G_{mc} of the familiar form

$$G_{mc}(s) = K_{mc}\left(1 + \frac{1}{\tau_{mc}s}\right) \tag{2-51}$$

where K_{mc} is the controller gain and τ_{mc} is the controller integral time constant.

2.4.2.1 Open-loop response of the contact area model to step changes in input concentration and tuning parameters of a master PI controller

With the inner slave loop operating, a step change in the variable $C_0(t)$ is passed through the entire system to obtain an open-loop response for the contact area. Figure 2-10 shows the results. The top plot shows the output concentration $C_L(t)$ as a function of time, the center plot shows that the setpoint $C_0(t)$ (*i.e.* r_{sc}) is changed from 9.25 ppm to 10.25 ppm at time 2 hr, and the bottom plot shows that the disturbance Q(t) is held constant at $Q = 0.2\ m^3/s$. In addition, ammonia chlorine demand is again held constant at $\delta = 3$ ppm, but not shown.

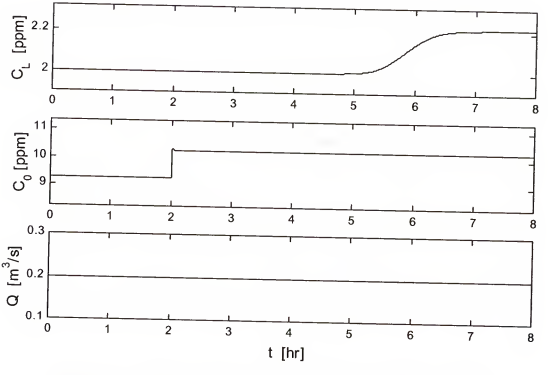

Figure 2-10. Open-loop response of the contact area with the slave controller in operation about the dosing area.

Inspection of the first two graphs reveals that setpoint adjustments of the slave controller cause changes in the output variable $C_L(t)$ that are representative of a very high

order system. However, the response can be effectively approximated with a FODT model. The results of the FODT fit are in turn used to tune the master controller.

The FODT fit of the concentration output $C_L(t)$ of the contact area for the open-loop step change in input $C_0(t)$ from 9.25 ppm to 10.25 ppm (the top plot in Figure 2-10) is shown in Figure 2-11. Output from the simulation is represented with a solid line, and the FODT model is represented with a dashed-dot line. The criterion used to decide which curve gives the best fit is again minimization of the SSE.

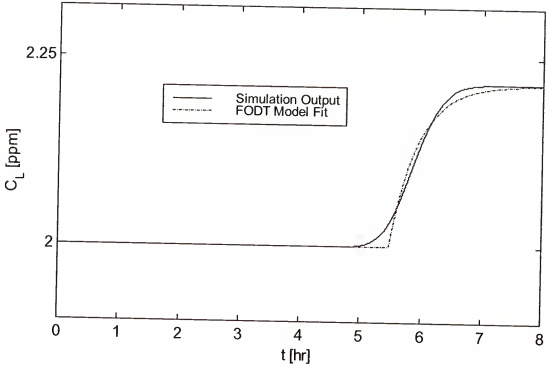

Figure 2-11. FODT fit of the contact area (while the slave controller is in operation around the dosing area) for step change in $C_0(t)$ from 9.25 ppm to 10.25 ppm with the flow held constant at Q = 0.2 m^3/s; the observed parameters are K_{ca} = 0.216 ppm-s/g, τ_{ca} = 1650 s, and θ_{ca} = 12510 s.

When the process of obtaining an open-loop response and a FODT model fit is repeated for several operating conditions, the resulting values are compared in an effort to

find parameters most representative of the system at all conditions. The values found to minimize the error for various operating conditions are listed in Table 2-7. The first two columns represent the beginning and ending steady-state inputs, and the next two columns report the beginning and ending steady-state outputs. The fifth column gives the plant disturbance Q(t) value during the trial. Finally, the last three columns list the values of K_{ca}, τ_{ca}, and θ_{ca} that minimize the error of the FODT model, respectively. The averages of all five trials are found across the bottom row. (Note that since steps up and steps down yield the same results for a given disturbance, more flowrate operating points are considered in lieu of redundant information.)

Table 2-7. Contact area transfer function parameters for various steps in input variable $C_0(t)$ for various values of disturbance Q(t).

Initial S.S. Input $C_0(t)$ [ppm]	Final S.S. Input $C_0(t)$ [ppm]	Initial S.S. Output $C_0(t)$ [ppm]	Final S.S. Output $C_0(t)$ [ppm]	Plant Flowrate Q(t) [m^3/s]	K_{ca} [ppm-s/g]	τ_{ca} [s]	θ_{ca} [s]
9.25	10.25	2.00	2.22	0.2	0.216	1650	12510
5.57	6.57	2.00	2.36	0.3	0.359	1100	8390
4.31	5.31	2.00	2.46	0.4	0.464	820	6310
3.70	4.70	2.00	2.54	0.5	0.540	660	5060
3.34	4.34	2.00	2.60	0.6	0.599	550	4220
				Average	0.436	960	7300

Using the average values for the contact area, it follows that the ratio θ / τ again does not fall into the standard range $0.1 \le \theta / \tau \le 1.0$. As a result, the controller is tuned as before via trial-and-error. Finally, recall that because the master controller must

primarily maintain a value of output concentration $C_L(t)$, it is tuned for optimal regulatory performance, rather than setpoint tracking.

Table 2-8. Estimated contact area transfer function parameters and resulting master controller disturbance-rejection parameters found by trial-and-error tuning.

Transfer Function Parameters	Numerical Value	Controller Parameters	Numerical Value
K^*_{ca}	0.436 ppm-s/g	K_{mc}	0.6 g/ppm-s
τ^*_{ca}	960 s	τ_{mc}	2500 s
θ^*_{ca}	7300 s		

The combined performance of the two controllers is assessed next when applied to the linear plant model for various disturbance Q(t) conditions. Even though the controller designs must ultimately be applied to the more realistic, nonlinear plant model, the linear closed-loop response is important for several reasons. First, the controller that is being applied to the system is linear; hence, if it cannot yield satisfactory results for the linear plant model, then it is extremely unlikely that it would be effective on the original nonlinear model. In addition, because software used for simulation (Matlab) is matrix-based, it can simulate a state-space model ten to one hundred times faster than a user-defined function. This is extremely useful in areas of debugging, tuning, and preliminary validation.

2.4.2.2 Closed-loop response of the entire model for step changes in flowrate

After the tuning choices are tested and verified on the linear model, they are used to attempt to control the nonlinear model. Figure 2-12 records the response of the system when subjected to a small early step-up in disturbance Q(t) at time 2 hr, followed by a large step-down in disturbance at time 12 hr, and finally another step-up at time 34 hr,

returning to the original flowrate Q(t). The first plot shows the output concentration for the linear plant (dashed-dot line), the nonlinear plant (solid line), and the setpoint (dotted line) as functions of time. Because regulations require a minimum of 1 ppm chlorine in water discharged from the plant (Florida Department of Environmental Protection, 1996), a value of 2 ppm is chosen for the setpoint, providing a margin of safety. The second plot shows the chlorine concentration entering the contact area $C_0(t)$ for each of the two models over time. Finally, the disturbance Q(t) is shown in the third plot as a function of time.

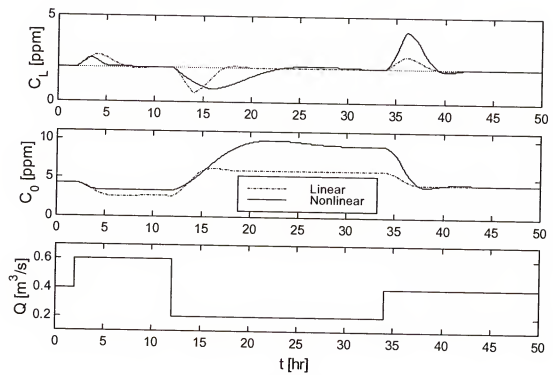

Figure 2-12. Closed-Loop response of linear and nonlinear models with a pair of controllers arranged in cascade configuration and subjected to a step changes in flowrate.

The well-tuned controller accomplishes an excellent response for both the linear and nonlinear plant. As expected, it performs better on the linear plant, returning the

output concentration $C_L(t)$ to the desired value within eight hours, even for the large step change in disturbance Q(t) at time 12 hr. The large step is designed to represent a condition of low residence time (less than 1 ½ hours) immediately followed by a condition of high residence time (approximately 4 hours), creating a worst-case scenario. As a result, eight hours (two residence times) is not an unacceptably large amount of time for the master controller to bring the system back to the setpoint. Furthermore, careful selection of the tuning parameters also results in a nonlinear closed-loop response with acceptable performance, almost matching that of the closed-loop linear system.

2.4.2.3 Closed-loop response of the entire model for a dynamic flowrate

Figure 2-13 shows the performance of the same control systems applied to the entire plant model when the flowrate is modeled as sinusoidal wave, which is chosen to approximate a smooth, cyclical water consumption profile of a typical day. The sine wave begins at time 2 hr, its period is 24 hr, and the amplitude is three-fourths of the nominal flowrate (0.4 m^3/s), or 0.3 m^3/s. The result is a disturbance Q(t) that varies from 0.1 m^3/s to 0.7 m^3/s. These values are chosen because they represent a 7:1 ratio of maximum-to-minimum flowrate, which is not an unrealistic occurrence.

The linear plant is controlled with acceptable performance, experiencing only low-amplitude fluctuations in output $C_L(t)$ that lag predictably behind the flowrate profile. However, it is clear that a sinusoidal flow of significant amplitude severely degrades the quality of the controller performance for simulations of the nonlinear plant. Figure 2-13 shows that output concentration values $C_L(t)$ are as high as 6.0 ppm and as low as 0.5 ppm. The conclusion is that cascade control of a wastewater treatment plant

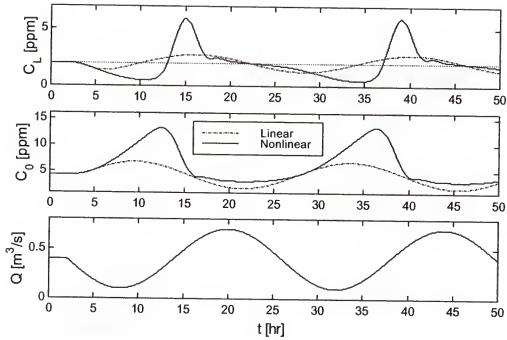

Figure 2-13. Closed-Loop response of linear and nonlinear models with a pair of controllers arranged in cascade configuration subjected to varying flow.

with a PI slave controller and a PI master controller is viable if the plant is linear, but it is inadequate in more realistic circumstances that include the nonlinear dynamics of the system.

2.4.3 Description and Tuning of the Master PI Controller and Smith Predictor

A PI master controller with a Smith Predictor (Ogunnaike and Ray, 1994) can be used in an attempt to reduce the effect of the delay and improve performance. The structure of a Smith Predictor applied to a PI master controller is given by the expression

$$G_{mc}(s) = \frac{K_{mc}(1+\frac{1}{\tau_{mc}s})}{1+K_{mc}(1+\frac{1}{\tau_{mc}s})K^{*}_{ca}\frac{1}{\tau^{*}_{ca}s+1}(1-e^{-\theta^{*}_{ca}s})} \qquad (2\text{-}52)$$

where the numerator factors $K_{mc}(1+\frac{1}{\tau_{mc}s})$ represent a standard PI controller, K^*_{ca} is the anticipated value of the contact area gain, τ^*_{ca} is the anticipated value of the contact area time constant, and θ^*_{ca} is the expected delay of the contact area.

As in the case of simple PI master controller, the tuning parameters K_{mc} and τ_{mc} must be selected to achieve optimum performance. With the effect of the delay reduced, however, the controller tunings change, and may become more aggressive. Furthermore, with the delay theoretically removed from the model, the trial-and-error tuning method is again the most reliable. Using the same FODT model for the contact area found in Table 2-7, the new values of K_{mc} and τ_{mc} are reported in Table 2-9. Note that K^*_{ca}, τ^*_{ca}, and θ^*_{ca} are simply the contact area model parameters found in Table 2-7.

Table 2-9. Contact area transfer function parameters and resulting disturbance rejection trial-and-error tunings when a Smith Predictor is incorporated.

Transfer Function Parameters	Numerical Value	Controller Parameters	Numerical Value
K^*_{ca}	0.436 ppm-s/g	K_{mc}	0.6 g/ppm-s
τ^*_{ca}	960 s	τ_{mc}	1000 s
θ^*_{ca}	7300 s		

2.4.3.1 Closed-loop response of the entire model for step changes in flowrate using a Smith Predictor

Figure 2-14 shows the simulation results for the system under PI control with a Smith Predictor subject to three separate constant delays. The flowrate profile (three step changes) and setpoint (held constant at 2 ppm) are identical to that used in Figure 2-12, using the same line-type convention as well. It is anticipated that the response is

improved over the case of a standard, single PI controller, provided that the model values K^*_{ca}, τ^*_{ca} and θ^*_{ca} are sufficiently accurate.

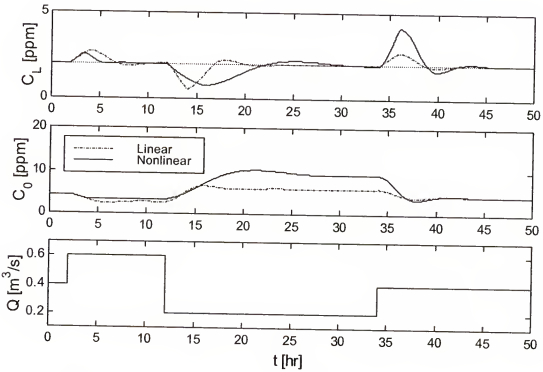

Figure 2-14. Closed-Loop response of linear and nonlinear models with a pair of controllers and a Smith Predictor arranged in cascade configuration subjected to a step changes in flowrate.

For these conditions, the cascade control configuration with a Smith Predictor added to the PI controller in the master loop yields an almost identical response to that with a standard PI in the master loop, both for the linear and nonlinear cases.

2.4.3.2 Closed-loop response of the entire model for a dynamic flowrate using a Smith Predictor

When the flowrate profile Q(t) of the system under cascade PI control with the addition of a Smith Predictor to the master loop is changed to a sine wave, the benefit of the Smith Predictor is again unapparent, as shown in Figure 2-15 Similarly to Figure 2-

11, the periodic flowrate Q(t) profile begins at time 2 hr, has a period of 24 hr, and has an amplitude of 0.3 m^3/s.

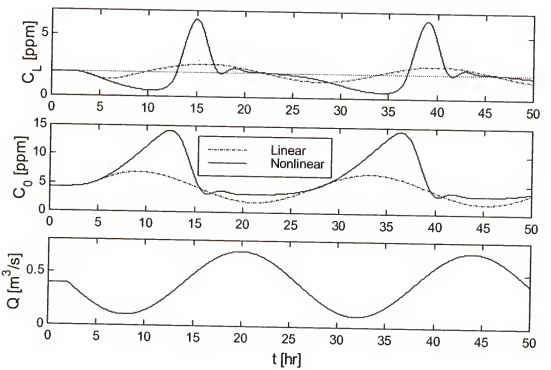

Figure 2-15. Closed-Loop response of linear and nonlinear models with a pair of controllers and a Smith Predictor arranged in cascade configuration subject to varying flow.

In the continuously varying flowrate scenario, only the linear plant simulation produces a satisfactory response. As in Figure 2-11, the output is a smooth sine wave that lags behind the disturbance. However, the controller fails almost completely to counter the effects of continuously varying delay when applied to the nonlinear plant, and the output is virtually the same as that obtained without a Smith Predictor under varying flow conditions. The result is in fact slightly worse than for simple cascade control, since the given that the output ranges from 0.5 ppm to 6.4 ppm.

Because the Smith Predictor is generally considered effective only within the range ±30% of the estimated delay (Seborg, Edgar, and Mellichamp, 1989), and given that the deadtime can often vary five-to-tenfold in a wastewater treatment plant, the lack of performance of the Smith Predictor observed is easily explained. Although a standard PI controller is adequate for the slave loop, a PI controller either with or without a Smith Predictor should not be used as a master controller. A more sophisticated controller form is needed to achieve satisfactory performance.

2.4.4 Description and Tuning of the Master PI Controller and Adaptive Smith Predictor

The response of the system under a PI master controller with a Smith Predictor (Ogunnaike and Ray, 1994) is not adequate, at least partly because the value of the delay θ_{ca} changes dramatically from one operating point to the next. This can be seen in Table 2-7, which lists the FODT fit parameters of the model for open-loop steps changes in input concentration C_0 at various constant disturbance values Q. Note also that the values of the other parameters, K_{ca} and τ_{ca}, vary with operating point. As a result, it is clear that a Smith Predictor with parameter estimates at the nominal flowrate (*i.e.* 0.4 m^3/s in this study) will experience error in *all three* parameters as the system moves to different operating points. It must be assumed that this will serve to only exacerbate the degradation of performance. However, each parameter follows a trend, and the three parameters are fit extremely well by the equations

$$K(Q) = -1.407Q^2 + 2.073Q - 0.140 \tag{2-53}$$

$$\tau(Q) = (0.003Q - 0.000001)^{-1} \tag{2-54}$$

$$\theta(Q) = (0.0004Q - 0.000001)^{-1} \tag{2-55}$$

where each parameter is updated continually in the controller as a function of flowrate. This variation of a Smith Predictor is an *adaptive* Smith Predictor. The structure of a PI master controller with an adaptive Smith Predictor is given by the expression

$$G_{mc}(s) = \frac{K_{mc}(1 + \frac{1}{\tau_{mc}s})}{1 + K_{mc}(1 + \frac{1}{\tau_{mc}s})\hat{K}_{ca}\frac{1}{\hat{\tau}_{ca}s + 1}(1 - e^{-\hat{\theta}_{ca}s})} \tag{2-56}$$

where the numerator factors $K_{mc}(1 + \frac{1}{\tau_{mc}s})$ represent a standard PI controller, $\hat{K}_{ca}$ is the current anticipated value of the contact area gain, $\hat{\tau}_{ca}$ is the current anticipated value of the contact area time constant, and $\hat{\theta}_{ca}$ is the current expected delay of the contact area.

As in the previous cases, the tuning parameters K_{mc} and τ_{mc} must be selected to achieve optimum performance. By using a dynamic algorithm, the controller tunings may become even more aggressive than for the case with a traditional Smith Predictor. The FODT model for the contact area found in Table 2-7 is again used as the starting point, the new values of K_{mc} and τ_{mc} are reported in Table 2-10.

Table 2-10. Contact area transfer function parameters and resulting disturbance rejection trial-and-error tunings when a Smith Predictor is incorporated.

Transfer Function Parameters	Numerical Value	Controller Parameters	Numerical Value
K^*_{ca}	0.436 ppm-s/g	K_{mc}	0.6 g/ppm-s
τ^*_{ca}	960 s	τ_{mc}	200 s
θ^*_{ca}	7300 s		

Note that controller gain does not increase, as is the case for many deadtime-compensated systems, but the integral action is much greater, implying that there is potential for improved performance. Interestingly, these parameters are valid for the nonlinear case *only*. While many systems tolerate more aggressive tunings for the linear case, the PI master controller with an adaptive Smith Predictor does not. In order to keep the linear system stable, the integral time constant of 2000 s must be used.

2.4.4.1 Closed-loop response of the entire model for step changes in flowrate using an adaptive Smith Predictor

Figure 2-16 shows the simulation results for the system under PI control with an adaptive Smith Predictor subject to the same three separate constant delays as in Section

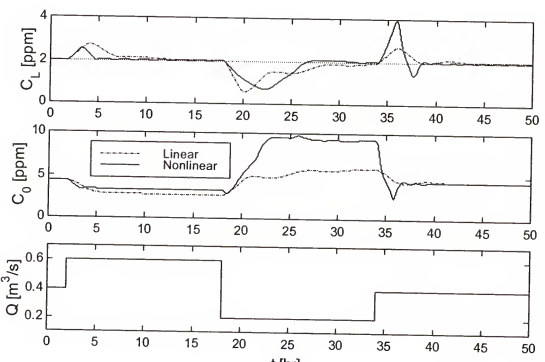

Figure 2-16. Closed-Loop response of linear and nonlinear models with a pair of controllers and an adaptive Smith Predictor arranged in cascade configuration subjected to a step changes in flowrate.

2.4.3. The flowrate profile (three step changes) and setpoint (held constant at 2 ppm) are identical to that used in Figure 2-12, using the same line-type convention as well. It is anticipated that the response is improved over the cases of a standard, single PI controller, as well as that of the PI master controller with a traditional Smith Predictor.

For these conditions, the cascade control configuration with an adaptive Smith Predictor added to the PI controller in the master loop yields a response that is significantly better than with a standard PI in the master loop, at least for the nonlinear case. The reason is likely to be that the master controller tunings for simple cascade and cascade with a Smith Predictor cannot tolerate such an aggressive integral time.

2.4.4.2 Closed-loop response of the entire model for a dynamic flowrate using a Smith Predictor

When the flowrate profile Q(t) of the system under cascade PI control with the addition of an adaptive Smith Predictor to the master loop is changed to a sine wave, the benefit of the adaptive Smith Predictor is reduced, as shown in Figure 2-17. Similarly to Figure 2-11, the periodic flowrate Q(t) profile begins at time 2 hr, has a period of 24 hr, and has an amplitude of 0.3 m^3/s.

In the continuously varying flowrate scenario, only the linear plant simulation produces a satisfactory response. As in Figure 2-11, the output is a smooth sine wave that lags behind the disturbance. For the nonlinear model, the controller appears to provide even poorer control than with a traditional Smith Predictor. It appears poorer because the output ranges from 0.2 ppm to 6.1 ppm. However, the extremely low level of 0.2 ppm is only observed in the first cycle. In the second, a minimum of 0.5 ppm is again accomplished. In regard to reducing the size of the peak for over-chlorination, it is slightly lower and much narrower, both of which are improvements. It is clear that,

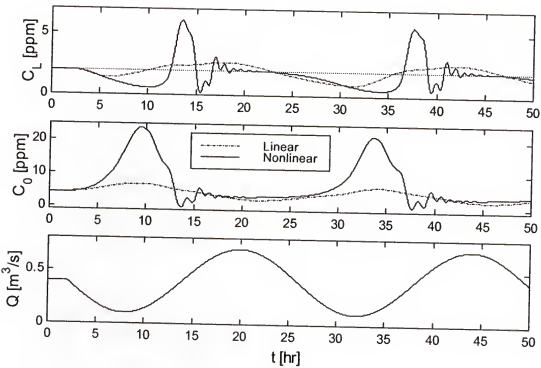

Figure 2-17. Closed-Loop response of linear and nonlinear models with a pair of controllers and an adaptive Smith Predictor arranged in cascade configuration subject to varying flow.

although there is some improvement, a different yet controller form is necessary to achieve satisfactory performance.

2.5 Novel Process Modification—Dynamic Weir

None of the traditional control strategies are fully effective when the flowrate of influent varies throughout the range typically plaguing wastewater treatment plants. Because the delay is so large, compensation is necessary, yet variations in the delay cause a Smith Predictor to fail. Primarily, this is because there are, in fact, two variables that must be controlled to guarantee consistent performance, not one. The first, of course, is the chlorine concentration itself, and the second is the residence time of the fluid in the reactor. Because the fluid is experiencing ongoing chemical reaction for as long as it is

retained in the reactor, it is necessary to control how long it remains in the reactor in order to guarantee concentration control.

Controlling the residence time of the fluid is achieved by controlling the bulk velocity of the fluid while in the reactor (assuming the length of the reactor does not change). Recall that the velocity is defined as $v(t) = Q(t) / A$ (in Section 2.2.3). In other words, the coefficient of $\frac{\partial C}{\partial z}$ in (2-28) is time-varying, making it extremely difficult to predict the value C(t,L) for random v(t) profiles. However, if it is possible to manipulate A over time such that $v(t) \cong$ constant, significantly better control of chlorine concentration may be achieved. Physically, adjusting the width of the contact basin is not likely to be feasible; the height, however, could be easily set with the implementation of a movable weir located at the end of the reactor. A reactor with such a modification is shown in Figure 2-18

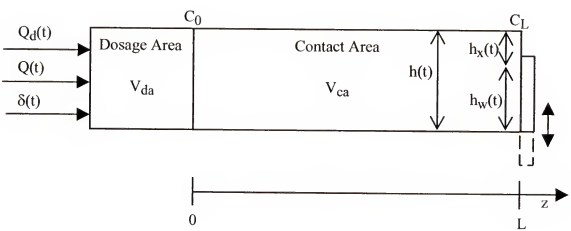

Figure 2-18. Wastewater chlorination reactor modified with a dynamic weir.

where h(t) is the height of the fluid in the reactor, $h_x(t)$ is the excess height of fluid above the weir, or weir head, $h_w(t)$ is the height of the weir, and all other variables are the same as given previously.

It is assumed that the height of fluid in the reactor is the same along the entire length of the reactor, and that it responds uniformly with respect to z for changes in either incoming flowrate or weir height. The assumption is based upon two principles. The first is the Manning equation (Sturm, 2001), which calculates the slope that is needed to supply the driving force required for a given flow

$$S = \frac{n^2 v^2}{R^{4/3}} \tag{2-57}$$

where S is the slope of the channel (dimensionless), n is a roughness factor specific to the channel (dimensionless), v is the velocity of the water in the channel in meters per second (m/s), and R is the hydraulic radius in meters (m). Not shown is a conversion factor of 1 with the dimensions necessary to make the equality true. Under any realistic conditions, flow of such low velocity will only cause a height gradient of a fraction of a centimeter per meter of channel length. In other words, at steady-state, h is essentially not a function of z.

The second reason that h is assumed not to be a function of z is the velocity of propagation of small disturbances (Lencastre, 1987)

$$u = \sqrt{gh} \tag{2-58}$$

where u is the *wave* velocity in meters per second (m/s), g is the gravitational constant in meters per second squared (m/s^2) and h is the depth of the fluid in meters (m). Also

given as a form of the Froude number, the ratio of this wave velocity u to bulk velocity v shows that perturbations in the system pass through the reactor much faster than the fluid. In other words, transients attenuate quickly, and the system can be assumed to be of uniform height with respect to location in the reactor.

2.5.1 Dynamic Weir Controller Design

2.5.1.1 Embodiment one—a model-based ratio controller

As implied by the relationship $v(t) = Q(t) / A(t)$, manipulation of height is simply a form of ratio control. Because the incoming flowrate is already being measured, the information is readily available. It is next necessary to consider the flowrate of fluid over the weir at the exit of the reactor. There are many different flow correlations to choose from, and each contains parameters specific to each plant. In practice, significant investigation may be required to determine the precise flow correlation for a given plant. The correlation used here is the modified Francis weir formula (Geankoplis, 1993) for the case of no suppressions (*i.e.* both ends of weir are flush with the side of the reactor)

$$Q_w = 0.415 w\, h_x^{1.5} \sqrt{2g} \tag{2-59}$$

where Q_w is the flow over the weir in cubic meters per second (m^3/s), g is the gravitational constant in meters per second squared (m/s^2), h_x is the weir head in meters (m), and w is the width of the basin (m). The result is an additional state for the system

$$\frac{dV}{dt} = Q(t) - Q_w \tag{2-60}$$

which upon substitution becomes

$$\frac{dh}{dt} = \frac{1}{Lw}(Q(t) - 0.415(w - h_x(t))\, h_x(t)^{1.5}\sqrt{2g}) \qquad (2\text{-}61)$$

In addition, we must recognize that

$$h_x(t) = h(t) - h_w(t) \qquad (2\text{-}62)$$

Substituting

$$\frac{dh}{dt} = \frac{1}{Lw}(Q(t) - 0.415(w - h(t) + h_w(t))\, (h(t) - h_w(t))^{1.5}\sqrt{2g}) \qquad (2\text{-}63)$$

where Q(t) is a measured disturbance and $h_w(t)$ is the input. By modeling the height as a state, it is now possible to determine if transient periods where $Q \neq Q_w$ affect the behavior of the reactor significantly.

The final obstacle to implementing a ratio control is knowledge of how to set the height of the weir $h_w(t)$ based upon the incoming flowrate Q(t) to yield the proper fluid volume. This is done by subtracting a term that represents the height of the head for that flowrate from the total height desired.

$$h_w = h - h_x(Q) \qquad (2\text{-}64)$$

The relationship $Q(h_x)$ is given in (2-59); however, the controller requires $h_x(Q)$. Although (2-59) is explicitly invertible (once the value of w is known), many flow correlation equations are not. If necessary, the inverse may be approximated with a polynomial fit; for example, if the Kanapaha facility is approximated to have a width of 8 m and flowrate in the range 0.1 $m^3/s < Q(t) < 0.7$ m^3/s, the weir head is well-described in terms of flowrate by the equation

$$h_x(Q) = -0.0762Q(t)^2 + 0.2188Q(t) + .0156 \qquad (2\text{-}65)$$

The total height desired must also be calculated. It is based upon the desired residence time, τ^{o}_{res}, which set by the operator (*i.e.* it is the setpoint of the ratio controller). It is related to the flowrate and the volume by

$$\tau^{o}_{res} = \frac{V(t)}{Q(t)} \tag{2-66}$$

where V(t) is the dynamic volume. Equivalently,

$$\tau^{o}_{res} = Lw\frac{h(t)}{Q(t)} \tag{2-67}$$

Rearranging and substituting into (2-64) yields

$$h_w(t) = \frac{Q(t)\tau^{o}_{res}}{Lw} - h_x(Q) \tag{2-68}$$

where $h_w(t)$ is the output of the ratio controller in meters (m), τ^{o}_{res} is the setpoint of the ratio controller in seconds (s), and $h_x(Q)$ is the estimated weir head. It is now clear that this second ratio controller is in fact a residence time controller, and therefore designated

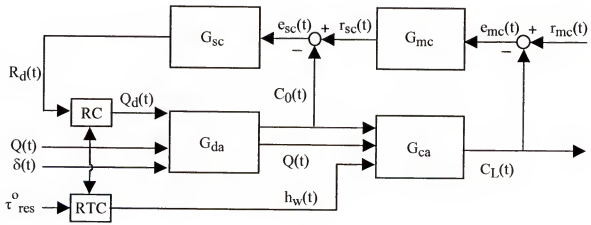

Figure 2-19. Block diagram of a wastewater treatment plant with a dynamic weir and model-based ratio controller under cascade chlorine concentration control.

RTC (recall that the input concentration is also implemented through ratio control). It is incorporated into the control scheme as shown in Figure 2-19. It is otherwise identical to the previous cascade control scheme. The RTC also uses flowrate Q(t) as an input, and calculates the desired height of the weir $h_w(t)$ for that operating condition. This signal is the passed to end of the contact basin, where it is implemented. Finally, as in the case of the concentration input ratio controller, changes in the weir position are assumed to be fully realized far faster than the time scale of the system; this eliminates the need to model weir movement dynamics. Note, however, that the total height of the fluid is now a state of the model, and may or may not change slowly enough to affect concentration.

The primary advantage of this embodiment is the necessity of only one measurement, Q(t). Coincidently, that measurement is frequently already available, producing no additional burden on the operator. It does, however, rely upon a model of the flow over a weir. Since the physical dimensions of each wastewater treatment plant are unique, the flow correlation must be identified on a case-by-case basis. Exhaustive experimentation may be required to define it. In addition, if the model is not accurate, degradation of controller performance may be may be observed.

2.5.1.2 Embodiment two—a feedback PI controller

A standard PI controller can also be utilized to achieve residence time control. In digital position form, it is given as

$$h_w^o(t) = h_w^{bias} + K_c[e(t) + \frac{T}{\tau_I}\sum_{k=0}^{t/T} e(t - kT)] \qquad (2\text{-}69)$$

where Kc is the proportional constant of the controller, τ_I is the integral time constant of the controller, h_w^{bias} is the reference position of the weir, and T is the sampling period. Furthermore, the feedback error e(t) is calculated as follows

$$e(t) = \tau^{o}_{res}(t) - LW\frac{h(t)}{Q(t)} \tag{2-70}$$

where e(t) is interpreted as the difference between the set-point τ^{o}_{res} and the estimated residence time τ_{res} given as the last term in (2-70). Again it clear that controller is

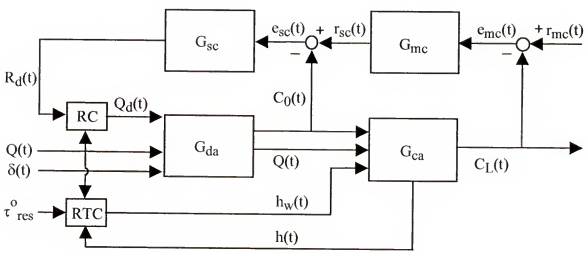

Figure 2-20. Block diagram of a wastewater treatment plant with a dynamic weir and Feedback PI controller under cascade chlorine concentration control.

charged with residence time control, and this embodiment is also referred to as a RTC. It is incorporated into the control scheme as shown in Figure 2-20, which is identical to Figure 2-19 except for the addition of a fluid height measurement.

In this formulation, the RTC again uses flowrate Q(t) as an input, and additionally uses fluid height h(t) as a second input. With these two pieces of information, it calculates the current residence time for fluid in the reactor. The PI controller tries to then eliminate any discrepancy between this value and the setpoint by sending a signal to adjust the height of the weir. As in the case of the model-based ratio controller, changes in the weir position are assumed to be fully realized far faster than the time scale of the system; this eliminates the need to model weir movement dynamics. Finally, the total

height of the fluid is again now a state of the model, and may or may not change slowly enough to affect concentration.

The primary advantage of this embodiment is that no flow correlation is needed; in contrast, recall that the model-based ratio controller (*i.e.* Embodiment 1) requires one. However, in addition to a measurement of Q(t), it needs a measured or estimated value of h(t)—something not needed by the ratio controller. Furthermore, the additional PI controller will require tuning. Again, since the physical dimensions of each wastewater treatment plant are unique, exhaustive experimentation may be required to achieve the proper parameters.

Finally, for either embodiment, it must be decided what the bounds of weir height are. The upper bound is modeled simply as the present height of the fixed weir. This is because it can be assumed that plants are sized according to their maximum expected capacity. For that maximum value, they must be large enough to retain the fluid some minimum amount of time. Therefore, it is never expected that the flow will go higher, causing the prescribed weir height to exceed the present value. A very different consideration governs the choice for minimum weir height. It is limited either by physical on-site constraints, or by a limit of how shallow a channel of water may become before uniform flow assumptions break down. It has been suggested in literature that a realistic lower bound is 1 ft, so 0.3 m is chosen for the purposes of simulation.

2.5.2 Closed-Loop Response of the Entire Model for Step Changes in Flowrate Using a Dynamic Weir

By reusing the tuning parameters given for a cascade chlorine concentration control system with standard PI controllers (Table 2-8), any improvement gained by implementing a dynamic weir can be observed. In the case of the model-based ratio

controller, this constitutes all necessary controller parameters. However, for the PI feedback system, the RTC itself is an additional PI controller, and requires tuning; trial-and-error tuning methods show that $K_w = 0.01\ m/s$ and $\tau_w = 1000s$ are effective choices for these parameters for this plant. Figure 2-21 records the response of the system equipped with a model-based ratio weir controller when subjected to the same series of step changes described in the previous section: a small early step-increase in disturbance Q(t) at time 2 hr, then a large step-decrease in disturbance at time 12 hr, and finally another step-increase at time 34 hr, returning to the original flowrate Q(t). The first plot shows the output concentration (solid line) and the setpoint (dotted line) as

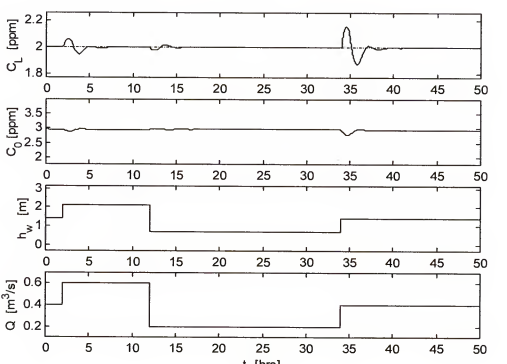

Figure 2-21. Closed-loop response of model with a pair of chlorine concentration controllers arranged in cascade configuration and a model-based ratio-controlled dynamic weir, subjected to a step changes in flowrate.

functions of time. A value of 2 ppm is again chosen for the setpoint, with 1 ppm being the minimum allowable threshold. The second plot shows the chlorine concentration entering the contact area $C_0(t)$ for each of the two models over time. The third plot is new, and gives the height of the weir as a function of time. Finally, the disturbance Q(t) is shown in the fourth plot as a function of time. In addition, the setpoint of the RTC is chosen as $\tau_{res}^{o} = 3600$ s.

Figure 2-22 is the identical simulation performed for the case when the RTC is a PI feedback controller. In other words, a value of 2 ppm is chosen for the setpoint, with 1 ppm being the minimum allowed value. Also, the setpoint of the RTC is $\tau_{res}^{o} = 3600$ s. Finally, each of the plots in Figure 2-22 represents the same value it did as explained for Figure 2-21.

The responses of the two types of RTCs are almost identical. Furthermore, it is clear that the dynamic weir arrangement yields an excellent chlorine concentration control response for the conditions described. They do an excellent job returning the system to setpoint, only deviating approximately 0.2 ppm in the most extreme case. Furthermore, they achieve the disturbance rejection at most in about three hours, much faster than the case with a fixed weir height. This behavior confirms that the dynamics of the system are fast enough to ensure that gravity flow should be sufficient to deliver the system to the desired height in a reasonable amount of time.

Interestingly, the most problematic step change is now a large step-up, in contrast to the fixed-weir case, where a dramatic step-down causes severe control problems. This cause of this phenomenon is the uncontrolled nature of the inlet flowrate. When flowrate surges from a low-flow to a high-flow condition, and the weir attempts to quickly create a

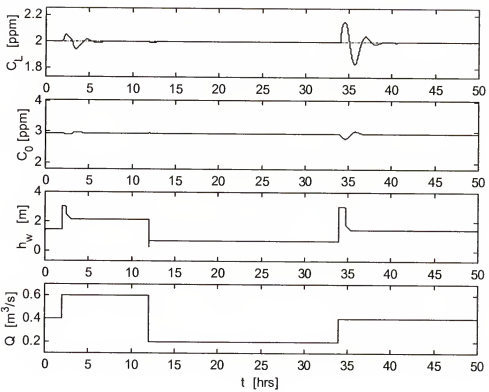

Figure 2-22. Closed-loop response of model with a pair of chlorine concentration controllers arranged in cascade configuration and a PI feedback-controlled dynamic weir, subjected to a step changes in flowrate.

greater volume of fluid in the reactor, the rate at which it can be accomplished is fully dependent upon how quickly the new flowrate can supply the needed amount of fluid. This fill-time can be approximated using the formula

$$t_{fill} \cong \frac{Lw(h_f - h_i)}{Q_f} \tag{2-71}$$

where h_f and h_i are the final and initial heights, respectively, and Q_f is the final flowrate. The maximum fill-time is specific each plant, depending upon the values of the parameters given in (2-71). As an example, for the plant detailed throughout this study, which is described by $L = 120$ m, $w = 8$ m, $h_f = 2.62$ m, $h_i = 0.37$ m, and

$Q_f = 0.7\ m^3/s$, it is calculated that $t_{fill} = 51$ minutes. While this is a highly undesirable situation, it should be noted that such a surge in flowrate is equally undesirable in a plant with a fixed weir, and even when added to the described residence time (60 minutes), the resulting fluid is retained for less time than is frequently observed in plants with a fixed weir.

2.5.3 Closed-Loop Response of the Entire Model for Varying Flowrate Using a Dynamic Weir

Figure 2-23 shows the performance of the standard cascade control system (the tuning parameters remain unchanged) supplemented with a feedforward RTC and a

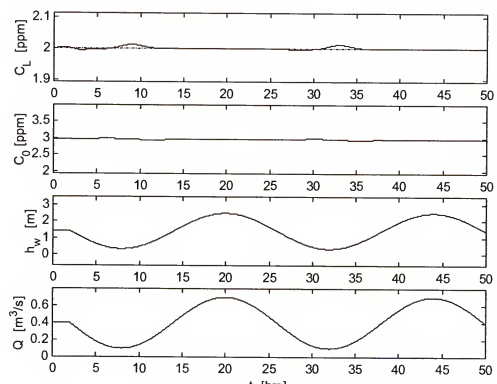

Figure 2-23. Closed-loop response of the plant with a pair of chlorine concentration controllers arranged in cascade configuration and a model-based ratio-controlled dynamic weir, subjected to varying flow.

dynamic weir when the flowrate is modeled as the previously described sinusoidal wave. As in previous sections, the sine wave begins at time 2 hr, has a period of 24 hr, and has an amplitude that is three-fourths of the nominal flowrate (0.4 m^3/s), or 0.3 m^3/s. The result is again a disturbance Q(t) that varies from 0.1 m^3/s to 0.7 m^3/s. As in the previous section, the setpoint of the second ratio controller is chosen as $\tau_{res}^{o} = 3600$ s.

Similarly to Section 2.5.2, Figure 2-24 is exactly the same simulation performed to generate Figure 2-23, except that the RTC is instead a PI feedback controller with tuning parameters $K_w = 0.01$ m/s and $\tau_w = 1000$s.

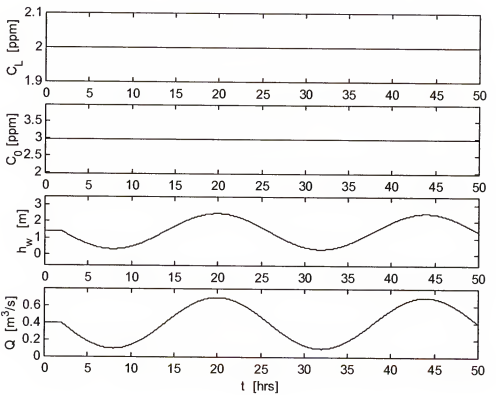

Figure 2-24. Closed-loop response of the plant with a pair of chlorine concentration controllers arranged in cascade configuration and a PI feedback-controlled dynamic weir, subjected to varying flow.

Again, it is clear that the performance of the two different RTC embodiments is practically identical. In comparing this result to other control strategies described, it is clear that the value of C_L is controlled much more tightly, falling in the approximate range $1.99\ ppm < C_L(t) < 2.01\ ppm$. This is in contrast $0.5\ ppm < C_L(t) < 6.0\ ppm$ in the simulation of a weir with fixed height shown in Figure 2-13. This means that a dynamic weir can virtually eliminate the effect that flowrate fluctuations have on the outlet chlorine concentration.

It is important to note that perfect control cannot be expected. Only the most dramatic disturbance (variable flow and its effect upon residence time) has been modeled; in practice, the system suffers from other, less severe disturbances. The simulation study serves to show that, even while ignoring lesser disturbances, a traditional control strategy is inadequate to control a system with a fixed weir. The dynamic weir solves problem of the most severe disturbance (variable flow, and therefore, residence time), leaving only less severe disturbance-related problems to be addressed.

2.5.4 Robustness Analysis for the Model-Based Residence Time Controller

It should be noted that no weir correlation is exactly accurate. Similar to measurement error, when the actual flow over the weir differs from that which is predicted by the correlation, performance may be degraded. In order to quantify how far the calculated control variable (*i.e.* the residence time) can be from its true value, consider error possible in the model of flow over a weir as a function of weir head $h_x(t)$. Rearranging (2-62) and substituting into (2-67)

$$\tau_{res}^{o} = Lw\frac{h_w(t) + h_x(t)}{Q(t)} \tag{2-72}$$

If the weir correlation being used (2-59) can be inverted directly, the error can be cast as a multiplicative factor of the correlation

$$Q_w^{'} = 0.415w\, h_x^{'1.5}\sqrt{2g}(1+\varepsilon) \tag{2-73}$$

where $Q_w^{'}$ is the actual, or true, flowrate and 100ε is the percent error in weir-flow rate. Rearranging this equation to yield h_x in terms of $Q_w^{'}$, the relationship is

$$h_x^{'} = \left(\frac{Q_w^{'}}{0.415w\sqrt{2g}}\right)^{\frac{2}{3}}(1+\varepsilon)^{-\frac{2}{3}} \tag{2-74}$$

Equivalently, $h_x^{'}$ can be represented in terms of h_x and ε

$$h_x^{'} = h_x(1+\varepsilon)^{-\frac{2}{3}} \tag{2-75}$$

Substituting (2-75) into (2-72) to find the true residence time yields the equation used for control design at steady-state

$$\tau_{res}^{'}(\varepsilon) = \frac{Lw}{Q(t)}\left(h_w(t) + h_x(t)(1+\varepsilon)^{-\frac{2}{3}}\right) \tag{2-76}$$

Next, solve (2-72) for $h_w(t)$ in the case where $\tau_{res}(\varepsilon = 0)$ (i.e., $\tau_{res} = \tau_{res}^0$)

$$h_w(t) = \frac{\tau_{res}Q(t)}{Lw} - h_x(t) \tag{2-77}$$

and substituting into (2-76), after rearrangement, yields $\tau_{res}(\varepsilon)$ in terms of additive perturbations in τ_{res}^0

$$\tau_{res}(\varepsilon) = \tau_{res}^0 + \frac{Lwh_x(t)}{Q(t)}\left((1+\varepsilon)^{-\frac{2}{3}} - 1\right) \tag{2-78}$$

which can also be expressed in terms of percent error from the target value

$$\Delta\tau_{res}(\varepsilon) = \frac{Lwh_x(t)}{\tau_{res}^0 Q(t)}\left((1+\varepsilon)^{-\frac{2}{3}} - 1\right) \tag{2-79}$$

where

$$\Delta\tau_{res}(\varepsilon) := (\tau_{res}(\varepsilon) - \tau_{res}^0)/\tau_{res}^0. \tag{2-80}$$

Finally, substituting (2-67) into (2-79) and canceling terms yields the expression

$$\Delta\tau_{res}(\varepsilon) = \frac{h_x(t)}{h(t)}\left((1+\varepsilon)^{-\frac{2}{3}} - 1\right) \tag{2-81}$$

Although typical weir correlations are accurate to within a few percent, the robustness of this control design can be shown by plotting wide range of errors. Figure

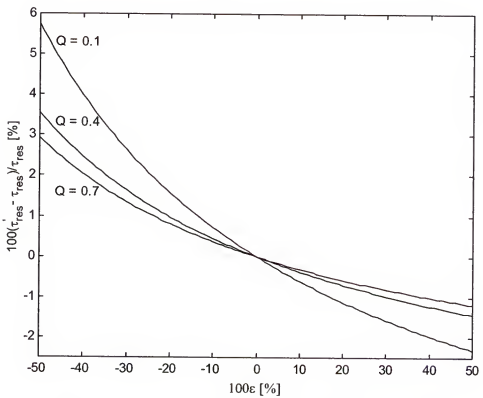

Figure 2-25. Plot of observed per cent error in τ_{res} for various values of weir correlation error ε.

2-25 illustrates the results for low, middle, and high-flow conditions. In other words, the flowrate Q(t) is fixed at three separate points, and a curve is generated for each by varying the value of ε. Each calculation assumes that L = 120 m, w = 8 m, and $\tau_{res}^{o} = 3600s$. In addition, the weir height $h_w(t)$ is set at the appropriate height (but not reported) for each of the three flowrates.

It is clear that the controller is extremely robust, given that it can easily tolerate errors in the weir correlation of up to 50% while yields errors in residence time of < 6%. The reason is that in general, $h(t) >> h_x(t)$, so errors in $h_x(t)$ simply do not have an extremely significant effect. The trend is evident in (2-81). This, however, underscores the importance of having an accurate value of $h_w(t)$; therefore, it is critical to monitor whether effects such as hysteresis cause significant error in weir position. If the are any problems, however, the problem is easily remedied by making the RTC control signal the setpoint to a slave PI controller designed to guarantee that the weir is in exactly the position prescribed by the RTC. Finally, while the robustness analysis would be more complicated if the correlation is not invertible, it can be assumed from the insensitivity of the system to correlation errors that the result would not be significantly different.

2.5.5 Propagation of Error Analysis for the PI Feedback-Controlled System

Errors in the measurement of key variables can cause degradation of controller performance. In the model-based embodiment of the controller, the analysis is relatively simply. The true value of the only measurement, Q(t), can be characterized to fall within certain bounds above or below the observed value. These high and low values directly limit the range of possible true residence time for a given moment in time, since all other variables are assumed to be known exactly.

In contrast, the PI feedback controller requires two measurements, and each contributes to the overall error separately. In addition, if the two variables are not independent, then a convoluted interaction can contribute as well. The possible range of error is therefore significantly more complicated than in the single variable case. One way of quantifying it is through a propagation of variance analysis, which is given by the equation

$$\sigma_\tau = \sqrt{\left(\frac{\partial G}{\partial Q}\right)^2_{\bar{Q},\bar{h}} \sigma_Q^2 + \left(\frac{\partial G}{\partial h}\right)^2_{\bar{Q},\bar{h}} \sigma_h^2 + \left(\frac{\partial G}{\partial Q}\right)_{\bar{Q},\bar{h}} \left(\frac{\partial G}{\partial h}\right)_{\bar{Q},\bar{h}} \sigma_{Qh}^2} \qquad (2\text{-}82)$$

where σ_τ is the variance of residence time, σ_Q is the variance of the flowrate measurement, σ_h is the variance of the height measurement, σ_{Qh} is the covariance between the measurements of Q and h, $\bar{Q}$ and $\bar{h}$ are operating point values, and G is a function that describes the relationship between the variables. Determining the values of σ_Q and σ_h are straightforward, and achieved by considering the specifications given for the appropriate measurement device.

For a representative magnetic flow meter of appropriate capacity, the specification is given as ($\pm$ 0.5 % of flowrate). Consequently, the error observed for a measurement with this device is a function of operating point (*i.e.* the value of Q). Assuming that the observed values from the flow meter fall within three standard deviations of the true value

$$3\sigma_Q^2 = 0.005\bar{Q} \qquad (2\text{-}83)$$

which can easily be substituted into (2-82) for different values of $\bar{Q}$.

In examining the variance of the height measurement σ_h, it is found that error of a representative piece of hardware for the appropriate height range is given as ($\pm$ 0.1 % of span). In contrast to the flow criterion, this value does not change for different operating conditions, since it is assumed that the height measurement device will be subject to constant maximum and minimum values, regardless of the present value of the variable. Therefore, in the case of the described plant, with the aforementioned maximum and minimum height values of 0.3 and 3.0 m, respectively, and the same standard deviation assumption given for the flow meter, it found that

$$3\sigma_h^2 = 0.0027\text{m} \tag{2-84}$$

which can also be subsequently substituted into (2-82).

The identification of the value of σ_{Qh} is generally more difficult that either σ_Q or σ_h. It is necessary to investigate how one affects the other. In the case of the wastewater treatment plant, the value of Q directly affects the value of h, and their covariance σ_{Qh} can be estimated by generating Q and h signals of appropriate variance (as defined by (2-83) and (2-84)) and sufficient length (vectors of 1000 points were

Table 2-11. Summary of the square of the covariance for low, middle, and high-flow operating points.

$\overline{Q}$ (m^3/s)	σ_{Qh}^2
0.1	4.719E-9
0.4	2.132E-8
0.7	3.927E-8

generated in Matlab for this exercise) and calculating the resulting covariance. When performed for the previously described low, middle, and high-flow conditions (0.1, 0.4, and 0.7 m^3/s), the observed standard deviations are as given in Table 2-11.

Finally, the function G must be defined. It is simply the relationship between the variables, which is in reality a slightly more general form than is already given by (2-67)

$$\tau_{res} = Lw\frac{h(t)}{Q(t)} \tag{2-85}$$

Partial derivatives of (2-85) produce the remaining terms in (2-82), with the appropriate

Table 2-12. Summary of the range of error in τ_{res} for low, middle, and high-flow operating points.

$\overline{Q}$ (m^3/s)	$\overline{h}$ (m)	Error in τ_{res}
0.1	0.337	± 31 s
0.4	1.409	± 19 s
0.7	2.492	± 18 s

values of $\overline{Q}$ and $\overline{h}$ used for each operating condition, as given in Table 2-12. Finally, the previously given values of $L = 120$ m and $w = 8$ m are also used. Considering that the setpoint for these simulations is 3600 s, it is clear that the measurement error tends introduce a deviation of less than a percent.

2.5.6 Additional Benefits of the Dynamic Weir Design

There are benefits in addition to the highly improved performance associated with using a dynamic weir to control residual chlorine concentration. Primarily, it is much easier to guarantee sufficient levels of microbe disactivation, thereby virtually eliminating the risk of exposing humans to numerous varieties of bacteria, viruses and

protozoa, including *Salmonella, Shigella* and *Vibrio cholera.* Furthermore, with chlorine levels no longer reaching the 5 to 10 ppm level, or higher, the risk of THM formation is greatly reduced as well.

Equally attractive to the wastewater treatment industry is the potential of the dynamic weir to significantly reduce operating costs. Some of the reduction can be realized indirectly; for instance, the need for equalization basins (Foess *et al.,* 1976; Ongerth, 1979), which are designed to attenuate the highly varied flow into the chlorination basin, is gone. In addition, it should be much easier to avoid fines for non-compliance. Furthermore, if sophisticated, expensive advanced control techniques are used to control a particular plant, they can be abandoned in favor of the dynamic weir with its easily programmed residence time controller.

However, the most notable economic benefit is that less chlorine is required to achieve the same level of safety. (Of course, the dynamic weir can be used with any chemical treatment; chlorine is simply used throughout this study for both simplicity and consistency.) For example, assuming a constant ammonia chlorine demand of 3 ppm, the four basin designs covered previously require a daily supply of chlorine as given in Table 2-13. Each simulation was again run for 50 hours, with the sinusoidal flow beginning at t = 2 hrs, and a day-long period with flow ranging between 0.1 and 0.7 m^3/s. This corresponds approximately to an 8 mega-gallon per day (MGD) average plant that is subjected to fluctuations from to 2 to 14 MGD, respectively. Total chlorine use for a single day is calculated simply by integrating the dosing flowrate for the second 24 hr flow cycle; as before, this is done to eliminate any transient effects caused by beginning

the simulation at steady-state with respect to flowrate. Finally, it is assumed that the cost of chlorine gas is $320.00 per US ton.

Table 2-13. Comparison of the daily chlorine usage cost for each of the plant configurations studied.

Weir Type	fixed	fixed	fixed	dynamic
Master Controller Type	PI	PI w/ Smith Predictor	PI w/ Adaptive SP	PI
Daily Cost ($)	**100**	**98**	**93**	**73**

The observed chlorine usage reduction is therefore approximately 25%. The percentage savings can vary, though, if the actual ammonia chlorine demand deviates from 3 ppm. However, the absolute savings remain the same. For a plant of the given size, the dynamic weir system will save the treatment plant approximately $10,000 per year over the most common type of system utilizing a fixed weir (*i.e.* one that uses a PI master controller). Furthermore, with much more effective control possible, the setpoint (*i.e.* presently 2 ppm) may be moved closer to the allowable threshold (*i.e.* 1 ppm in this case), thereby saving even more in chlorine costs (perhaps an additional $5000 yearly) without the risk of failure to comply with regulations. This savings is realizable primarily because, even when flow is equalized in a fixed-volume reactor, the reactor is still not being operated optimally in the sense that the residence time of wastewater within the reactor is greater than it needs to be, requiring more chlorine for disinfection.

Finally, reduced chlorine use alone provides safety benefits. With the demand for chlorine reduced, it is necessary to store less on-site, which in turn would likely reduce the scale of the problem should an accident occur.

2.6 Conclusions

The effect of ammonia nitrogen demand dictates that failure to utilize cascade control will most likely result in degraded outlet chlorine concentration performance. Hence, a cascade controller is needed; however, for dosage adjustment, a cascade control strategy alone does not guarantee acceptable performance, primarily because it does not address the effect that varying flowrate has on residence time. The implementation of a residence time controller (RTC) supplementary to existing dosage control techniques can bring about excellent performance.

Because the RTC scheme reduces the observed variation in residence time from several-fold to just a few percent, the pre-existing control structure becomes much more effective in delivering acceptable outlet chlorine concentration control. A fundamental explanation for this trend is that a disturbance in the form of varying flowrate has two distinct and independent effects on the system. The first is the interruption of constant input concentration, an undesirable effect that is commonly rejected using a ratio controller. However, the flowrate fluctuations also cause a second effect—varying residence time, for which the concentration ratio controller is ineffective. The feedforward RTC can be interpreted as a novel form of a ratio control, with the task of maintaining approximately constant the ratio of fluid height in the reactor to flowrate (2-67), resulting in an approximately constant residence time of fluid in the reactor. Thus, although there are two primary disturbances, namely $Q(t)$ and $\delta(t)$, they induce three effects on the system (*i.e.,* (i) input concentration interruption, (ii) variable residence time, and (iii) a load on the system that consumes chlorine in the dosage area); therefore,

three controllers (ratio, RTC, and slave controllers) are required to adequately reject all effects of the disturbances.

Both the feedforward and feedback configurations of the RTC perform adequately when the measured data is not filtered. It is anticipated, however, that performance can be improved by employing a digital filter. In fact, a first-order exponential filter (Ogunnaike and Ray, 1994) with filter parameter $\lambda = 0.01$ should yield satisfactory performance. Despite the low value of the parameter, data can be taken several times per second; high-frequency data acquisition assures that no significant additional delay is introduced by the filter, since the residence time requirement is likely to be thirty minutes or more.

There are two alternative ways to implement the RTC scheme: namely, a feedforward model-based; and a feedback non-model-based configuration. Trade-off exists between them, and plant-specific considerations should be used to determine the best control configuration. For example, the feedforward algorithm requires an inverted model of flow over a weir. In contrast, the feedback algorithm does not require a model, but does require a fluid height measurement as well as controller tuning. The ability of the engineer to acquire the requisite information ultimately determines the appropriate choice.

Both the feedforward and feedback RTC schemes are capable of yielding excellent control, provided that the weir is placed in the proper position. It is possible that the weir will not always move to the position prescribed by an RTC; however, the problem is easily remedied by making the RTC control signal become the setpoint to a slave PI controller designed to guarantee that the weir is in exactly the position prescribed

by the RTC. Furthermore, the feedforward RTC is an extremely robust controller with respect to weir-flow modeling error, making weir head estimation much less critical than weir position in terms of guaranteeing good performance. Finally, while the robustness analysis would be more complicated if the correlation for flow over a weir is not explicitly invertible, it can be expected from the insensitivity of the system to correlation errors that the result would not be significantly different.

The most notable economic benefit is that, under the conditions of the simulation, the RTC scheme has the potential to realize an average 25-30% annual reduction in the amount of chlorine used while facilitating better control. This is possible because presently, virtually all wastewater passing through the disinfection tank remains far longer than required by the regulations; consequently, the water must be dosed with more chlorine than would otherwise be necessary. For example, assuming an average ammonia nitrogen chlorine demand $\delta(t)$ of 3 ppm, the fixed-weir cascade design with a PI master controller and moving weir with a feedforward RTC control design are compared, and found to require an annual supply of chlorine of 115 and 83 US tons , respectively (*i.e.,* a difference of 32 US tons). To determine yearly usage, simulation of each control shceme is again run for 50 hours, with the sinusoidal flow beginning at $t = 2$ hrs, and a day-long period with flow ranging between 0.1 and 0.7 m^3/s. This corresponds approximately to an 8 mega-gallon per day (MGD) average plant that is subjected to fluctuations from to 2 to 14 MGD. Total daily chlorine use is calculated by integrating the dosing flowrate for the second 24 hr flow cycle; this is done to eliminate any initial transient effects. The daily consumption is then extrapolated to a yearly usage.

The extent of percentage chlorine savings can vary, however, if the average ammonia chlorine demand deviates from 3 ppm. Nonetheless, the absolute savings remain the same. In other words, the amount of chlorine presently required to react with the ammonia nitrogen in the dosage area must remain the same under all control schemes; however, the required amount of chlorine remaining available in the system for disinfection reactions in the contact area is significantly reduced. For a plant of the given size, the dynamic weir system can save the treatment plant approximately 32 US tons per year over the fixed-weir design. Furthermore, with much more effective control possible, the setpoint (*i.e.,* presently 2 ppm) may be moved closer to the allowable threshold (*i.e.,* 1 ppm in this case), thereby saving even more in chlorine costs without the risk of failure to comply with regulations. Finally, while the setpoint of the RTC is 3600 s throughout this study, regulations are usually closer to 1800 s, providing for the potential to save even more chlorine. For example, additional simulations show that the yearly average chlorine usage for a plant this size with a new outlet concentration setpoint of 1.2 ppm and a residence time setpoint of 1800 s would be further reduced to approximately 63 US tons. The yearly total chlorine savings for an 8 MGD plant then becomes approximately 52 US tons, which represents a savings ceiling of up to 45%.

CHAPTER 3
STABILITY OF PI-CONTROLLED RUN-TO-RUN STATIC SYSTEMS WITH SIGNIFICANT DELAY

3.1 Introduction

There are numerous industrial processes that may be automated using run-to-run control schemes. Such processes are inherently discrete, and consequently, they are very similar to batch systems, with the subtle, yet important, distinction that information about each batch is only measurable after the batch is completed. The semiconductor industry is rich with examples of run-to-run control applications, such as plasma etching (Card el al., 1998) and polishing (Boning *et al.*, 1996; Moyne *et al.*, 2001). Additional examples include the serial pressing, sputtering, and coating operations in compact disc production (Gillet *el al.,* 2001) and the roasting, cooling, and screening stages that are necessary for peanut and hazelnut processing (Nagaraju *el al.,* 1997; Ozdemir and Devres, 2000; Ozdemir and Devres, 2000).

In addition, many unit operations that are automated with run-to-run control are contained within of a series of production stages. Therefore, a significant characteristic of the run-to-run control schemes considered here is that properties created in an early stage cannot be measured immediately after that stage; rather, they must complete a series of steps before data can be gathered (Kosut *et al.,* 1998). When coupled with large throughputs, a large measurement delay may result. Additionally, the assumption is made in this study that dynamic effects from one batch to the next are negligible. In reality, some limited dynamic effects may linger from one run to the next, such as latent

heat in a reactor that is repeatedly heated and cooled. These effects, however, are ignored here, resulting in a process that is static but that suffers from measurement delay. More specifically, the plant open-loop model is given as

$$y_M(k) = K_P u(k - D) \tag{3-1}$$

where K_P is gain of the plant, D is the measurement delay, k is an indexing notation used to number batches sequentially, $y_M(\cdot)$ is the measured output, and $u(\cdot)$ is the input.

The goal of this study is to provide a comprehensive theoretical description for the single-input, single output (SISO) case of a static run-to-run plant with significant delay. In Section 3.2, a suitable proportional-integral (PI) controller form is derived, and compared with a standard discrete PI controller. Various strategies are outlined in Section 3.3 for characterizing the parameters of a plant. This knowledge is required for safe and effective tuning of the controller for closed-loop feedback control. The application of a Smith Predictor is investigated in Section 3.4 as a possible technique to counter the degrading effect of large delays on closed-loop performance. It is shown that even linear static run-to-run systems with significant delay are deceptive in their simplicity, as a Smith Predictor can lead to closed-loop instability for very small uncertainties in the plant. Finally, Section 3.5 provides conclusions and suggestions for the development of future work.

3.2 Derivation of a PI Run-to-Run Controller

The controller for a run-to-run system can consider only past data. This is due to the fact that a batch must be finished completely before the property of interest can be measured. In other words, the output y(k) is first available for use in calculating u(k+1). This is in marked contrast with the situation encountered in standard sample-and-hold

data systems, where it is assumed that the output y(k) is obtained via measurement at a sampling instant and utilized to calculate an appropriate control input u(k) at the same sampling instant. For the run-to-run system in question, one may employ a proportional-integral control law that calculates the input from knowledge of the measured error e(k) obtained from the processed batch k via the time-domain control law

$$u(k+1) = K_c\varepsilon(k) + K_cR_I[\varepsilon(0) + \varepsilon(1) + \ldots + \varepsilon(k)] \quad , \; R_I \geq 0 \tag{3-2}$$

where K_c is the proportion gain of the controller, and R_I is the reset rate of the controller. Taking the z-transform yields the relationship

$$u(k)z = K_c\varepsilon(k) + K_cR_I[z^{-k} + z^{-k+1} + \ldots + z^{-1} + z^0]\varepsilon(k) \tag{3-3}$$

Recognizing that $\sum_0^k z^{-i} = \frac{z}{z-1}$ and rearranging terms as needed gives

$$u(k) = K_c\frac{1}{z}\varepsilon(k) + K_cR_I\frac{1}{z-1}\varepsilon(k) \tag{3-4}$$

or

$$u(k) = K_c\left(\frac{1}{z} + R_I\frac{1}{z-1}\right)\varepsilon(k) \tag{3-5}$$

It should be noted that R_I must always be positive since a negative value for reset rate is physically meaningless. Equation (3-5) is similar to a standard discrete PI controller in position form

$$u(k) = K_c\left(1 + R_I\Delta t\frac{z}{z-1}\right)\varepsilon(k) \tag{3-6}$$

where Δt is the sampling period of the controller (Seborg *et al.,* 1989). A main difference, however, is that (3-5) has an extra unit delay on the right-hand side. The final subtle difference is that absolute time is no longer a reference; alternatively, the number

of batches marks in an indirect fashion the passage of time. The differences arise because a discrete controller can, in general, be applied to a continuous plant, which has both an input and an output at any instant in time, while a discrete plant only has an input and output value for each batch that is processed. Appendix C provides a brief review of how a discrete controller (Seborg *et al.,* 1989) uses the current error to implement the current input—a task that is impossible for the run-to-run controller to accomplish.

3.3 Plant Stability under Feedback Control

Figure 3-1 shows a block diagram of the closed-loop system considered

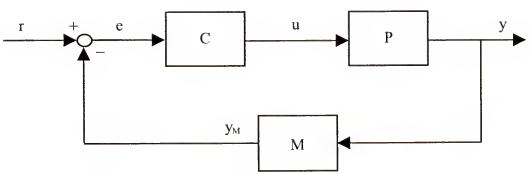

Figure 3-1. Generalized block diagram for a feedback loop with measurement delay.

where $C = K_c\left(\frac{1}{z} + R_I \frac{1}{z-1}\right)$ is the controller, $P = K_P$ is the plant gain, $M = z^{-D}$ is the measurement delay, y is the output, and y_m is the measured output. Basic block diagram algebra shows that

$$\frac{y}{r} = \frac{CP}{1 + CPM} \tag{3-7}$$

Upon substitution of C, P, and M, closed-loop stability depends upon the location of the uncancelled poles of the expression

$$\frac{y}{r} = \frac{K_C\left(\frac{1}{z} + R_1\frac{1}{z-1}\right)K_P}{1 + K_C\left(\frac{1}{z} + R_1\frac{1}{z-1}\right)K_P z^{-D}} \tag{3-8}$$

When rearranged algebraically, the denominator of (3-8) is given by the polynomial

$$P(z) = z^{D+2} - z^{D+1} + [K_C K_P(R_1 + 1)]z - K_C K_P \tag{3-9}$$

Appendix D shows that (3-8) never has unstable pole-zero cancellations when unstable poles are present, provided that: (i) $R_1 \geq 0$, and (ii) the additional constraints required by the Jury Array are met, as given in Section 3.3.1. Therefore, all roots of (3-9) that lie outside of the open unit disk on the complex plane are in fact unstable poles of (3-8).

Also, inspection of (3-9) reveals that there are only three lumped parameters that are relevant for closed-loop stability, given that K_C and K_P always appear as the product $K_C K_P$. Therefore, the locations of the roots of equation (3-9) dictate whether or not the system is stable for a given triplet of parameters ($K_C K_P$, R_1, D).

3.3.1 Nominal Stability Region

It is necessary and sufficient for the poles of (3-9) to lie within the unit circle to guarantee stability, based on the analysis provided in Appendix D. The Jury Test (Ogunnaike and Ray, 1994) provides criteria in two steps that establish necessity and sufficiency for the roots of a polynomial to lie within the unit circle. The first step of the Jury Test states that given the polynomial

$$P(z) = a_0 z^n + a_1 z^{n-1} + \ldots + a_{n-2} z^2 + a_{n-1} z^1 + a_n = 0 \tag{3-10}$$

where the leading term a_0 is positive, there are three necessary conditions for the roots of a polynomial to lie within the unit circle:

$$
\begin{aligned}
&1.\ |a_n| < a_0 \\
&2.\ P(1) = \sum_{i=0}^{n} a_i > 0 \\
&3.\ P(-1) = \sum_{i=0}^{n} (-1)^{n-i} a_i > 0, \text{ for n even, or} \\
&\qquad P(-1) = \sum_{i=0}^{n} (-1)^{n-i} a_i < 0 \text{ for n odd}
\end{aligned}
\qquad (3\text{-}11,12,13)
$$

Applying (3-11)-(3-13) to the system (3-9) under consideration yields

$$
\begin{aligned}
&1.\ |K_C K_P| < 1 \\
&2.\ P(1) = K_C K_P R_1 > 0 \\
&3.\ P(-1) = 2 - K_C K_P (R_1 + 2) > 0, \text{ for D even, or} \\
&\qquad P(-1) = -2 - K_C K_P (R_1 + 2) < 0 \text{ for D odd}
\end{aligned}
\qquad (3\text{-}14,15,16)
$$

The implications of this set of necessary conditions are immediate. First, from the knowledge that $R_1 > 0$, based on (3-15), it is necessary for both $K_C K_P > 0$ and $R_1 > 0$. Consequently, because of (3-14), it is necessary that $0 < K_C K_P < 1$. Both conclusions are reinforced by (3-16) for the case where D is even, since $R_1 > 0$ implies that $K_C K_P < 1$. Finally, given $R_1 \geq 0$, the case where D is odd implies that $K_C K_P > -1$, which is subset of the constraint just established that implied $0 < K_C K_P < 1$. In effect, (3-14) and (3-15) can be reduced to yield the constraints

$$
\begin{aligned}
&1.\ 0 < K_C K_P < 1 \\
&2.\ R_1 > 0 \\
&3.\ P(-1) = 2 - K_C K_P (R_1 + 2) > 0, \text{ for D even, or} \\
&\qquad P(-1) = -2 - K_C K_P (R_1 + 2) < 0 \text{ for D odd}
\end{aligned}
\qquad (3\text{-}17,18,19)
$$

The second step in applying the Jury Test requires construction of the Jury Array. It is a table composed elements that are calculated from the coefficients of the polynomial (3-10), and has the following form:

$$
\begin{array}{lccccc}
\text{Row 1} & a_n & a_{n-1} & \cdots & a_1 & a_0 \\
\text{Row 2} & a_0 & a_1 & \cdots & a_{n-1} & a_n \\
\text{Row 3} & b_{n-1} & b_{n-2} & \cdots & b_0 & \\
\text{Row 4} & b_0 & b_1 & \cdots & b_{n-1} & \\
\vdots & \vdots & & & & \\
\text{Row } 2n-5 & p_3 & p_2 & p_1 & p_0 & \\
\text{Row } 2n-4 & p_0 & p_1 & p_2 & p_3 & \\
\text{Row } 2n-3 & q_2 & q_1 & q_0 & & \\
\text{Row } 2n-2 & q_0 & q_1 & q_2 & &
\end{array}
\tag{3-20}
$$

where

$$
\begin{aligned}
b_k &= \begin{vmatrix} a_n & a_{n-1-k} \\ a_0 & a_{k+1} \end{vmatrix}; \quad k = 0,1,\cdots,n-1 \\
&\vdots \\
q_k &= \begin{vmatrix} p_3 & p_{2-k} \\ p_0 & p_{k+1} \end{vmatrix}; \quad k = 0,1,2
\end{aligned}
\tag{3-21}
$$

The elements calculated within the array are then used to verify whether the following additional conditions for the roots of the polynomial (3-10) to lie within the unit circle are met:

$$
\begin{aligned}
|b_{n-1}| &> |b_0| \\
&\vdots \\
|q_2| &> |q_0|
\end{aligned}
\tag{3-22}
$$

When applied to a polynomial with real coefficients, equations (3-11)-(3-13) and (3-22) comprise a set of necessary and sufficient conditions.

Example

Let $D = 2$ and consider $P(z) = z^4 - z^3 + [K_C K_P (R_1 + 1)]z - K_C K_P$. Since D is even, the conditions (3-17)-(3-19) reduce to

$$
\begin{aligned}
&1.\ \ 0 < K_C K_P < 1 \\
&2.\ \ R_1 > 0 \qquad\qquad (3\text{-}23,24,25) \\
&3.\ \ 2 - K_C K_P (R_1 + 2) > 0
\end{aligned}
$$

Then the Jury Array for the problem is as follows:

Row 1	$-K_C K_P$	$K_C K_P (R_1+1)$	0	-1	1
Row 2	1	-1	0	$K_C K_P (R_1+1)$	$-K_C K_P$
Row 3	$K_C^2 K_P^2 - 1$	$-K_C^2 K_P^2 (R_1+1)+1$	0	$K_C K_P - K_C K_P (R_1+1)$	
Row 4	$K_C K_P - K_C K_P (R_1+1)$	0	$-K_C^2 K_P^2 (R_1+1)+1$	$K_C^2 K_P^2 - 1$	
Row 5	$(K_C^2 K_P^2 - 1)^2 *$ $(K_C K_P - K_C K_P (R_1+1))^2$	$(K_C^2 K_P^2 - 1) *$ $(-K_C^2 K_P^2 (R_1+1)+1)$	$(K_C K_P - K_C K_P (R_1+1)) *$ $-(-K_C^2 K_P^2 (R_1+1)+1)$		
Row 6	$(K_C K_P - K_C K_P (R_1+1)) *$ $-(-K_C^2 K_P^2 (R_1+1)+1)$	$(K_C^2 K_P^2 - 1) *$ $(-K_C^2 K_P^2 (R_1+1)+1)$	$(K_C^2 K_P^2 - 1)^2 *$ $(K_C K_P - K_C K_P (R_1+1))^2$		

where the symbol "*" denotes multiplication. Therefore, the three original constraints (3-17,18,19) are supplemented by two additional constraints defined by (3-22) for this particular example

$$
\begin{aligned}
&\left| K_C^2 K_P^2 - 1 \right| > \left| K_C K_P - K_C K_P (R_1+1) \right| \\
&\left| (K_C^2 K_P^2 - 1)^2 (K_C K_P - K_C K_P (R_1+1))^2 \right| > \left| (K_C K_P - K_C K_P (R_1+1)) * -(-K_C^2 K_P^2 (R_1+1)+1) \right|
\end{aligned}
\qquad (3\text{-}26)
$$

Figure 3-2 represents graphically the results of the analysis described above when it is repeated for various values of D. The curves are the *nominal stability conditions* for different sets of the three parameters ($K_C K_P$, R_1, D). The x-axis represents the values of R_1, and the y-axis represents the product $K_C K_P$. Each curve defines the stability limit for a fixed value of the measurement delay D, with the topmost curve corresponding to $D = 0$, the curve immediately below it corresponding to $D = 1$, and so on down to $D = 20$. If for a given D, the point defined by the ordered pair $(R_1, K_C K_P)$ lies below the line, the system is stable for the parameters $(R_1, K_C K_P, D)$. A point on the line is critically stable, and above the line, unstable. All stability regions are also framed by the

x-axis and y-axis, meaning that they all lie entirely within the first quadrant, as dictated by (3-17) and (3-18).

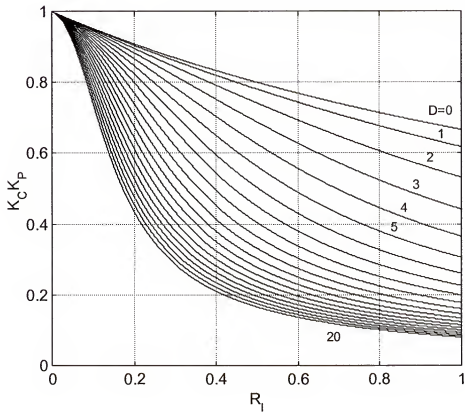

Figure 3-2. Nominal stability limit curves under PI control for various delay values.

These curves of Figure 3-2 are generated using the root finding function of Matlab for computational efficiency, but confirmed with representative Jury Table plots. Also, for clarity, recall that the controller introduces a unit delay; the controller delay is separate from the measurement delay D.

3.3.2 Robustness Analysis

A static plant with measurement delay of the form (3-1) under PI control has two parameters that are known exactly—the gain K_c and the reset time R_I of the controller,

since they are set by the operator. In contrast, it is possible that the plant gain K_P and the measurement delay D may not be known precisely, or may change with time. More specifically, the delay D may be uncertain, but is restricted to be a whole number. As a result, if D changes, the stability limit simply migrates between the appropriate curves of Figure 3-2. The gain K_P of the plant, however, is a continuous parameter that may be affected by error, and is modeled by the multiplicative uncertainty

$$K_P = K_P^0(1+\varepsilon) \tag{3-27}$$

with

$$\underline{\varepsilon} \le \varepsilon \le \bar{\varepsilon} \tag{3-28}$$

and

$$0 \ge \underline{\varepsilon} > -1 \tag{3-29}$$

$$\bar{\varepsilon} > 0 \tag{3-30}$$

where K_P^0 is the exactly known nominal plant gain, and ε is a scalar that quantifies the extent of modeling error. Equation (3-27) defines the unknown actual plant gain K_P as a multiple of the exactly known nominal plant gain K_P^0. The range of possible variation is restricted by the dual inequality (3-28), where $\underline{\varepsilon}$ is the lower bound and $\bar{\varepsilon}$ is the upper bound. Taken together, (3-29) and (3-30) ensure that K_P^0 is in fact one of the possible values of K_P (*i.e.,* $\varepsilon = 0$). Finally, Equation (3-29) further restricts the error so that K_P and K_P^0 have the same sign; this is necessary to guarantee (3-17) once the value of K_C is set.

Let $f(R_1, D)$ represent an arbitrary curve in Figure 3-3. The robust stability criterion becomes $K_C K_P < f(R_1, D)$ for all values of ε satisfying (3-28). Using (3-27), this condition can be written as

$$K_C K_P^0 (1+\varepsilon) < f(R_1, D) \tag{3-31}$$

or equivalently, since $(1+\varepsilon) > 0$

$$K_C K_P^0 < \frac{1}{(1+\varepsilon)} f(R_1, D) \tag{3-32}$$

Using the upper constraint bound $\varepsilon = \bar{\varepsilon}$ yields the *robust stability condition*

$$K_C K_P^0 < \frac{1}{(1+\bar{\varepsilon})} f(R_1, D) \tag{3-33}$$

In other words, the product of K_C and K_P must remain below the upper bound given by $f(R_1, D)$ to ensure robust stability. The nominal stability limit is obtained for the case where $K_P = K_P^0$ (*i.e.,* $\varepsilon = 0$); hence, (3-33) yields the nominal stability condition

$$K_C K_P^0 < f(R_1, D) \tag{3-34}$$

Figure 3-3 shows a comparison of the boundaries of the robust stability region given by (3-33) and the nominal stability region given by (3-9) for the case $D = 5$ and $\bar{\varepsilon} = 0.25$. Note that the robust stability region is always a constant fraction of the nominal stability region: namely, the fraction $\frac{1}{(1+\bar{\varepsilon})}$ that results from taking the ratio of the right-hand sides of (3-33) and (3-34).

The robust stability limit is, in effect, a gain margin that reduces the ordinate of each critically stable ordered pair by the factor $1/(1+\bar{\varepsilon})$. The graph resulting from a value of $\bar{\varepsilon} = 1/9$ is shown in Figure 3-4. Note that the graph has the same general shape

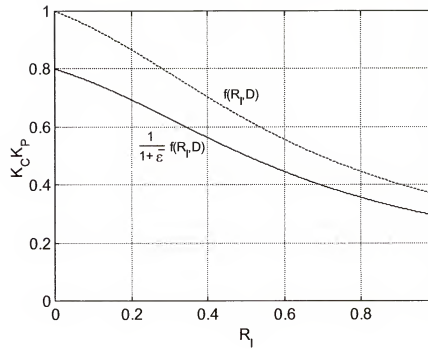

Figure 3-3. Representation of the boundary robust stability region given by (3-33) (solid line) and the boundary of the nominal stability region given by (3-34) (dashed line) for a delay $D = 5$.

as that shown in Figure 3-2 for the nominal stability region, except that each y-value has been scaled by the factor $\frac{1}{1+(1/9)} = 0.9$.

Given a static plant of the form (3-1) including a measurement delay D, a key engineering task is to identify the error bounds in the modeling parameters K_p and D. A systematic design of experiments (Box *el al.,* 1978) may be an effective strategy for determining the range of gain values K_P, or equivalently, finding bounds on the error parameter ε. In fact, standard linear regression studies (Kreyszig, 1999) using experimental data can be used to yield confidence intervals directly related to the uncertainty parameter ε. In addition, if the process is already in operation, historical data

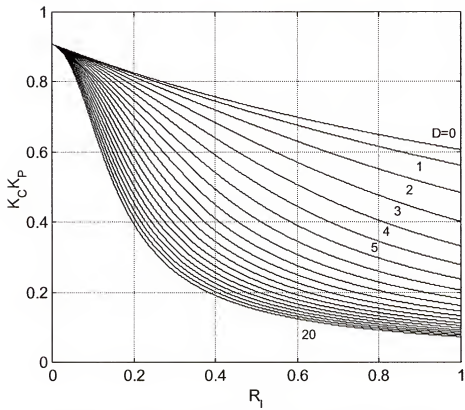

Figure 3-4. Robust stability limit curves under PI control for $\bar{\varepsilon} = (1/9)$ and various delay values.

may be used to help reverse-engineer the range of the plant gain values.

Identifying the value of D is generally more straightforward. Whether in the design stage or already in operation, it should be trivial to count the number of units that are en route from the point at which the input value is applied to the point at which the output is measured. However, it should be noted that it is possible for the delay to vary since not all unit operations are necessarily occupied by a batch at a given time. The importance of this scenario is discussed in detail in Section 3.4.

3.3.3 Tuning Correlations

Generating the curves represented by $f(R_I; D)$ is computationally expensive, since the polynomials generated by the Jury Table are of order $(D+1)^2$. It is observed that

they resemble the frequency response for a sinusoidal input (Levine, 1996), and can be approximated by a two-parameter (α,β) model

$$f'(R_1, D) = \frac{1}{(\alpha R_1)^4 + 2(\alpha R_1)^2 (2\beta - 1) + 1} \tag{3-35}$$

Hence, $f'(R_1, D) \cong f(R_1, D)$ for appropriate values of parameters α and β. As a model with only two parameters, the optimal values of $\alpha = \alpha(D)$ and $\beta = \beta(D)$ can be found easily through a computationally inexpensive exhaustive numerical search. This fit can be optimized at the discretion of the user with least squares, minimum absolute error, etc. Results are given in Appendix E for the case of minimum absolute error, and the

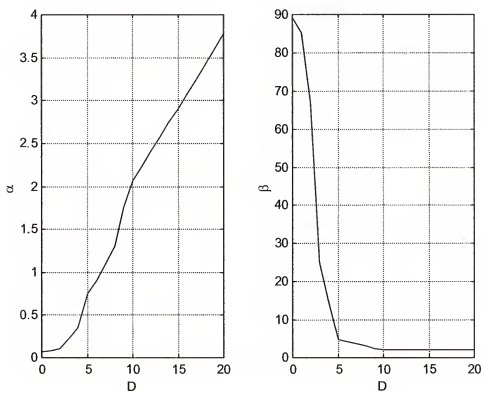

Figure 3-5. Optimal-fit parameters for the model (3-35) using the minimum absolute error criterion: (a) parameter α, (b) parameter β.

resulting values of α and β as a function of D are given in Figure 3-5. In addition, Figure 3-6 shows the plots of the exact curves $K_C K_p = f(R_1, D)$ and of the approximate curves $K_C K_p = f(R_1, D)$. Note that only the curves for delay values of 2, 5, 8, 11, 14, and 17 are plotted; this shows the performance of the fit over a wide range of values of D, while retaining graphical clarity.

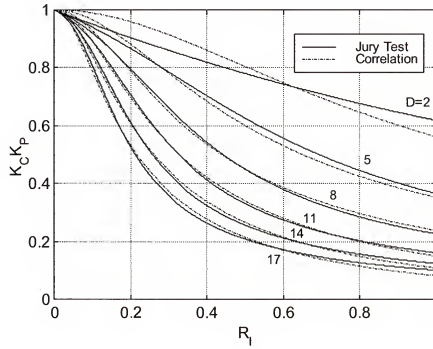

Figure 3-6. Visual comparison of actual stability curves with those generated by 2-parameter correlation.

Figure 3-6 shows that some of the approximations do not provide a close fit, but the approximate curves are nonetheless useful when considering how tuning heuristics are implemented. For instance, a common method is to begin along the y-axis and select one half of the maximum value allowed, in this case $K_C K_P = 0.5$ for all delays. The abscissa of the point found in this fashion is the recommended value of $K_C K_P$. Next,

select the relevant delay curve for the problem, and move out one third of the way to the curve in the x-direction while keeping $K_C K_P = 0.5$. This resulting point is the suggested initial tuning. With such gross approximations, it should be clear that the small amount of error introduced using the two-parameter fit is negligible. Moreover, with suggested tunings so far from the limits of stability, robustness is typically ensured.

3.4 Plant Stability under PI Control with a Smith Predictor

The application of a Smith Predictor (Marlin, 2000) for deadtime compensation is a potential remedy for a system affected with significant delay values. When added to the system discussed in Section 3.3, the closed-loop diagram becomes as illustrated in Figure 3-7

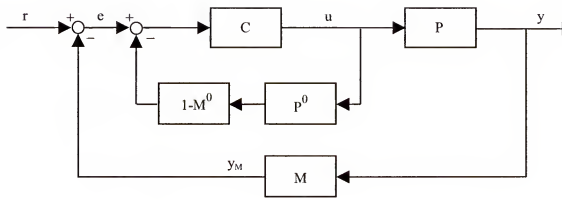

Figure 3-7. Generalized block diagram for a feedback loop of a static plant and measurement delay using a PI controller with a Smith Predictor.

As discussed in Section 3.3, the plant P and the measurement system M have two uncertain parameters: namely K_P and D. To implement the Smith Predictor, estimated values K_P^0 and D^0 are required to build the Smith Predictor operators $P^0 = K_P^0$ and $M^0 = z^{-D^0}$. It is desirable to investigate the robustness of the Smith Predictor scheme with respect to errors in the estimates of the parameter K_P and D.

3.4.1 Closed-loop dynamics under PI control with a Smith Predictor

Standard block diagram algebra on Figure 3-7 yields the transfer function for the inner loop

$$\frac{u}{e} = \frac{C}{1 + CP^0 - CM^0P^0} \tag{3-36}$$

Using (3-36) in the relationship $y = Pu$ and recognizing that $e = r - y$ yields

$$y = P\left(\frac{C}{1 + CP^0 - CM^0P^0}\right)(r - My) \tag{3-37}$$

which can be readily rearranged into the form

$$\frac{y}{r} = \frac{CP}{1 + CP^0 - CM^0P^0 + CMP} \tag{3-38}$$

As in the case considered in Section 3.3, the stability region is determined by the roots of the characteristic polynomial $P(z) = 1 + CP^0 - CM^0P^0 + CMP$, as shown in Appendix F. Substituting the values for C, M, and P defined in Section 3.3, as well as those for P^0 and M^0 defined in Section 3.4 yields the characteristic equation

$$\begin{aligned} &1 + K_C\left(\frac{1}{z} + R_I\frac{1}{z-1}\right)K_P^0 - K_C\left(\frac{1}{z} + R_I\frac{1}{z-1}\right)K_P^0 z^{-D^0} \\ &+ K_C\left(\frac{1}{z} + R_I\frac{1}{z-1}\right)K_P z^{-D} = 0 \end{aligned} \tag{3-39}$$

Multiplying each term by $z(z-1)z^D z^{D^0}$ and grouping like terms yields

$$\begin{aligned} &z^{D^0+D+2} + [K_C K_P^0(R_I + 1) - 1]z^{D^0+D+1} - (K_C K_P^0)z^{D^0+D} \\ &-[K_C K_P^0(R_I + 1)]z^{D+1} + (K_C K_P^0)z^D \\ &+[K_C K_P(R_I + 1)]z^{D^0+1} - (K_C K_P)z^{D^0} = 0 \end{aligned} \tag{3-40}$$

Provided $P = P^0$ and $M = M^0$, inspection reveals that the last four terms of (3-40) sum to zero, leaving the simplified nominal characteristic equation $z^2 + [K_C K_P^0 (R_1 + 1) - 1]z - K_C K_P^0 = 0$, which is equivalent to (3-9) for the special case of an undelayed plant (*i.e.,* D=0).

3.4.2 Stability Region as a Function of Model Uncertainty

As the true plant parameters are allowed to deviate from their estimations, the loop may become unstable. For illustration purposes, the stability space is depicted in Figure 3-8 for the set of conditions $K_C K_P^0 = 0.5$, $R_1 = 0.2$, and $D^0 = 6$. At zero on either axis, the estimated parameter matches the true parameter exactly. Moving away from zero represents increasing the mismatch, with negative values representing underestimates and positive values representing overestimates.

For example, in the case where $D^0 - D = 0$, the stability range for $K_C K_P$ is approximately $-0.45 < K_C(K_P^0 - K_P) < 0.48$. In contrast, at $D^0 - D = \pm 1$, there are no stabilizing $K_C K_P$ values. Similarly, for $D^0 - D = \pm 2$, the system remains stable for the approximate range $0.1 < K_C(K_P^0 - K_P) < 0.45$, and so forth for greater values of mismatch. Note that the space is *not* symmetrical, which is most dramatically shown by a significant stability range for $D^0 - D = 5$, where none exists for $D^0 - D = -5$. In addition, for the subset of cases in which $K_P^0 = K_P$, the only stable value of $D^0 - D$ is zero. Therefore, for all practical purposes, it is essential to know the value of the delay precisely in order to consider using a Smith Predictor on this type of system.

To interpret this diagram, first recognize that, while not explicitly shown, there are physical limits to underestimates (negative numbers), and no bound to overestimates

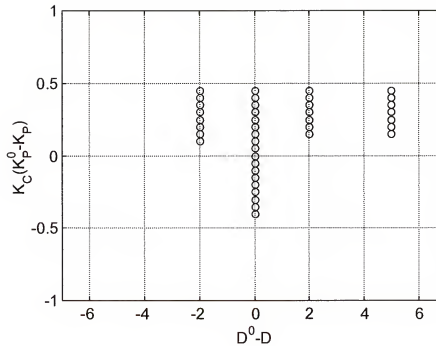

Figure 3-8. Stability region for a run-to-run controller applied to a discrete plant. The exact nominal parameters are $K_C K_P^0 = 0.5$, $R_I = 0.2$, and $D^0 = 6$ and uncertain parameters, plant gain, K_P, and measurement delay, D, are allowed to vary.

(positive numbers). Second, the delays must be whole numbers (and therefore errors in them must be whole numbers), while errors in gains are differences of real numbers. That is why the stability space only shows discrete values across the x-axis. In addition, the stability space is continuous vertically within each grouping of circles; they are spread out only for clarity. The most important feature of the diagram is the intolerance of the system to error of as little as one unit in delay. Furthermore, at any error in delay of other than zero, the system in unstable for a perfect match of the gain and its estimate. Clearly, unless the engineer has complete confidence in the value and constancy of the

delay, a Smith Predictor will result in unstable behavior even for little or no error in the in the gain estimate.

For contrast purposes, Figure 3-9 shows the analogous stability space for a discrete controller applied to a continuous system. Specifically, the pertinent simulation parameters are $K_C K_P^0 = 0.5$, $R_I = 0.2$, and $D^0 = 6$. The area is represented by groups of crosses, and is continuous vertically; they are spaced only for clarity. The circles represent the same stability space depicted in Figure 3-8. It is clear that the stability region for the discrete controller applied to a continuous system is much larger and not

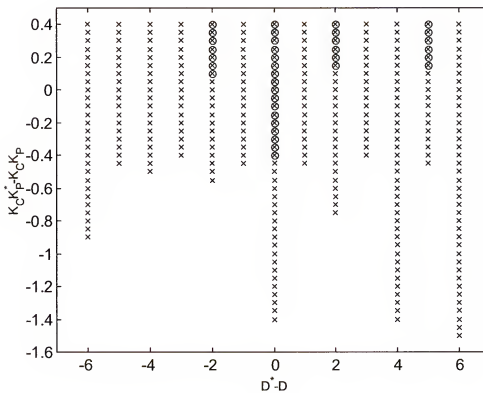

Figure 3-9. Stability region for a discrete controller applied to a continuous plant. The exact nominal parameters are $K_C K_P^0 = 0.5$, $R_I = 0.2$, and $D^0 = 6$ and uncertain parameters, plant gain, K_P, and measurement delay, D, are allowed to vary.

fragmented, unlike the similar run-to-run controller/discrete plant stability region (*i.e.,* the circles). Most notably, it shows that a continuous system with a discrete controller can tolerate errors in the estimation of the delay for every value within the range from $D^0 - D = -6$ to $D^0 - D = 6$ when there is no error present in the plant gain value. Furthermore, the discrete controller system is stable for the approximate range $-1.4 < K_C(K_P^0 - K_P) < 0.4$ when the error in delay is zero. Recall that that is not the case for the run-to-run controller/discrete plant system. In other words, the discrete controller with Smith Predictor/continuous plant system depicted in Figure 3-9 is robust enough to tolerate small errors in either of the two variable parameters, while the run-to-run controller with Smith Predictor/discrete plant system is not.

In summary, while the two types of systems may appear very similar, there are fundamental differences that significantly affect the performance and stability space of each configuration. Therefore, it is important that a control designer recognize the distinction between the two subtly difference arrangements. If the system is continuous, a Smith Predictor is a potential candidate to remedy the adverse effects of measurement delay. However, it is concluded from the robustness analysis (Section 3.3.2) and the tuning correlations (Section 3.3.3) that PI control is a safer strategy for a run-to-run controller applied to a discrete system, despite the fact that limited performance can be expected because of the significant delay.

3.5 Conclusions

The PI form of the run-to-run controller has been derived. In addition, tuning heuristics have been provided for a wide range of possible plant gain and delay values. With them, stable plant behavior can be guaranteed, although limited performance must

be tolerated. However, it has been shown that stability cannot be guaranteed when applying Smith Predictors to run-to-run static systems with measurement delay in the presence of even very small modeling error. The implication of Figure 3-8 is that the root locus of the characteristic equation for the system with a Smith Predictor moves around as a function of $D^0 - D$ and $K_C(K_P^0 - K_P)$. Furthermore, as D changes, it is apparent that one or more roots migrate into and out of the unit circle (the critical limit of stability). Therefore, it is recommended that simple PI control be used for run-to-run static systems with significant delay. Furthermore, a set of tuning heuristics are provided that will yield satisfactory performance.

A comprehensive study of the behavior of the roots of the characteristic polynomial may be helpful in finding ways to modify the controller to be more robust with a Smith Predictor. Without that development, it is necessary to use more traditional control approaches, even though performance will be limited. A possible starting point may be to study the discrete analog of the findings of (Adam *et al.,* 2000), who have shown that discrete stability ranges exist for a Smith Predictor applied to a continuous system with an uncertain time-delay parameter. In their work, the frequency response in the Nyquist plane is shown to rotate about the origin as the delay value varies, which can alter the number of encirclements of the critical point (Latchman and Crisalle, 1995), which is a parameter that is central to the stability of a continuous system.

CHAPTER 4
CONTROL OF pH USING A NOVEL OPTICAL SENSOR

4.1 Introduction

The pH of a solution can have extreme effects on the environment. For example, river ecology is extremely sensitive to pH, and manufacturing facilities that discharge materials into river water must be careful to not create a toxic environment. In many chemical reactions, the pH determines both extent of reaction and selectivity, and hence it can be a determining factor for the profitability of a design (Fogler, 1992). Finally, pH is also an important attribute of the final product for goods ranging from car batteries to soft drinks.

Measurement of pH is a commonly accepted exercise, but the true range of the measurement demands involved is unusually large. The definition of pH is

$$pH = -\log[H^+] \tag{4-1}$$

where $[H^+]$ is the hydrogen ion concentration in moles per liter (mol/L or M). More accurately, it is a function of hydrogen ion activity, but the two are essentially equivalent for the purposes of pH measurement in most systems (McMillan, 1994). Furthermore, it is believed that hydrogen ions exist as hydronium ions $[H_3O^+]$ in aqueous solution; this can also be ignored for simplicity. Therefore, the problem of controlling pH is really the problem of controlling concentration of the chemical species it represents, namely, hydrogen ion concentration. Even when considering an operating range of $2 < pH < 12$ (more extreme values are not uncommon), this constitutes a tremendous range (0.01 to

0.000000000001 M) of hydrogen ion concentration conditions that must be taken into account. Additionally, some electrodes can respond to changes of as little as .001 pH units, and under certain conditions at neutrality (pH = 7), that corresponds to a hydrogen ion concentration change of less than 0.000000001 M (McMillan, 1994). The combination of range and sensitivity demands makes it a major challenge to design a control scheme that that can work for such varied conditions with acceptable precision due to the fundamental laws governing signal-to-noise ratio (Williams, 1991).

From the viewpoint of control engineering, the plant (a solution with an arbitrary pH value residing in a vessel or flowing in a stream) is highly non-linear over its operating range. The chemistry involved in acid/base reactions is a major underlying reason for this trait (see Appendix G). Furthermore, when considering a system including at least one weak acid or base, the amount of additional acid or base needed to bring a volume of fluid to a desired pH varies according to the strengths of the acid(s) or base(s), their dissociation constants, and the initial pH. In addition, pH regions exist where the fluid volume resists a change in pH when additional acid or base is added—a phenomenon referred to as buffering (Zumdahl, 1989). In other words, different fluids of the same volume and pH can require significantly different amounts of acid or base to achieve the same shift in pH, and proceed along the transition with very different trajectories. Buffering contributes significantly to an underlying difficulty of pH control, namely, that the gain of a pH system can vary by several orders of magnitude from point to point throughout the operating range.

Finally, in most realistic pH control applications, the acidic and basic components of the stream that must have its pH adjusted changes over time. This introduces different

dissociation constants, and therefore makes the already highly variable gain (with respect to operating range) time-varying as well. Even though this phenomenon can still be controlled in the traditional manner (feedback control strives to eliminate offset), the continuous variations often severely degrade control performance, especially when the tuning parameters are static. The complicated nature of describing the pH of a combination of streams has inspired considerable work in the area of open-loop pH reactor modeling (McAvoy, 1972; McAvoy *et al.,* 1972; Gustafsson *et al.,* 1995).

There have been many attempts to devise schemes for closed-loop control that are effective despite the problems of range, sensitivity, and plant gain. These include the implementation of dual base injectors (Williams *et al.,* 1990), and the use of a smaller, separate reactor (Sung and Lee, 1995) to quickly identify the behavior of the system and use that knowledge to improve control performance. Furthermore, advanced control strategies such as adaptive control (Mahuli *et al.,* 1993; Sung *et al.,* 1998) have been used to ensure that the controller remains optimally tuned for the observed operating conditions. Finally, it has been proposed that using alternative control variables may be an effective way to improve pH control (Gustafsson and Waller, 1983; Waller and Makila, 1981; Narayanan *et al.,* 1998). In one way or another, these arrangements attempt to produce a system that is easier to control despite the problems stemming from range, sensitivity, and variable gain.

One common feature of most methods is that they use a standard electrode as a measurement device to close the control loop. Because of the physics that govern electrodes (see Section 4.2.2), the electronic signal sent to the controller is proportional to pH. This introduces an additional and significant non-linearity to the system, since $[H^+]$

is the chemical species being controlled. An optical pH sensor (Janowiak, 2003), commonly referred to as an optrode (see Section 4.2.3) being developed at the University of South Florida generates a signal proportional to $[H^+]$, not pH, and therefore holds potential for eliminating the non-linearity of the feedback portion of the loop. While not addressing the non-linear physics that govern the chemistry in the plant, the optical sensor with a signal proportional to the true variable of interest ($[H^+]$) could affect the closed-loop dynamic behavior of the system dramatically. The goal of this study is to determine if a linear optical pH sensor achieves feedback control performance superior to that of the traditional, highly non-linear, electrode.

There are several components required to achieve the project goal. First, an accurate model must be developed to simulate a pH control system; Section 4.2 discusses the process in detail. Section 4.3 outlines a simulation study designed to access the relative performance of the two probes over a range of response characteristics, both without noise and with realistic noise injected. Section 4.4 addresses issues pertinent to the construction of a pilot-scale pH control system for the purpose of experimental trials. Conclusions are drawn about the relative effectiveness of the two sensors with respect to dynamic control in Section 4.5.

4.2 Modeling and Simulation of a pH Control System

There are three primary components to a basic feedback control scheme. Their relative arrangement is represented in the abstract block diagram that is Figure 4-1, where C represents the controller, P is the plant, M is the measurement device, r is the system setpoint, u is the input to the system, and y and y_m are the output and measured output of the system, respectively. Each of the three components C, P, and M is modeled separately before the dynamic response of the closed system is evaluated.

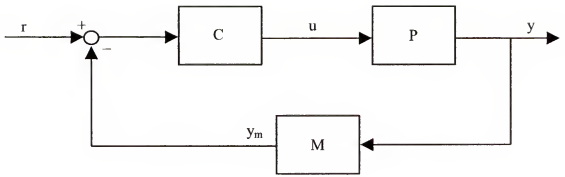

Figure 4-1. Abstract block diagram of a simple feedback control system.

When modeling the plant P, it is noted that chemical reactions among acids and bases are relatively fast (Zumdahl, 1989). Therefore, using a continuously stirred tank reactor (CSTR) is a plausible equipment choice for pH control. It is assumed that sufficient agitation allows any reaction to proceed to equilibrium well before the fluid exits the reactor. Additionally, the simplicity of the apparatus helps minimize the number of parameters associated with the entire control system. As a result, a more confident determination can be made of the relative advantages and disadvantages of using an optical pH sensor in lieu of a traditional electrode. Section 4.2.1 is a step-by-step description of the modeling process adopted to describe a CSTR for pH control.

The most common control instrument C used for pH control systems is the proportional-integral (PI) controller

$$u(s) = K_C\left(1+\frac{1}{\tau_I s}\right)e(s) \tag{4-2}$$

where K_C is the gain of the controller, τ_I is the integral time constant of the controller, e is the error, and u is the input to the CSTR. Derivative action is not used, since measurement noise typically degrades the response to a point where the benefits of

derivative action are significantly outweighed by the deleterious effects of noise. In addition, more advanced control schemes, such as cascade or Smith Predictor configurations, are assumed to be unnecessary. They are generally used in situations where input disturbances or long transport delays degrade the quality of control performance, problems not associated the chosen CSTR model.

The control loop is closed with the addition of a measurement device M. Both the electrode and optrode work by continuously undergoing chemical reaction; see Sections 4.2.2 and 4.2.3 for a detailed discussion as well as a mathematical model for each device. Because the physics of the two instruments are different, the closed loop response can be expected to be different as well. Establishing a quantitative criterion to evaluate performance should indicate whether or not there is a significant difference in the behavior of the closed-loop system when utilizing one sensor versus the other.

4.2.1 Process Model of pH Control in a CSTR

The process model consists of a mixing tank and three streams—two entering the CSTR and one leaving it, as shown in Figure 4-2. One of the inbound streams is the influent, and typically consists of a mixture of a number of weak acids that is typical of industrial process by-products. The other incoming stream is the reagent, which is a strong base used to neutralize the acids. The effluent should have the desired pH for the next destination of the stream. Note that in a production process, the influent may change from acidic to basic, or back again. A control system for such a process would require an additional input stream of acidic reagent. Only the case of an acidic stream being treated with a basic reagent is considered in this study because this scenario is no more illustrative in sensor comparison.

A schematic of the reactor with volume V used in this study is shown in Figure 4-2. The influent stream with flowrate Q_1 is chosen to be acetic acid of concentration $[A]_{in}$, a commonly available weak acid with a well-known dissociation constant. Second, the reagent stream with flowrate Q_2 is chosen to be sodium hydroxide (also commonly available) of concentration $[NaOH]_{in}$. Note that the following inlet concentration holds: $[NaOH]_{in} = [Na^+]_{in} = [OH^-]_{in}$. Finally, the effluent stream leaving the tank at a flowrate Q_3 is a mixture of both acetic acid and sodium hydroxide in concentrations, [A] and $[Na^+]$, respectively. The flowrates $Q_1, Q_2,$ and Q_3 are measured in liters per second (L/s), and [ ] denotes a concentration of species ( ) in moles per liter (mol/L or M).

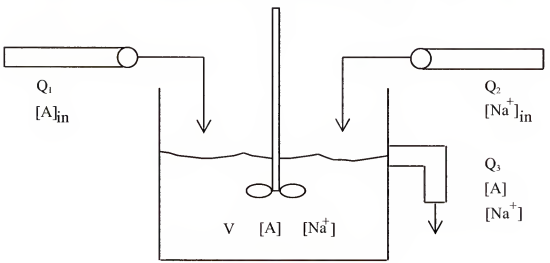

Figure 4-2. Schematic of a CSTR used for pH control.

The entire system is described by a set of six equalities, of which two are differential equations and four are algebraic equations

$$\frac{d[A]}{dt} = -\left(\frac{Q_1 + Q_2}{V}\right)[A] + \left(\frac{Q_1}{V}\right)[A]_{in} \tag{4-3}$$

$$\frac{d[Na^+]}{dt} = -\left(\frac{Q_1 + Q_2}{V}\right)[Na^+] + \left(\frac{Q_2}{V}\right)[Na^+]_{in} \tag{4-4}$$

$$K_a = \frac{[H^+][A^-]}{[HA]} \tag{4-5}$$

$$K_w = [H^+][OH^-] \tag{4-6}$$

$$[A] = [HA] + [A^-] \tag{4-7}$$

$$[Na^+] + [H^+] = [A^-] + [OH^-] \tag{4-8}$$

An important feature of the system is that the effluent stream Q_3 is created by spillover from the CSTR, ensuring that the volume V is constant. Assuming that all fluid streams are aqueous with approximately the same density, a total mass balance yields

$$\frac{d(\rho V)}{dt} = \rho Q_1 + \rho Q_2 - \rho Q_3 \tag{4-9}$$

Assuming that the density ρ is constant and using the fact that V is also constant, it follows that

$$Q_1 + Q_2 = Q_3 \tag{4-10}$$

The two differential equations represent chemical species that do not change in the reactor, and are derived via mass balances. The first is total acetic acid concentration, denoted [A], which is the sum of the concentrations of the protonated and unprotonated molecules, *i.e.* $[A] = [HA] + [A^-]$.

$$\frac{d([A]V)}{dt} = [A]_{in} Q_1 - [A] Q_3 \tag{4-11}$$

Now using the fact that V is constant and the flowrate equality (4-10)

$$V\frac{d[A]}{dt} = [A]_{in}Q_1 - [A](Q_1 + Q_2) \tag{4-12}$$

or

$$\frac{d[A]}{dt} = -\left(\frac{Q_1 + Q_2}{V}\right)[A] + \left(\frac{Q_1}{V}\right)[A]_{in}$$

which is the first of the six equations (4-3) that describe the system. The second species balance required is for sodium ions, yielding

$$\frac{d([Na^+]V)}{dt} = [Na^+]_{in}Q_2 - [Na^+]Q_3 \tag{4-13}$$

which can be manipulated as before to give

$$\frac{d[Na^+]}{dt} = -\left(\frac{Q_1 + Q_2}{V}\right)[Na^+] + \left(\frac{Q_2}{V}\right)[Na^+]_{in}$$

or the second of the six equations (4-4) that describe the system.

Equations (4-3) and (4-4) define the two states of the reactor. Because there are a total of six unknowns

$$[A],[Na^+],[H^+],[A^-],[HA], \text{ and } [OH^-]$$

four additional equations are required to account for all of the relevant species. First, both acetic acid and water have dissociation constants, K_a and K_w, which are reported as (4-5) and (4-6) respectively, such that

$$K_a := \frac{[H^+][A^-]}{[HA]}$$

and

$$K_w := [H^+][OH^-]$$

so that

$$[OH^-] = \frac{K_w}{[H^+]} \tag{4-14}$$

Second, there is the aforementioned total acid concentration (4-7)

$$[A] = [HA] + [A^-]$$

Third, charge neutrality is required for a mixture of neutral liquids, and is given by (4-8) in the form

$$[Na^+] + [H^+] = [A^-] + [OH^-]$$

The quantity of interest, hydrogen ion concentration, is found through repeated substitutions. Rearranging (4-5) in the form

$$K_a[HA] = [H^+][A^-] \tag{4-15}$$

and then rearranging (4-7) to find that

$$[HA] = [A] - [A^-] \tag{4-16}$$

yields after (4-16) is substituted into (4-15) and a rearrangement of terms

$$K_a[A] = [H^+][A^-] + K_a[A^-] \tag{4-17}$$

Solving now for the concentration of the anion

$$[A^-] = \frac{K_a[A]}{[H^+] + K_a} \tag{4-18}$$

Now using (4-18) and (4-14) in the charge neutrality equation (4-8) and rearranging terms yields

$$[Na^+] + [H^+] - \frac{K_a[A]}{[H^+] + K_a} - \frac{K_w}{[H^+]} = 0 \tag{4-19}$$

or

$$[Na^+]([H^+]+K_a)[H^+]+([H^+]+K_a)[H^+]^2 - K_a[A][H^+]-([H^+]+K_a)K_w = 0 \quad (4\text{-}20)$$

which is easily cast in the form of a third-order polynomial

$$[H^+]^3+\left([Na^+]+K_a\right)[H^+]^2 + \left(K_a[Na^+]-K_a[A]-K_w\right)[H^+]-K_aK_w = 0 \quad (4\text{-}21)$$

It is critical to select the proper root of the polynomial (4-21) to find $[H^+]$. Using Descartes' Rule of Signs (Borowski and Borwein, 1991) to analyze the coefficients proves that Equation (4-21) has exactly two negative real roots and one positive real root (see Appendix H). Because negative concentration values have no physical meaning, the correct solution is given by the positive root.

4.2.2 Traditional Electrodes

4.2.2.1 Theory of operation

The basic design of traditional pH electrode sensors consists of a coated glass electrode filled with a fluid of known pH. The coated glass is pH sensitive, and if immersed in a fluid, galvanic half-cell potentials develop across the external fluid-glass boundary and the glass-fill solution boundary (McMillan, 1994). If care is taken to ensure that the hydrated gel layers on each side of the glass are suitably similar, and that sufficient free ions are available to migrate, the two potentials can be compared directly. The resulting voltage difference is a function of both pH and temperature.

The ability of a standard glass electrode to measure pH is rooted in the free energy present in the system, and is described by the classic thermodynamic equation (Zumdahl, 1989)

$$\Delta G = \Delta G^0 + RT\ln(Q) \quad (4\text{-}22)$$

where ΔG^o is the free energy change of the system for the given reaction with all species at 1 atmosphere of pressure, ΔG is the free energy change of the system for the given reaction at the given conditions, R is the gas constant, and T is the temperature. Also,

$$Q = \frac{[H^+]_{inner}}{[H^+]_{outer}} \tag{4-23}$$

is the reaction quotient, and $[H^+]_{inner}$ and $[H^+]_{outer}$ are the hydrogen ion concentrations of the glass-fill solution and the surrounding fluid, respectively. Substituting the definitions

$$\Delta G := -nFE \tag{4-24}$$

$$\Delta G^0 := -nFE^0 \tag{4-25}$$

where n is the number of electrons exchanged in the reaction, F is the electrical charge of a mole of electrons, and E and E^o are the half-cell potentials created by the reactions respectively at the current and standard conditions, gives the classical Nernst Equation:

$$E = E^0 - \left(\frac{RT}{nF}\right) \ln(Q) \tag{4-26}$$

Theoretically, then, the electrical potential $E - E^0$ is a function of T, n, and Q (R and F are constants). In the glass electrode system, T can be considered a known quantity, as in practice it is simply compensated for using a thermocouple, and n is always equal to one (because hydrogen ion always has a charge of one). The remaining term is the ratio of $[H^+]$ in the glass-fill solution (*i.e.,* $[H^+]_{inner}$) to $[H^+]$ in the solution of unknown pH (*i.e.,* $[H^+]_{outer}$). From (4-26), the natural log of the ratio is proportional to the electric potential being generated. A mathematical transformation can be

employed to change the natural logarithm to the base-ten logarithm. Recall that pH is defined as given by (4-1) as

$$pH = -\log[H^+]$$

Given that the standard hydrogen potential is the reference potential (*i.e.,* $E^0 := 0$ in this case) against which all half-reactions are assigned (Zumdahl, 1989), it can be seen that the standard pH probe develops an electrical potential that is linear with respect to $\log[H^+]$, *i.e.,* with respect to pH. In addition to reasons of brevity, this explains why hydrogen ion control is commonly referred to pH control.

4.2.2.2 Sensing capabilities

As an inherent result of the way that electrode sensors are designed, there are numerous sources of error. Because of the fact that two half-cells (whether or not they are physically combined into one probe, a pH electrode always consists of two separate reactions), a temperature compensator, and an external power supply are required, there are at least five potentials and ten resistances that become involved in the analysis (McMillan, 1991). Furthermore, although most of these should theoretically be constant, it is common for them to vary to some extent, resulting in a significant amount of compounded error. In addition, because the sensors are constructed of glass, they are generally limited to pressures of no more than 100 pounds per square inch (psi) and temperatures of no higher than 100°C, although specially constructed (and therefore more expensive) devices can improve these bounds (Moore, 1990). In fact, by reinforcing the glass wall with metal, 250 psi and 140°C can safely be monitored. Unfortunately, these sensors are extremely prone to erosion (e.g. when exposed to slurries with metallic particles), corrosion (hydrofluoric acid), and coating (black liquor

streams). Also, extreme conditions (pH < 3, pH > 12, or water content less than 40 wt% in the stream) tend to leach hydronium ions present in the gel layers, which degrade both the accuracy and response time of the sensors. When all of these factors are taken into account, the best reliable accuracy of pH electrodes that can be expected is about ± 0.1 pH units, even under well controlled laboratory conditions.

4.2.2.3 Dynamic model

To formulate a dynamic model for a pH electrode, it is easiest and most useful to study how one responds to a controlled change in input. A step input can be simulated by quickly transferring the pH probe from one solution to another. An experimental curve from such an experiment is shown in Figure 4-3. In the experiment, the probe was held

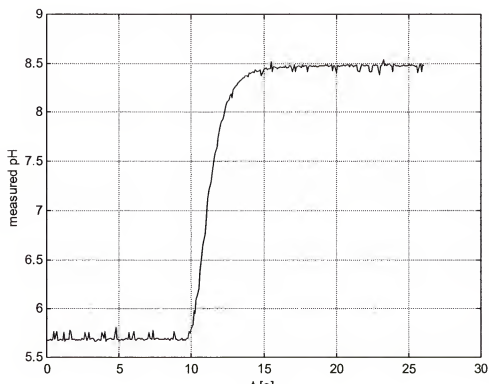

Figure 4-3. Typical dynamic response of a pH electrode to a step change in input.

in the first solution of $pH = 5.7$ until approximately $t = 9$ s, when it was quickly transferred to a second solution, and the ion exchange was allowed to proceed to equilibrium, yielding the stable final pH reading of 8.5.

Based upon the shape of the curve, a first-order model is appropriate. A time constant of approximately two seconds is observed. This is consistent with values reported in the literature (MacMillan, 1994), although it is also stated that the time constant can vary (Section 4.3 investigates the behavior of the system when it does vary in the range from 1 to 5 seconds). Figure 4-4 shows the model structure in block diagram form

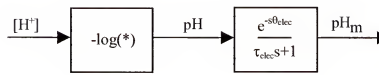

Figure 4-4. Block diagram of the model of a traditional pH measuring electrode.

where $[H^+]$ is the hydrogen ion concentration in the tank, θ_{elec} is the delay of the electrode, τ_{elec} is the time constant of the electrode, and pH_m is the measured pH produced by the sensor and sent to the controller. Note that the transformation from $[H^+]$ to pH occurs before the transfer function; this means that a sensor gain of 1 (dimensionless) is implied in the transfer function, and is therefore omitted for clarity. The corresponding differential equation for the transfer function block that represents the probe model *only* (*i.e.,* the rightmost block) in Figure 4-4 is then given as

$$\frac{d(pH_m)}{dt} = -\frac{1}{\tau_{elec}} pH_m + \frac{1}{\tau_{elec}} pH(t - \theta_{elec}) \qquad (4\text{-}27)$$

It is less certain what a reasonable estimate of the delay of the electrode would be, given that it is difficult to identify exactly at what time the probe was immersed in the second solution. It is assumed that ion exchange begins quickly after the probe contacts the new solution, creating little delay. A value of 1 second is chosen throughout the study for the sensor ($\theta_{elec} = 1$ s). Finally, since temperature could easily be detected and passed into the pH calculation algorithm, it can be assumed as a constant in simulation. These assumptions will be retained unless experimental results (see Section 4.4) indicate that they must be revised.

4.2.3 Novel Optical Sensors

4.2.3.1 Theory of operation

An alternative to pH sensor technology employs the use of fiber optics. Chromophores (indicator dyes that are optically sensitive, in this case, to $[H^+]$) dissolved in a solution can be used to accurately determine the pH of the solvent, with the aid of spectrophotometers. It has been further demonstrated that the indicator dyes can be immobilized in a polymer film (Seitz, 1988; Rao *et al.,* 1991), implying that there is the potential to create sensors that can determine the pH of flow streams. This is accomplished by analyzing the light passing through a fiber optic sensor coated with polymer containing the indicator dyes.

The apparatus can be placed into a flow stream, where the pH of the fluid determines what fraction of the immobilized dye molecules accept a proton. Because the bond structures of the protonated and unprotonated molecules are different, their absorbance spectra also differ. An appropriate light source is then placed near the end of the sensor, and the light passing through is analyzed for absorbency at wavelengths

critical to each form of the dye. If the total number of sites is known, the fraction protonated, and therefore the $[H^+]$, can be deduced.

The dye or dyes that are present in the polymer obey the Henderson-Hasselbalch equation (Zumdahl, 1989)

$$pH = pK_a - \log\frac{[HA]}{[A^-]} \tag{4-28}$$

which establishes the relationship between pH and the pK_a of an acid as a function of the relative concentration of its protonated and unprotonated forms. Values of pK_a for various acids are well documented, leaving the measurement of acid and conjugate base concentrations as the primary obstacle. Note that this weak acid and its accompanying dissociation constant are not related to acetic acid and its dissociation constant. When coupled with the Beer's law (Skoog *et al.,* 1998), the spectrophotometer is used to accomplish the measurement of the needed concentration. Beer's Law is

$$A = abc \tag{4-29}$$

where A is the absorbance, a is the absorptivity (a proportionality constant), b is the path length, and c is the chromophore concentration. By choosing an optimum wavelength of light, and knowing the absorptivities of the two species that constitute the immobilized dye being used, the thickness of the film (*i.e.,* the path length) and total density of the chromophore sights in the polymer (*i.e.,* the concentration), the absorbance detected can be correlated to the corresponding acid and base concentrations.

Using Beer's law to calculate the hydrogen ion concentration is a straightforward process. First, a wavelength of light is selected such that the absorptivity of $c_{HA_{opt}}$ is

high and the absorptivity of $c_{A^-_{opt}}$ is low, or vice versa. Next, knowing the path length b, the absorbance can be expressed

$$A = a_{HA_{opt}} b c_{HA_{opt}} + a_{A^-_{opt}} b c_{A^-_{opt}} \tag{4-30}$$

where the only remaining unknown terms are A, $c_{HA_{opt}}$, and $c_{A^-_{opt}}$. Since the total chromophore concentration is also known, is observed that

$$c_{HA_{opt}} = c_{A_{opt}} - c_{A^-_{opt}} \tag{4-31}$$

in a fashion analogous to, but not directly related to, (4-16). Finally, (4-31) is substituted into (4-30) and the spectrometer is used to obtain a measurement of absorbance A. After suitable rearrangement

$$c_{A_{opt}} = \frac{A - a_{HA_{opt}} b c_{A_{opt}}}{a_{A^-_{opt}} b - a_{HA_{opt}} b} \tag{4-32}$$

With $c_{A^-_{opt}}$ determined, (4-31) can easily be used to find $c_{HA_{opt}}$, and both can then be substituted into the final term of (4-28).

As with glass electrodes, there are physical limitations inherent to the design of polymer sensors that must be recognized, analyzed, and accounted for (Janowiak, 2003). First, the pK_a of an indicator dye can be affected when it is immobilized. In addition, it has been found that both the ionic strength of the flow stream as well as the temperature have significant effects on the apparent pK_a value of the acid. Ionic strength can be deduced from the conductivity of a solution, which can be measured easily by assembling an electrical circuit around the solution. Furthermore, temperature is also easy to measure, and its dependency is no additional burden when compared to traditional pH

sensors. A model has been proposed (Chang *et al.,* 1995; Janowiak, 2003) to describe the effects of ionic strength and temperature on the observed pK_a value:

$$pK_a = pK_a^0 + P\ \log(\Omega) + M\frac{1}{T} \tag{4-33}$$

where pK_a^0 is simply a known reference value for pK_a, P is an interaction factor between the dye and the electrolytes present, Ω is the conductivity of the solution, and M is a parameter related to the activation energies of dye-hydrogen ion reactions. Assuming that this is an accurate model, the pK_a term in the Henderson-Hasselbalch equation (4-28) can be well defined. As in the case of temperature, many sensors are available to make conductivity measurements. With conductivity and temperature measurements, the pKa of the immobilized dye can be calculated. Therefore, using a spectrophotometer and Beer's Law to determine $c_{A^-_{opt}}$ and $c_{HA_{opt}}$, the ratio $c_{HA_{opt}} / c_{A^-_{opt}}$ can easily be used with (4-28) and (4-33) to determine the pH of a solution in which the probe is immersed.

4.2.3.2 Sensing capabilities

As a result of their simplicity, optrode sensors offer several physical advantages to conventional probes (Seitz, 1984; Janowiak, 2003). First, only one sensor is needed, as opposed to two for the conventional configuration (recall that even combination probes contain two half-cell reactions); fewer signals limit the potential for compounded error. Also, optrodes are much more rugged than their glass counterparts, allowing higher operating temperatures and pressures. Individually, they have comparably limited dynamic pH range (Seitz, 1984), but are constructed using optic fibers of very small diameter (Borman, 1992), which can potentially be clustered together to achieve equal or greater dynamic range than conventional electrodes. In addition, they are much less

prone to erosion, corrosion, and coating. Because the dyes can be bonded directly into the polymer matrix, leaching is not a significant problem, which means that signal drift is negligible. Also, optrodes sense at the speed of light, and are therefore limited by the dynamics of the spectrophotometer and dye-hydrogen ion reactions, making them potentially quicker than traditional electrodes. Finally, the most attractive characteristic of the optical probe is that pH measurement is linear with respect to $\log\frac{[HA]}{[A^-]}$, and therefore the $[H^+]$ measurement is linear with respect to $\frac{[HA]}{[A^-]}$. In this fashion, the optical sensor promises to achieve an objective that may potentially outweigh other shortcomings, namely linear feedback. This property could serve to enhance closed-loop control performance.

4.2.3.3 Dynamic model

Similar to the electrode, the optical probe works via a concentration-driven ion exchange, and it is assumed to be described by a first order model. In this case, however, the two species of the immobilized indicator dye are either a weak acid-conjugate base or weak base-conjugate acid pair. Similarly to the weak acid in the influent stream (4-5), the total concentration and concentrations of protonated and unprotonated species are related by a unique dissociation constant, K_a^{opt} as given by

$$K_a^{opt} := \frac{[H^+][A^-]^{opt}}{[HA]^{opt}} \tag{4-34}$$

where $[A^-]^{opt}$ is the concentration of unprotonated sites and $[HA]^{opt}$ is the concentration of protonated sties. Note that $[A^-]^{opt}$ and $[HA]^{opt}$ are the same quantities given by $c_{A^-_{opt}}$ and $c_{HA_{opt}}$ in Section 4.2.3.1.

As with the electrode, the actual value of the time constant is assumed to vary for different process conditions. Figure 4-5 is a block diagram description of the model

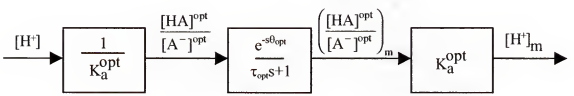

Figure 4-5. Block diagram of the model of an optical pH measuring probe.

where θ_{opt} is the delay of the optrode, τ_{opt} is the time constant of the optrode, $\frac{[HA]^{opt}}{[A^-]^{opt}}$ is the real-time acid-to-base ratio of the system, $\left(\frac{[HA]^{opt}}{[A^-]^{opt}}\right)_m$ is the measured acid-to-base ratio sent to the controller, and $[H^+]$ is the measured hydrogen ion concentration measured by the sensor and sent to the controller. Note that while the sensor in fact measures the acid-base ratio, it is trivial to multiply this quantity by the dissociation constant of the optrode K_a^{opt} to obtain $[H^+]$, and this conversion is therefore included in the model. As with the electrode model, there is a sensor gain of 1 (dimensionless) that is omitted for clarity. The corresponding differential equation for the transfer function block that represents the probe model *only* (*i.e.,* the middle block) in Figure 4-5 is then given as

$$\frac{d\left(\frac{[HA]^{opt}}{[A^-]^{opt}}\right)_m}{dt} = -\frac{1}{\tau_{opt}}\left(\frac{[HA]^{opt}}{[A^-]^{opt}}\right)_m + \frac{1}{\tau_{opt}}\frac{[HA]^{opt}}{[A^-]^{opt}}(t-\theta_{opt}) \qquad (4\text{-}35)$$

In order to compare the optrode performance directly to electrode performance, a the identical range of time constant values varying form 1 to 5 seconds is selected for simulation. In addition, to preserve the direct comparison between the two sensors, a value of $\theta_{opt} = 1$ s (recall that $\theta_{elec} = 1$ s as well) is chosen throughout the simulation study. Finally, both temperature and conductivity can be assumed to be readily measurable (*i.e.,* pK_a^{opt} is known exactly) eliminating the need to use (4-33) in the simulation model.

4.3 Closed-Loop Simulations

A simulation study is performed to examine if there an advantage to using an optical probe rather than a traditional pH electrode for closed-loop control. The study utilizes the plant model P, controller model C, and measurement device (electrode and optrode) models M described in Section 4.2. Throughout the study, a number of parameters remain unchanged: namely, simulation start time is always equal to $t = 0$ s, step changes always occur at $t = 20$ s, simulation end time is always equal to $t = 200$ s, and each trial uses simple Euler algorithm with a stepsize of 0.1 s. In addition, the volume is defined as $V = 1.75$ L, and the concentration values $[A] = [NaOH] = 0.1$ M and the flowrate value $Q_2 = 0.0025$ L/s are valid for all initial steady-state operating points throughout the simulation study. Finally, it should be noted that the equivalence point for this system is always $pH = 8.728$ in the study.

Each closed-loop trial is tuned separately to guarantee the optimal response according to the integral of time-averaged error (ITAE) criterion (Seborg, Edgar, and Mellichamp, 1989; Ogunnaike and Ray, 1994)

$$\text{ITAE} = \int_0^{t_f} t\, e\, dt \tag{4-36}$$

where t_f is the final time, t is the time, and e is the error between pH value and pH setpoint. One major benefit of this method is that the best theoretical response attainable can be identified, without additional complication introduced by the fact that optimal tunings for controllers using either an optrode or electrode vary throughout the operating range. In other words, introducing different amounts of additional error by fixing the controller tunings is avoided. Finally, the ITAE is calculated for the period between step change ($t = 20$ s) and the end of the simulation ($t = 200$ s). Note that a few simulations are unable to reach final steady-state before $t = 200$ s; in these cases, the simulation ending time is increased for the purpose of identifying the optimal controller tunings only. After the optimal tunings are identified, they are fixed, the simulation is re-run with a simulation stop time of $t = 200$ s, and the resulting ITAE value recorded.

A set of tuning heuristics for the definition of an optimal tuning of the PI controller is developed. An exhaust numerical search is employed with an adaptive step size for gridding, as explained in Appendix I. For each of the simulation variations described later in this section, the controller gain K_C is identified to two significant figures (as defined in Appendix I), and the integral time constant τ_I of the controller is determined to one significant figure. Finally, while the gain K_C does not need to be

restricted in its range, the restriction $10\ s < \tau_1 < 1000\ s$ is imposed as a practical limitation to unrealistically extreme values.

In addition, the ITAE criterion is applied to the actual pH in all cases, rather than the measured pH, which is only used for the feedback signal. This is particularly important for the cases when noise is injected, since additional error would be artificially introduced by the noisy signal near the end of each simulation. Finally, it should be noted that ITAE applied to errors in terms of the respective control variables (*i.e.,* pH for the electrode and $[H^+]$ for the optrode) cannot be compared directly. Therefore, while the error for the electrode is calculated directly

$$e_{elec} = pH_{sp} - pH \tag{4-37}$$

where e_{elec} is the error when using an electrode, pH_{sp} is the setpoint in units of pH (this quantity is specified by the user, and therefore always available), and pH is the actual pH of the system (as opposed to the measured pH). In contrast, the error for the optrode is converted to pH units by defining the error as

$$e_{opt} = pH_{sp} - (-\log_{10}([H^+])) \tag{4-38}$$

where e_{opt} is the when using an optrode, and $[H^+]$ is the actual hydrogen ion concentration of the system.

The control diagrams for both the electrode and the optrode are derived from the basic closed loop system shown in Figure 4-1. The information specific to the control loop when an electrode is used as a measurement device is shown in Figure 4-6. Features present in Figure 4-6 that are not present in Figure 4-1 include disturbances Q_1, C_1, and C_2 as well as the injected noise signal n.

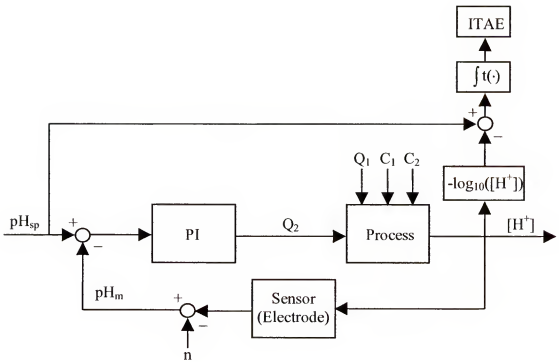

Figure 4-6. Block diagram of the control loop when using an electrode for pH control.

where C_1 is equivalent to $[A]_{in}$ and C_2 is equivalent to $[Na^+]_{in}$ as given in Figure 4-2. The diagram for a control loop using an optrode as a measurement device is shown in Figure 4-7, and includes the additional features included in Figure 4-6. Note that the setpoint must pass through an appropriate function to be in the same units as the feedback signal.

In each case, the process begins with the probe generating a signal that is a function of the hydrogen ion concentration $[H^+]$ of the fluid in which it is immersed. Noise n may then added to the output of the probe, and that measured value is compared to the setpoint by the controller. The controller then determines the proper input Q_2 to send to the system. Finally, the system adopts a new hydrogen ion concentration value as a result of the most current values of Q_1, Q_2, C_1, and C_2.

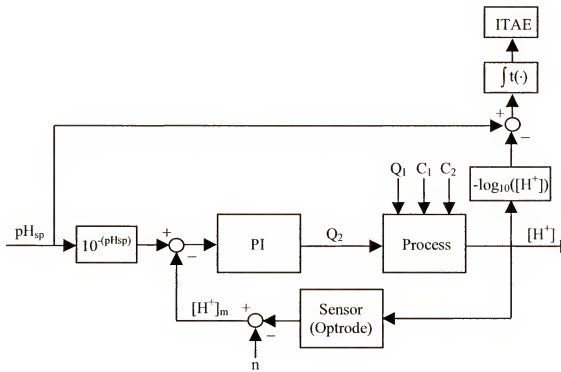

Figure 4-7. Block diagram of the control loop when using an optrode for hydrogen ion concentration control.

The total number of simulated responses investigated is 320, a number that results from each variation of six different parameters that are allowed to be assigned more than one value. The six variables are: (*i*) sensor choice, of which there are two, (ii) value of the sensor time constant, of which there are five (*iii*) , whether or not noise is injected, for which there are two choices, (*iv*) whether the response is due to a servo or regulation study (these terms are defined later in this section), of which there are two choices, (*v*) whether the disturbance is a step increase or a step decrease, for which there are two choices, and (*iv*) one of four initial operating points. These six variables should be noted, as they are referred to frequently in later sections of the study. Specifically, the time constant of either sensor (*i.e,* τ_{elec} or τ_{opt}) can be values of whole numbers from 1 to 5 seconds, inclusive. In addition, in the case of the servo responses, the initial pH values

are 6, 7, 8, and 9, for step-up responses, and 7, 8, 9, and 10 for step-down responses. Also, for the case of regulation responses, the initial pH values are 7, 8, 9, and 10, while the step-increases and step-decreases in concentration always have a value of ten percent of the original value. Furthermore, it is a primary objective that the responses avoid saturation effects as much as possible, and accordingly, the chosen initial operating points center around the equivalence point of an acetic acid-sodium hydroxide system ($\mathrm{pH} = 8.728$).

An automatic controller is typically required to respond to two types of changes in the system it is charged with controlling. One is known as a servo response, and occurs when the setpoint of the system is changed, and the controller must react properly to move the system form the original operating condition to the new desired operating condition. The second type of response is called a regulation response, and occurs when an uncontrolled system variable (as opposed to the input Q_2 of this system) causes the control variable (in this system, hydrogen ion concentration) to change. Both types of responses can commonly occur, necessitating that both types of responses should be studied.

4.3.1 Noise-Free Closed-Loop Performance

Figure 4-8 depicts the time-domain response of a single combination of variables (*ii*)-(*vi*) as given in Section 4.3 for both an electrode and an optrode. In particular, the time constant for each sensor (i.e., $\tau_{elec} = \tau_{opt}$) has a value of two seconds, and there is no noise injected into the signal. Additionally, curves represent a servo response to a unit step decrease beginning at $\mathrm{pH} = 10$. In the top plot, the closed-loop response of the electrode is given by a continuous line, while the closed-loop response of an optrode is

given by a dash-dot line. Furthermore, the value of the setpoint is also plotted using a dotted line. The bottom plot gives the corresponding input manipulations (*i.e.*, the value of the reagent flowrate Q_2) implemented by the controller, and uses the same line-type convention.

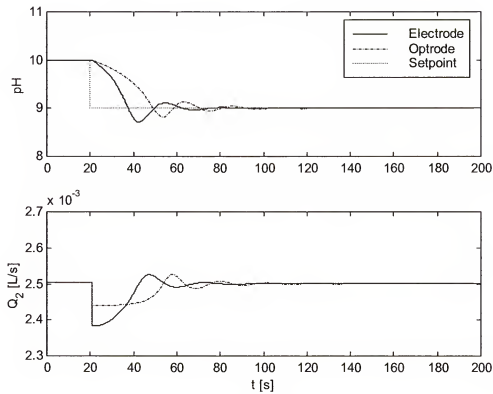

Figure 4-8. Noise-free time-domain servo responses of the electrode (continuous line) and the optrode (dash-dot line) sensors plotted against the setpoint (dotted line) for a unit step decrease in pH beginning at $pH = 10$.

It is clear that in this case, the electrode responds more quickly than does the optrode. While the two responses have approximately the same settling time (*i.e.*, the time required to reach each respective final steady-state), the rise time (*i.e.*, the time it takes to reach the final steady-state for the first time) is much lower for the electrode,

causing additional error to accumulate for the optrode. In fact, this is reflected in the ITAE values, which are 221 for the electrode and 378 for the optrode.

The closed-loop performance defined by the ITAE method is plotted in Figure 4-9 for forty of the responses described in Section 4.3. Specifically, they are noise-free servo responses to step increases. In other words, of the six variables given in Section 4.3, (*i*) and (*ii*) are not fixed, (*iii*) is restricted to the case of no noise, (*iv*) is restricted to the case of servo responses, and (*v*) is restricted to the case of step increases. Finally, each of the four subplots represents (*vi*) one of the four possible initial operating points. Within each subplot, there are two lines plotted. The electrode is depicted by the solid line, and the optimal ITAE value is plotted as a function of the time constant of the sensor, τ. Note that for this sensor, $\tau = \tau_{elec}$. Similarly, the optrode ITAE value is depicted by a dash-dot line, for which $\tau = \tau_{opt}$. Note that the line that is relatively lower represents better performance.

It should be noted that both servo and regulatory responses are grouped into (*1*) steps-up and (*2*) steps-down for clarity. An equally meaningful arrangement based upon the physics of the system might be (*a*) changes that require the controller to drive the system toward the equivalence point, and (*b*) changes that require the controller to drive the system away for the equivalence point. In other words, in general, some of the changes drive the neutralization reaction toward a more sensitive regime (*i.e.,* higher plant gain), while others toward a more sluggish regime (*i.e.,* lower plant gain). Note that this notion holds even for regulation responses, as the disturbance will serve to move the system either toward or away form the equivalence point, and it is the job of the

controller move it in the opposite direction soon thereafter. Trends pertinent to this phenomenon are also discussed.

As shown in Figure 4-9, there are operating regions where either the electrode or the optrode provides better control. Specifically, in subplot (a), the optrode is more effective and in subplot (c), the electrode is more effective. The two measurement devices work almost identically with respect to minimizing the ITAE criterion in subplot (b). Finally, subplot (d) represents a case where the optrode must be significantly detuned to maintain stability at the original operating point (*i.e.,* pH = 9), thereby making it

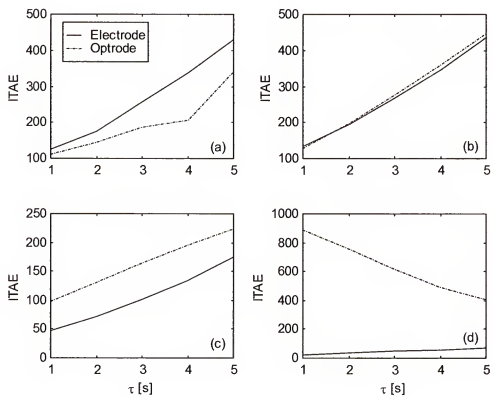

Figure 4-9. Noise-free servo performance of the electrode (continuous line) and the optrode (dash-dot line) sensors for steps increases in pH setpoint. Figure (a) shows a change of pH from 6 to 7, (b) from 7 to 8, (c) from 8 to 9, and (d) from 9 to 10.

extremely sluggish in obtaining the final operating point (*i.e.,* pH = 10). Note that subplots (a) and (b) represent circumstances in which the controller must move the system toward the equivalence point. Finally, subplots (c) and (d) are around the equivalence point and away from the equivalence point, respectively.

The plots shown in Figure 4-10 represent a different set of forty responses than do the plots of Figure 4-9. Specifically, they encompass the cases where the variables (*i*)-(*vi*) of Section 4.3 are the same as give for Figure 4-9, except that (*v*) is now restricted to the case of step decreases.

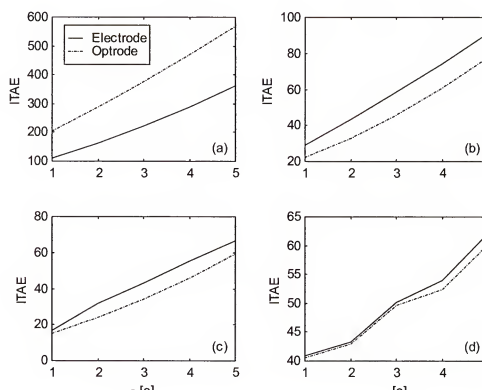

Figure 4-10. Noise-free servo performance of the electrode (continuous line) and the optrode (dash-dot line) sensors for steps decreases in pH setpoint. Figure (a) shows a change of pH from 10 to 9, (b) from 9 to 8, (c) from 8 to 7, and (d) from 7 to 6.

For the set of step-decrease servo responses given in Figure 4-10, similarly to the step-increase trials reported in Figure 4-9, operating regions exist where either probe is more effective at minimizing the error. For example, the electrode is significantly better in the case of subplot (a), which also corresponds to changes that move the system toward the equivalence point. In subplots (b) and (c), however, there is slightly better performance obtained when using the optrode, which are cases of moving toward and around the equivalence point, respectively. Finally, they are very comparable in subplot (d), where the system is being moved away from the equivalence point.

The eight comparisons of closed-loop performance given collectively by Figures

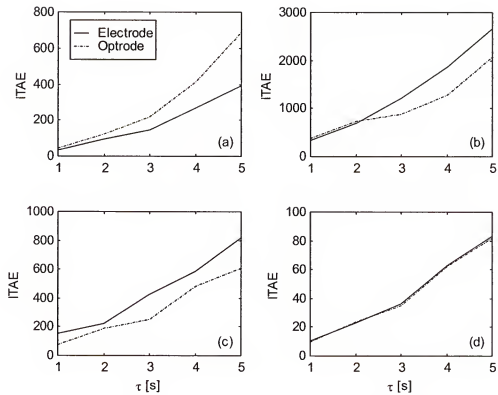

Figure 4-11. Noise-free regulation performance of the electrode (continuous line) and the optrode (dash-dot line) sensors for 10% step increases in influent acid concentration. Figure (a) shows a pH setpoint of 10, (b) 9, (c) 8, and (d) 7.

4-9 and 4-10 do not seem to suggest that an optrode is consistently better than an electrode for servo-response pH control. In fact, each sensor seems to be more effective under certain conditions, although there is no obvious pattern to predict which one will be.

Figures 4-11 and 4-12 have plots analogous to the Figures 4-9 and 4-10, but for the case of regulation trials rather than servo responses (*i.e.*, variable (*iv*) is now restricted to the case of regulation responses). Specifically, Figure 4-11 depicts the ITAE for ten percent increases in influent acid concentration at pH setpoints of (a) 10, (b) 9, (c) 8, and (d) 7. Furthermore, Figure 4-12 reports the ITAE for ten percent decreases in influent acid concentration at pH setpoints of (a) 7, (b) 8, (c) 9, and (d) 10.

For the set of step-up disturbance rejection responses shown in Figure 4-11, the results are inconclusive, with examples of better performance with the electrode, better performance with the optrode, and approximately equal performance. For example, subplot (a) favors use of the electrode, and is indicative of a change that requires the controller to move the system away from the equivalence point. Next, subplots (b) and (c) give the opposite result, indicating that the optrode would be a more effective choice; these changes are around the equivalence point and toward it, respectively. Finally, in (d), there is no substantial difference in error observed from using one probe to the other, with the controller driving the system toward the equivalence point.

Figure 4-12 shows the set of steps-down in influent acid concentration, and similarly to the results for step-up trials, operating regions appear to exist where the electrode or optrode minimizes the error more effectively, or they perform approximately the same. In subplot (a), the two sensors perform almost identically for a case where the

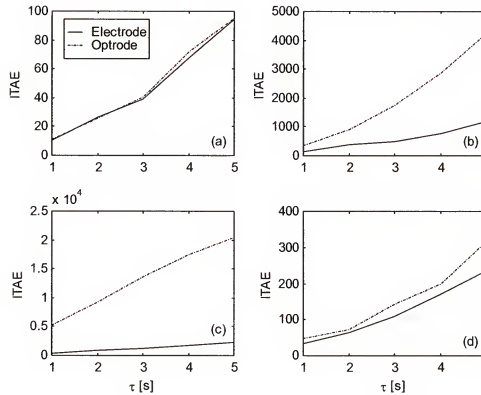

Figure 4-12. Noise-free regulation performance of the electrode (continuous line) and the optrode (dash-dot line) sensors for 10% step decreases in influent acid concentration. Figure (a) shows a pH setpoint of 7, (b) 8, (c) 9, and (d) 10.

disturbance moves the system toward the equivalence point. Next, subplots (b) and (c) clearly indicate that using the electrode is the better choice, and represent changes toward and around the equivalence point, respectively. Finally, subplot (d) indicates a marginal advantage for the optrode, and this for a case that moves the system away from the equivalence point.

Between Figures 4-11 and 4-12, eight comparisons of closed-loop performance are given for disturbance rejection, and similarly to the servo tests, there is no conclusive indication that an optrode performs better than an electrode for pH control. Again, each sensor seems to be more effective under some conditions, and they are approximately

equal under other conditions. Also of note is that in none of the sixteen cases given by Figures 4-9, 4-10, 4-11, and 4-12 does one line cross the other, representing a situation where one sensor surpasses the other in performance as a function of time constant.

4.3.2 Closed-Loop Performance with Realistic Noise

The ITAE trials performed in Section 4.3.2 are repeated with the addition of measurement noise and reported in an analogous arrangement. Therefore, Figures 4-13 and 4-14 represent the identical step-increase and step-decrease servo responses previously described, and Figures 4-15 and 4-16 report the results for step-increase and step-decrease disturbance input concentration. White noise is selected for injection, with magnitude sufficient to ensure that three standard deviations are equal to $\pm$ 0.1 pH units for the electrode and $\pm$ 0.001 pH units for the optrode, as reported by (Garcia-Rubio and Clavette,1991). Finally, the electrode is depicted as a solid line in each case, while the optrode is a dashed-dot line.

The addition of noise is equivalent to saying that the plots shown in Section 4.3.2 depict the cases where variable (*iii*) of Section 4.3 is being restricted to the case where noise is being injected. Therefore, coupled with the fact that Figures 4-13, 4-14, 4-15, and 4-16 otherwise analogously represent the same conditions as Figures 4-9, 4-10, 4-11, and 4-12, the forty responses shown in Figure 4-13 are: (*i*) and (*ii*) are not fixed, (*iii*) is restricted to the case that noise is injected, (*iv*) is restricted to the case of servo responses, and (*v*) is restricted to the case of step increases. Finally, each of the four subplots represents (*vi*) one of the four possible initial operating points.

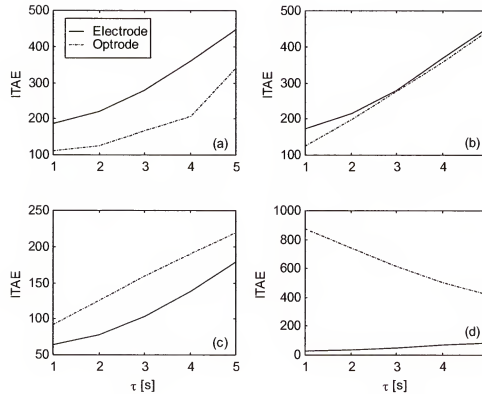

Figure 4-13. Servo performance of the electrode (continuous line) and the optrode (dash-dot line) sensors with realistic noise injected for steps increases in pH setpoint. Figure (a) shows a change of pH from 6 to 7, (b) from 7 to 8, (c) from 8 to 9, and (d) from 9 to 10.

Figure 4-13 illustrates the set of results obtained for step-increase servo responses. Cases exist for operating regions where the electrode provides better control, where the optrode provides better control, and where neither is significantly better than the other. In subplot (a), for a case that represents a move toward the equivalence point, the optrode is clearly superior. Moving into a region closer to the equivalence point, but still moving toward it, subplot (b) illustrates a case where the two probes are comparable. Next, subplot (c) centers around the equivalence point, and the electrode is favored. Finally, in subplot (d), the optrode suffers from instability at the original operating point (*i.e.,* pH = 9) unless it is detuned; hence (d) should be ignored.

The forty optimization represented in Figure 4-14 are determined by using the same values of the six variable (*i*)-(*vi*) given in Section 4.3 used to obtain Figure 4-13, except that (*v*) is restricted to cases of step decreases only.

In subplot (a) of the set of step-decrease servo responses given in Figure 4-14, which is indicative of a perturbation that drives the system toward the equivalence point, the electrode is shown to minimize ITAE more effectively. In subplots (b) and (c), behavior is observed not previously seen in this study. Specifically, the time constant of the sensors determine which is the better choice. For each, the optrode is indicated to exhibit better performance for low values of the time constant, but the electrode is

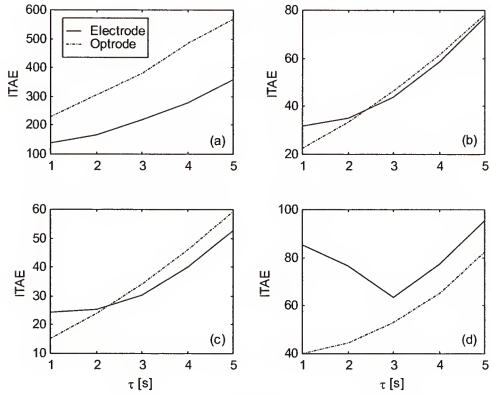

Figure 4-14 Servo performance of the electrode (continuous line) and the optrode (dash-dot line) sensors with realistic noise injected for steps decreases in pH setpoint. Figure (a) shows a change of pH from 10 to 9, (b) from 9 to 8, (c) from 8 to 7, and (d) from 7 to 6.

indicated at higher values of the sensor time constant. Note that (b) is in the region around the equivalence point (pH = 8.728) and (c) is a region where pH is moving away from the equivalence point for the described simulation. Finally, subplot (d) suffers from instability in much the same way that Figure 4-13 does, rendering it inconclusive.

It is observed that in the presence of noise, certain conditions can result in unstable behavior of the neutralization system. Therefore, some trials must be discarded, resulting in fewer meaningful comparisons. The six useful comparisons of closed-loop performance given collectively by Figures 4-13 and 4-14 do not suggest that an optrode

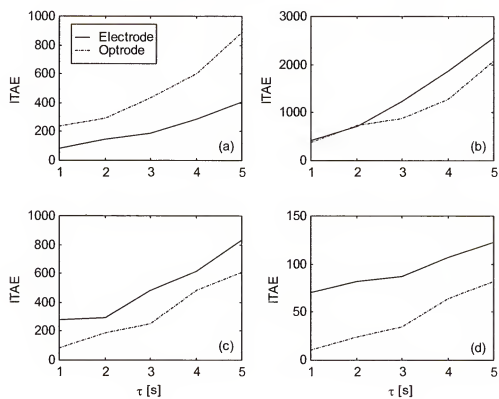

Figure 4-15. Regulation performance of the electrode (continuous line) and the optrode (dash-dot line) sensors with realistic noise injected for 10% step increases in influent acid concentration. Figure (a) shows a pH setpoint of 10, (b) 9, (c) 8, and (d) 7.

performs better than an electrode for pH control. In fact, each seems to be more effective under certain conditions, although there is no obvious pattern evident that can be used to predict which sensor should be more effective. Furthermore, there are two cases in which the sensor time constant plays a critical role. Note that in Figure 4-14 (b) and (c), the electrode is less effective only in the regime of fast sensor response; this can be attributed to the fact that measurement noise plays a larger role in performance degradation under those conditions. Figures 4-15 and 4-16 have plots analogous to the Figures 4-13 and 4-14, but for the case of regulation trials rather than servo responses (*i.e.*, variable (*iv*) is now restricted to the case of regulation responses). In other words, Figure 4-15 depicts the ITAE for ten percent step increases in influent acid concentration for beginning pH values of (a) 10, (b) 9, (c) 8, and (d) 7. Similarly, Figure 4-16 reports the ITAE for ten percent step decreases in influent acid concentration for beginning pH values of (a) 7, (b) 8, (c) 9, and (d) 10. Finally, the optrode minimum error is represented by the dotted line, while the electrode minimum error is represented by a solid line.

The set of step-increase disturbance rejection responses shown in Figure 4-15 represents the first indication of an obvious trend to this point in the simulation study. First, subplot (a) must be ignored, since it also suffers from instability problems. Consequently, subplots (b), (c), and (d) remain, and each indicates that the optrode is better able to minimize the ITAE, despite the fact that conditions moving both toward and away from the equivalence point are represented.

The set of step-decrease servo responses with noise are given by Figure 4-16, and contain examples that indicate that either the optrode or electrode can perform better, depending upon the conditions. For example, the neutralization process is moving

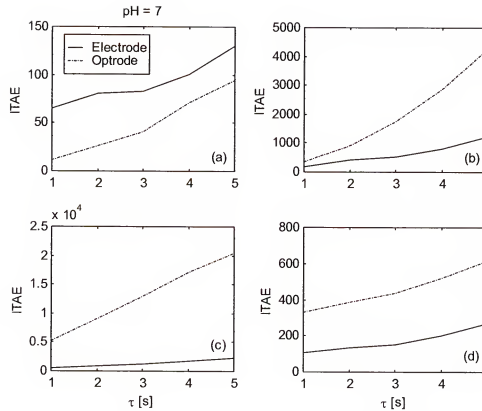

Figure 4-16. Regulation performance of the electrode (continuous line) and the optrode (dash-dot line) sensors with realistic noise injected for 10% step decreases in influent acid concentration. Figure (a) shows a pH setpoint of 7, (b) 8, (c) 9, and (d) 10.

toward the equivalence point in subplot (a), and the optrode is a significantly better choice. However, in subplots (b) and (c), the electrode is preferable for conditions representing a controller moving the system toward and around the equivalence point, respectively. Finally, (d) is ignored due to stability problems.

Between Figures 4-15 and 4-16, six meaningful comparisons of closed-loop performance are given for regulation, and similarly to the six meaningful servo tests, there is no suggestion that an optrode performs better than an electrode for pH control, even given a significantly lower level of measurement noise. Instead, the speed with which the sensor responds (*i.e.,* the sensor time constant) appears to be at least as critical.

Finally, it is observed that the injection of noise can cause the optrode to exhibit superior performance to that of the electrode in the case of very fast sensor response when it would not otherwise; this behavior is a product of the proportionally larger effect noise has on performance when response characteristics are fast.

4.4 Design of an Experimental System

An important aspect of validating simulation results is being able to confirm them with real data. To do this, an experimental pH control is constructed. Then a sensor is wired to a computer with data acquisition capabilities and control-capable software. Finally, the computer is wired to the control valve of the reagent stream. In addition, the proper algorithms are written and implemented with the software.

There are two important reasons for developing the simulation model parallel to the experiment setup. First, no optical sensor is available. Therefore, only simulations are possible for that portion of the project. However, if experiments with an electrode

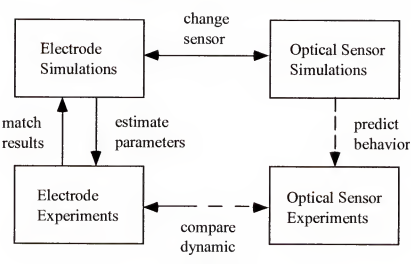

Figure 4-17. Flow diagram of a proposed way to compare dynamic response of the sensors with no optical sensor available.

match simulations using an electrode model, and the models for the sensors are developed with equal care, extrapolation can be made with confidence about the behavior of the system under control using an optical sensor. The process is illustrated as a flowchart in Figure 4-17.

The second reason for relying upon simulations is efficiency. They are less expensive, less dangerous, and much faster. Troubleshooting can be done in simulation, greatly speeding the processes of controller tuning and studying system behavior at a variety of operating points. It is only then that real experiments are performed to confirm the simulation results.

4.4.1 Apparatus

4.4.1.1 Experimental hardware

The core of the experimental setup is a pre-manufactured unit made by Armfield and designated PCT 16 (pH control accessory). A schematic of the equipment is shown in Figure 4-18. The most important components are the sump tanks, pumps, flow meters, control valve, impeller, and mixing tank.

The process begins with effluent being present in the left tank and reagent in the right tank. Pumps with recycle streams send a steady flow of each through separate flow meters. The flow meter for the effluent is adjusted to allow the desired flowrate. Dissimilarly, the flow meter for the reagent is adjusted to allow the maximum desired flowrate. The effluent then passes directly to the mixing tank. The reagent, however, goes through the control valve before it reaches the tank. The control valve is capable of receiving instructions from a controller that will further restrict the flow to the desired

rate. Finally, the mixture is agitated in the tank, and overflows to a drain as more fluid arrives.

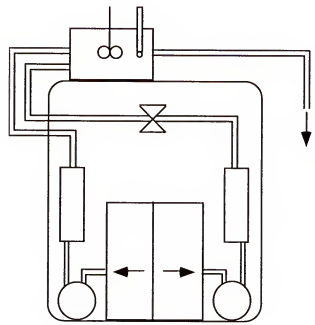

Figure 4-18. Schematic of the pH control experimental apparatus.

4.4.1.2 Computer hardware, data acquisition, and power supply

The computer used to run the software and send and receive data is a Macintosh Quadra 700 fitted with a PowerPC upgrade card. The electrical signals passing to and from the computer are managed by a National Instruments NB-MIO-16X data acquisition card (DAQ). Finally, a custom-built external power supply is need for two tasks—amplifying the signal from the DAQ to the control valve and transforming the power source for use by the impeller. The physical setup is shown in Figure 4-19.

For the chosen application, the output signals from the controller (computer) are voltages sent to the control valve of the experimental apparatus. They are generated by the algorithms programmed into the software, and are based upon the input signals. In

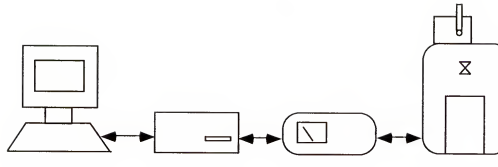

Figure 4-19. Physical setup of experimental equipment for pH control.

this system, the input signals to the controller are readings sent from the measurement device—the pH electrode.

4.4.1.3 Computer software

National Instruments also produces Labview (version 3.0), the software used for programming the computer with the control software. During construction and operation, the program presents the user with two windows for each file. The first step is to select the flow diagram screen (the window mostly used during construction) and code in the transfer function for a PI controller

$$u(k) = K_C\left[1+\frac{\Delta t}{\tau_I}\frac{z}{z-1}\right]e(k) \tag{4-39}$$

where Δt is the sampling interval in seconds (s), z is the complex z-domain argument (a shift operator), and K_C and T_I are the same as defined in Section 4.2 (Seborg *et al.,* 1989). To put this in a form immediately usable by Labview requires an input and an output

$$u(k) = K_C\left[1+\frac{\Delta t}{\tau_I}\frac{z}{z-1}\right]e(k) \tag{4-40}$$

Applying the shift operator

$$u(k) = K_C\left[e(k) + \frac{\Delta t}{\tau_I}\sum_{i=1}^{k} e(i)\right] \tag{4-41}$$

where k denotes the k-th sample, e(k) is the error (input) signal at sample k, u(k) is the signal calculated by the algorithm (output) at sample k, and other values are defined above.

4.4.2 Measurement Noise Analysis

4.4.2.1 Signal assessment

Measurements recorded with an electrical signal frequently suffer from the effects of noise. The experimental apparatus described in Section 4.4.1 utilizes such

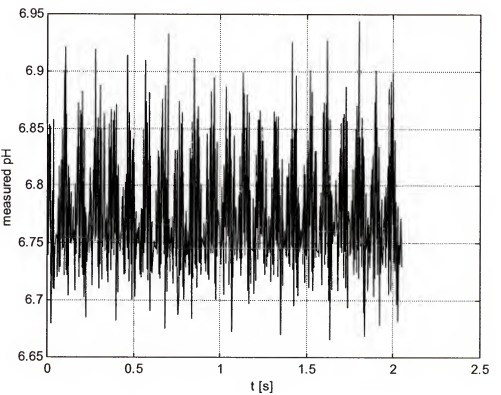

Figure 4-20. Noisy (raw) pH signal originating from the pH meter.

measurements, and a typical signal seen by the computer for a seemingly stable value of pH displayed by the pH meter is shown in Figure 4-20

It is, of course, desirable to reduce the amount of noise in the signal. First, the nature of noise must be investigated. With the results, it is possible to choose the method most appropriate for reducing it. Because noise can most effectively be filtered if it is random, identification and attenuation of non-random signals is the first step. Figure 4-21 shows the power spectral density (found by taking the Fourier Transform of the data to convert it to frequency domain representation) of the noisy signal in Figure 4-20. The actual value of each power is not particularly meaningful; it is the relative area under each spike that is of importance.

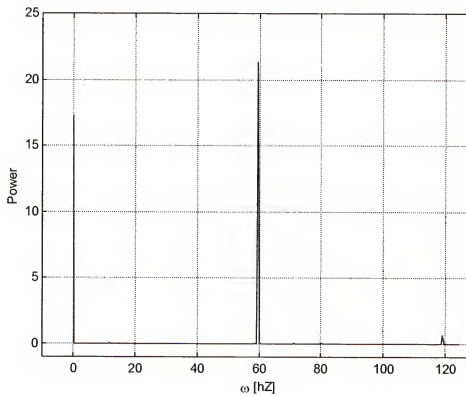

Figure 4-21. Power spectral density of the noisy signal in Figure 4-20.

There are essentially two signals, one at 0 hertz (Hz), or cycles per second, and the other at approximately 60 hertz. The signal at 0 Hz is the constant signal that is desired, while the 60 Hz signal is noise being introduced. Because the alternating current of the power supply runs at or near 60 Hz, this result is quite plausible. If a low-pass filter can be designed to eliminate or minimize the 60 Hz component, the random nature of the remaining signal can be confidently assumed. There are two main categories of filters—hardware and software, and each are explained further in turn.

4.4.2.2 Hardware filtering

Before the signal ever gets to the computer, it is possible to condition the signal using basic electronic components—resistors, capacitors, etc. While more complicated schemes are possible, a traditional RC (resistor-capacitor) circuit is chosen for its simplicity and ease of analysis. Essentially, they are low-pass filters with a cutoff frequency equal to RC. The unit of R is ohms, and the unit of C is Farads, the product of which is frequency in hertz. The physical configuration of an RC circuit is illustrated in Figure 4-22. The attenuation rate of the filter is smooth and continuous, so the 60 Hz signal is not completely eliminated. However, it drops off sharply at higher frequencies, so appropriate selection of the term RC can ensure adequate performance. Additionally, because there is no voltage (signal) drop across the filter, multiple filters in series can be employed without adverse effects. In this case, a cutoff frequency of 10 hertz is selected,

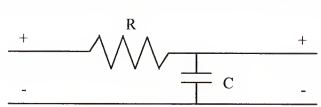

Figure 4-22. Schematic representation of an RC circuit.

and two such filters are used.

Although the signal appears unchanged to the naked eye in the time domain, Figure 4-23 proves that the contribution of the 60 Hz signal is greatly reduced.

Using an RC circuit has both advantages and disadvantages. First, they are of negligible cost, and extremely easy to implement. Second, they do not introduce any time delay to the system. However, they must appear before the DAQ component, meaning there will always be the potential for some signal corruption after it has been filtered. Finally, the discharging of the capacitor causes spikes in the reading (refer to Figure 4-3).

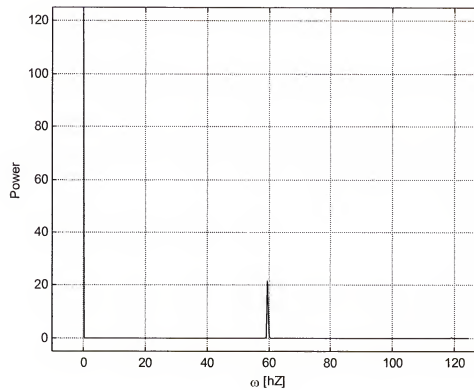

Figure 4-23. Power spectral density of the noisy signal in Figure 4-20 after RC filtering.

4.4.2.3 Software filtering

After the signal is delivered to the computer, there are additional ways to condition the signal that is ultimately sent to the controller. They are software filters, and two of the most basic types are considered—exponential and moving average. They are similar in concept, using some type of arithmetic average of a predetermined number of data points. When the associated parameters are chosen carefully, the result is a significantly smoothed version of the incoming data stream. See Appendix J for the equations of each, as well as qualitative visual representations of how they affect a raw set of data.

Using algorithms in the control software can help alleviate some of the shortcomings of hardware filtering. Because the signal has already been digitized, additional noise further downstream is not a consideration. In addition (for the same reason), the spikes in a signal that has been filtered continuously can be smoothed. Unfortunately, even though they are also inexpensive and easy to use, they introduce the most critical problem not present with a hardware filter—delay. There is no way to circumvent it, since each must spend a finite amount of time waiting on sufficient data to arrive before it can make the calculation. As a result, selection of the filter parameter (each has one) represents a tradeoff between smoothness and introduced delay.

The final decision of which type to use is made from experience, when experiments on the actual system indicate which type tends to achieve the best smoothness/delay compromise. In this case, preliminary results appear to show that a moving average filter will work more effectively; however, this is open to scrutiny, and could be amended as the experimental design evolves.

4.5 Conclusions

The simulation portion of the work is complete. A representative group of both servo responses and disturbance rejection responses have been performed for both the novel optical pH sensor and the traditional pH electrode. Furthermore, each was simulated for multiple values of sensor time constant. Tuning was done for each individual case via trial-and-error to ensure the best settings for that particular trial, based upon ITAE as the performance criterion.

The optical sensor is not consistently observed to guarantee better closed-loop performance when compared to the traditional pH electrode. In fact, there is a significant number of cases where the electrode is a better choice. While it is generally accepted that an entirely linear system (*i.e.,* controller, plant and sensor) is the easiest to control, the plant in this case is highly non-linear. The results to this point support the speculative idea that a linear sensor will not always provide the best control performance for a non-linear plant. Rather, a non-linear sensor that is non-linear in precisely the proper way may serve to somewhat 'cancel' the non-linearity of the plant under certain circumstances, thus creating a more linear overall system. This hypothesis, if proven correct, could theoretically be applied to other, unrelated, non-linear systems in order to improve performance.

Another possibility that may explain the results is that pH units are the basis of reference for the error criteria, as discussed for (4-38). These units were chosen because most rules concerning the allowable hydrogen ion concentration in a process stream are written in terms of pH; this is natural given that pH is the units being measured in such streams. However, the true issue is whether one hundred times the desired hydrogen ion concentration is really only twice as large an error as ten times the desired hydrogen ion

concentration (*i.e.,* in ITAE, an error of two pH units is weighed twice what an error of one pH unit is weighed for the same instant in time). If quality standards were revised to be expressed in the true unit of interest—hydrogen ion concentration—a similar study might reveal a clearer indication that the fiber-optic linear sensor is indeed consistently a better choice for closed-loop pH control than is a pH electrode.

Despite the lack of obvious superiority for either sensor, a number of conclusions can be made about the linear, optical sensor and its potential. First, the time constant plays a critical role with respect to performance for both sensors, so the optical sensor can yield a clear advantage to the electrode if it can be designed to respond quickly. Also, at the very least, an optrode whose output is converted to pH units would perform better than an electrode simply due to the lower measurement noise associated with it. Finally, the tunings for the electrode vary far more over a given operating range than do those of the optical probe; for applications where the controller tunings cannot be adapted in real-time efficiently, the fiber-optic sensor will provide better control as the operating point changes dynamically.

CHAPTER 5
CONCLUSIONS AND FUTURE WORK

A wastewater disinfection reactor that utilizes chlorine has been realistically modeled. A standard cascade control system is recommended to reject the effect that ammonia demand has on residual chlorine levels. However, many possible master controller algorithms fail to deliver the desired outlet chlorine concentration when the flow rate through the plant varies significantly. It is proposed that a supplemental control loop is required, where a residence time controller (RTC) manipulates the volume of the reactor, thereby dramatically increasing the effectiveness of the cascade system. Finally, the RTC can be implemented in either feedforward or feedback form, and the appropriate choice is application-specific.

Better control behavior and a minimum average 25-30% annual reduction in the amount of chlorine used can be expected by implementing this technology. For an 8 million gallon-per-day (8MGD) plant, the dynamic weir system can save the treatment plant approximately 32 US tons per year over the fixed-weir design. And this is the potential from flow equalization and a conservative residence time set point (3600 s) alone. Florida regulations, for example, require only 900 s of contact time, promising the possibility of more chlorine savings with a lower RTC set point. Finally, since much less outlet chlorine concentration fluctuation is seen with the dynamic weir implementation, the set point (*i.e.,* presently 2 ppm) can be moved closer to the minimum stipulated by the regulation (*i.e.,* 1 ppm in this case). Taken together, the aforementioned strategies can accomplish an even more dramatic chlorine savings. For example, for the same 8 MGD

plant, if the outlet concentration set point is fixed at 1.2 ppm and the residence time set point is fixed at 1800 s, the yearly total chlorine would then becomes approximately 52 US tons, representing a savings of up to 45%. This is possible because the volume of the chlorine contact basin is adjusted in real-time, and the chlorine dosage system is always operated optimally. In other words, wastewater is generally not retained within the reactor longer than necessary, consuming excessive chlorine, as is the case with a fixed-weir structure. Furthermore, high chlorine dosages that result in the formation of carcinogens can also be eliminated. Finally, a plant that uses less chlorine has a proportionally lower chlorine storage requirement, which helps promote a safer environment at the treatment facility.

Future work in this area of research would certainly involve experimental trials. To do so, the permission of regulatory bodies such as the EPA would be the first step. Next, a suitable wastewater treatment plant would need to be identified, and the moving weir installed. The effectiveness of the new control strategy could then be evaluated. It should be noted that pilot-scale trials are not recommended, since the scalability of a key dimensionless parameter of the system, the Froude number, would be difficult to preserve through any significant reduction in reactor size.

The derivation of run-to-run proportional-integral controllers is presented. With knowledge that robustness is described by a gain margin, a set of tuning heuristics is given for static plants with significant delay. With them, stable plant behavior can be guaranteed. In contrast, when a Smith Predictor is used to attempt to improve performance for this type of system, instability is observed even for small modeling error.

When a Smith Predictor is used, it is observed that this type of system can actually go from an unstable state to a stable one (and back again) as the difference between true measurement error and the estimated error of the Smith Predictor increases. Therefore, it is concluded that at least one root of the characteristic equation of the system with a Smith Predictor migrates in and out of the stable region for monotonically increasing error in delay. More importantly, even a mismatch in delay of only one unit can cause instability. Therefore, unless the delay of the system is known with certainty in real time, it is recommended that simple PI control be used for run-to-run static systems with significant delay.

To further develop this work, a comprehensive study of the behavior of the roots of the characteristic polynomial may be helpful in finding ways to modify the controller to be more robust with a Smith Predictor. Without that development, it is necessary to use more traditional control approaches, even though performance will be limited. A possible starting point may be to study the discrete analog of the findings of (Adam *et al.,* 2000), who have shown that discrete stability ranges exist for a Smith Predictor applied to a continuous system with an uncertain time-delay parameter. In their work, the frequency response in the Nyquist plane is shown to rotate about the origin as the delay value varies, which can alter the number of encirclements of the critical point (Latchman and Crisalle, 1995), which is a parameter that is central to the stability of a continuous system.

The closed-loop dynamic behavior of a CSTR for effluent pH control has been modeled with both a traditional pH electrode sensor and a fiber-optic sensor with a linear response to hydrogen ion concentration. Furthermore, a representative group of both

possible responses were performed over a realistic range of sensor time constant. Each trial was tuned individually based upon the ITAE performance criterion. When compared for the same sets of operating conditions, there is no indication that the linear optical sensor performs better than the traditional pH electrode. In addition, there are certain circumstances where the electrode is clearly more effective.

It is widely accepted that the neutralization process is highly non-linear, and the results suggest that substituting a linear measurement device into the control loop is, at best, only a partial remedy for the control-degrading non-linear nature of the system. In fact, a non-linear sensor with just the proper characteristics may better produce a quasi-linear composite system, although describing the necessary characteristics precisely would be challenging.

An additional explanation for the result that the optical sensor is not clearly superior to an electrode may come from the fact that their performance is judged in terms of pH units. If error were calculated in terms of hydrogen ion concentration, and the loops retuned accordingly, more obvious performance trends may manifest themselves. Regardless, there are a few clear conclusions that can be made about the behavior of the fiber-optic sensor with respect to a traditional electrode. For example, the time constant is critical to one measurement device outperforming the other, so a sufficiently fast response characteristic would be required to choose one over the other. Also, it may be possible to simply convert the output of an optrode to pH units, thus exploiting the advantage of lower measurement noise, with no other source of difference in their respective responses.

Future work for this area of investigation may involve changing the definition of the error for the purpose of ITAE calculation. In terms of hydrogen ion concentration, one sensor or the other may prove itself to be clearly superior in closed-loop performance tests. Additionally, experimental trials should be performed to verify that the closed-loop system behaves as predicted for each of the sensors. With experimental results, the conclusions drawn from the simulation study would be validated, and additional ways to exploit the nature of linear fiber-optic pH sensors could be investigated.

APPENDIX A
DISTRIBUTED PARAMETER EQUATION DERIVATION

This appendix presents a detailed derivation of the PDE that describes a PFR given in Section 2.2.4. It begins with a conservation of mass balance, and uses the result in a shell balance around a small portion of the reactor. Finally, it takes the limit as the incremental volume approaches zero. By the very derivation that results in a PDE, the reverse process (use of difference equations to approximate one differential term) is concluded to be a plausible alternative expression.

Consider a small section of the reactor

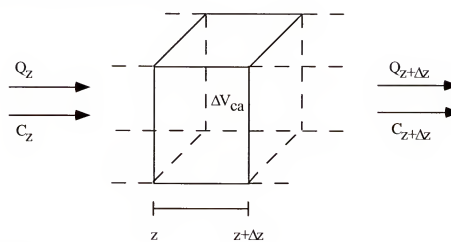

Mass Balance

Beginning with an overall mass balance

$$\frac{d(\rho \Delta V_{ca})}{dt} = \rho Q_z - \rho Q_{z+\Delta z} \tag{A-1}$$

Using the fact that input flow rate is equal to output flow rate for this system

$$Q_z = Q_{z+\Delta z} \tag{A-2}$$

Substituting (A-2) into (A-1) and simplifying

$$\frac{d(\rho \Delta V_{ca})}{dt} = 0 \tag{A-3}$$

$$\rho \Delta V_{ca} = \text{constant} \tag{A-4}$$

Noting that water is incompressible

$$\rho = \text{constant} \tag{A-5}$$

$$\therefore \Delta V_{ca} = \text{constant} \tag{A-6}$$

Shell Balance

Performing a shell balance around a small portion of the reactor

$$\frac{d[C\Delta V_{ca}]}{dt} = [CQ]_z - [CQ]_{z+\Delta z} + r_{rxn}\Delta V_{ca} \tag{A-7}$$

$$r_{rxn} = -k_{rxn}C \tag{A-8}$$

$$\Delta V_{ca} = A\Delta z \tag{A-9}$$

where A is the cross-sectional area

$$\frac{dC}{dt}A\Delta z = Q[C_z - C_{z+\Delta z}] - k_{rxn}CA\Delta V_{ca} \tag{A-10}$$

$$\frac{dC}{dt} = -\frac{Q}{A}\frac{[C_z - C_{z+\Delta z}]}{\Delta z} - k_{rxn}C \tag{A-11}$$

Let

$$\frac{Q}{A} = v \tag{A-12}$$

where v is the velocity of the fluid. Taking $\lim_{\Delta z \to 0}$ yields a PDE

$$\frac{\partial C}{\partial t} = -v\frac{\partial C}{\partial z} - k_{rxn}C \qquad \text{(A-13)}$$

Because the equation is based upon the differential volume model, it is logical that it can be approximated by a large number of extremely small reactors.

APPENDIX B
PERFORMANCE ASSESSMENT OF THE STANDARD
FEEDBACK CONTROL CONFIGURATION

This appendix contains information related to simulations using standard feedback control, including the block diagram, open-loop response of the plant, controller tunings, and closed-loop response. It is concluded in the text of the report that cascade control should be more effective, and the information below bears this out. As a result, the details related to standard feedback are omitted from the body of the text, and are presented below.

The block diagram for a standard feedback system (Figure B-1) is very similar to the one given for a cascade feedback system shown in Figure 2-6 of the main text. All variables given are the same as those listed for the cascade system in Section 2.4

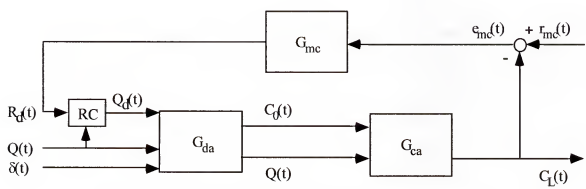

Figure B-1. Block diagram of a wastewater treatment plant under standard feedback control (in addition to a ratio controller).

When the derived models of the dosing area and contact are used for G_{da} and G_{ca}, and the controllers are turned off, the following open-loop response is obtained

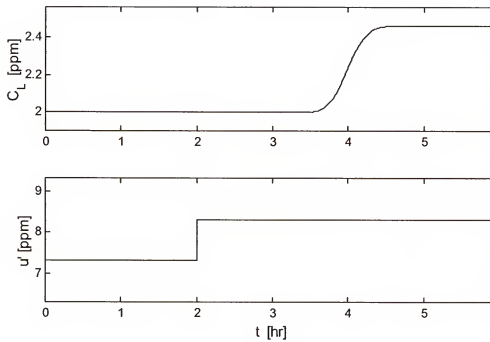

Figure B-2. Open-loop response of the entire plant when subjected to a step change in dosing rate Q_dC_d from 2.926 m^3/s to 3.326 m^3/s at time 2 hr.

The response shown in Figure B-2 is then fit to a FODT model exactly as those in Sections 2.4.1 and 2.4.2, and the resulting tuning parameters (also found through trial-and-error) are listed in Table B-1

Table B-1. Estimated transfer function parameters for the entire plant and resulting master controller parameters found by trial-and-error tuning.

Transfer Function Parameters	Numerical Value	Controller Parameters	Numerical Value
K^*_{ca}	1.16 ppm-s/g	K_{mc}	0.0003 g/ppm-s
τ^*_{ca}	850 s	τ_{mc}	2000 s
θ^*_{ca}	6430 s		

It happens that these are the tunings found for both a PI master controller and a PI master controller with a Smith Predictor. This in unusual, since a Smith Predictor usually

allows the operator to make the tuning parameters more aggressive; verification of this result is addressed in Section 2.6. Using these tuning parameters, the closed-loop performance of the standard feedback scheme is compared to that of a cascade scheme (using parameters given in Section 2.4.2) for a sinusoidal disturbance in ammonia chlorine demand, $\delta(t)$. The results are given in Figure B-3; note that Q(t) was held constant at 0.4 m^3/s.

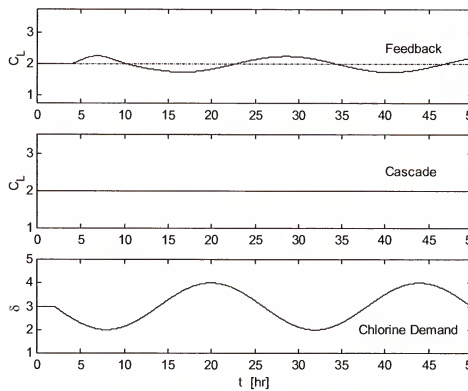

Figure B-3. Closed-loop comparison of a feedback control scheme versus a cascade control scheme for a sinusoidal disturbance in ammonia chlorine demand, $\delta(t)$.

Furthermore, the response of the system under feedback control is virtually the same regardless of what type of master controller is used. It is clear in Figure B-3 that, while the feedback control is not bad, the cascade control is clearly superior. It is for this

reason that it has been eliminated from consideration in the study as a viable control scheme.

APPENDIX C
REVIEW OF THE OPERATION OF A DISCRETE CONTROLLER
APPLIED TO A CONTINUOUS SYSTEM

Figure C-1 illustrates how a continuous output signal in the first plot is sampled every Δt time units. That value is passed to the digital control algorithm (3-6), which requires ε (note that this ε is different from $\varepsilon(k)$, the error of batch k) time units to calculate and implement the new input. A zero-order hold is then used to continue the input until a new value is calculated and implemented at the end of the next iteration.

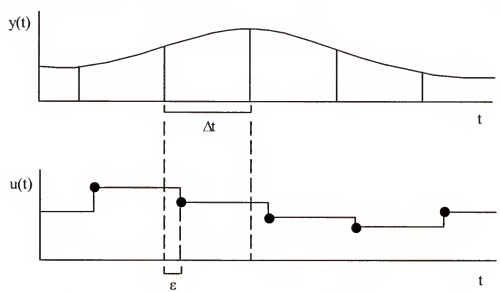

Figure C-1. Graphical representation of the implementation delay of a discrete controller.

Clearly, it is important for $\varepsilon << \Delta t$ to ensure that the approximation: $u(k+\varepsilon)$ is valid; given the speed of a typical digital computer this condition is easy to guarantee.

APPENDIX D

CONDITIONS FOR WHICH THE TRANSFER FUNCTION (3-8) HAS UNSTABLE POLE-ZERO CANCELLATIONS

The purpose of this appendix is to show that there are no unstable pole-zero cancellations for the transfer function

$$\frac{K_C\left(\frac{1}{z}+R_I\frac{1}{z-1}\right)K_P}{1+K_C\left(\frac{1}{z}+R_I\frac{1}{z-1}\right)K_P z^{-D}}=0$$

which is shown as (3-8) in the main body of the text. Multiplying through by the term $z(z-1)z^{-D}$ and rearranging terms yields the rational function

$$\frac{K_C K_P(R_I+1)z^{D+1}-K_C K_P z^D}{z^{D+2}-z^{D+1}+K_C K_P(R_I+1)z-K_C K_P}=0 \qquad \text{(D-1)}$$

Further factoring out the term $K_C K_P(R_I+1)$ gives

$$K_C K_P(R_I+1)\frac{\left(z-\frac{1}{R_I+1}\right)z^D}{z^{D+2}-z^{D+1}+K_C K_P(R_I+1)z-K_C K_P}=0 \qquad \text{(D-2)}$$

Recognizing that $R_I \geq 0$, it follows that there may be a zero on the unit circle only when $R_I = 0$.

Consider the cases (i) $R_I > 0$, and (ii) $R_I = 0$.

(i) If $R_I > 0$, then $0 < \frac{1}{R_I+1} < 1$ and the zero of (D-1) is strictly inside the unit circle. This zero cannot therefore be cancelled with an unstable pole.

(ii) If $R_I = 0$, there is a zero of (D-1) at $z = 1$, exactly on the unit circle. Now let $P(z) = z^{D+2} - z^{D+1} + K_C K_p (R_I + 1)z - K_C K_p$ and after recognizing that $P(1) = 0$ when $R_I = 0$, it follows $z = 1$ is also a pole of (D-1). Therefore, it can be concluded that there is always an unstable pole-zero cancellation if $R_I = 0$. Checking for repeated poles at $z = 1$, divide P(z) by $(z = 1)$ to obtain

$$P'(z) = \frac{z^{D+2} - z^{D+1}}{z-1} + \frac{K_C K_p (R_I + 1)}{z-1} z - \frac{K_C K_p}{z-1} \qquad \text{(D-3)}$$

Evaluating at $R_I = 0$ yields

$$P'(z) = \frac{z^{D+2} - z^{D+1}}{z-1} + K_C K_p \frac{z}{z-1} - \frac{K_C K_p}{z-1} \qquad \text{(D-4)}$$

or

$$P'(z) = z^{D+1} + K_C K_p \qquad \text{(D-5)}$$

Now since $P'(1) = 1 + K_C K_p$, it follows that $z = 1$ is a duplicated zero P(z) when $R_I = 0$ if and only if $K_C K_p = -1$. However, the first necessary condition of the Jury Test strictly requires that

$$\left| K_C K_p \right| < 1$$

so the Jury Test will always determine whether or not the system under consideration is stable provide that $R_I \geq 0$.

APPENDIX E

VALUES OF α AND β FOR THE 2-PARAMETER CURVE FITS OF THE FUNCTIONS GENERATED BY THE JURY TEST

Delay	Alpha	Beta
0	0.0700	89.2029
1	0.0800	85.3576
2	0.1100	67.1585
3	0.2239	25.1400
4	0.3502	14.874
5	0.7502	4.6984
6	0.9003	4.2589
7	1.106	3.6091
8	1.3046	3.2504
9	1.7642	2.2637
10	2.0646	2.0139
11	2.2345	2.0286
12	2.4063	2.0380
13	2.5717	2.0566
14	2.7430	2.0617
15	2.9119	2.0703
16	3.0820	2.0784
17	3.2550	2.0800
18	3.4226	2.0880
19	3.6014	2.0831
20	3.7728	2.0875

APPENDIX F
CONDITIONS FOR WHICH THE TRANSFER FUNCTION (3-38) HAS UNSTABLE POLE-ZERO CANCELLATIONS

The purpose of this appendix is to show that there are no unstable pole-zero cancellations for the transfer function (3-38) of a SISO static run-to-run system with measurement delay and a Smith Predictor. Equation (3-38) shows that the numerator of the transfer function is the same as for the case when no Smith Predictor is employed. Therefore, according to Appendix D, we must find conditions under which $z = 1$ is a root of the characteristic equation when $R_1 = 0$. Beginning with the characteristic equation (3-40)

$$z^{D^0+D+2} + [K_C K_P^0 (R_1 + 1) - 1] z^{D^0+D+1} - (K_C K_P^0) z^{D^0+D} - [K_C K_P^0 (R_1 + 1)] z^{D+1} + (K_C K_P^0) z^D + [K_C K_P (R_1 + 1)] z^{D^0+1} - (K_C K_P) z^{D^0} = 0$$

set $R_1 = 0$, factor out $(z-1)$, and then set $z = 1$ in all remaining terms

$$\left(1 + K_C K_P^*\right) - K_C K_P^* + K_C K_P = 0 \tag{F-1}$$

Solving this expression for zeros yields

$$1 + K_C K_P = 0 \tag{F-2}$$

Applying the first condition (3-17) of the Jury Test to (3-40) shows that the root $K_C K_P = -1$ is forbidden. There are there possible cases of the value of a_n, depending upon the value of D. Consider the cases (i) $D = D^0$, (ii) $D < D^0$, and (iii) $D > D^0$.

(i) If $D = D^0$, then the final four terms cancel each other, and the *third* term in (3-40) becomes that with the lowest power of z, therefore its coefficient

$(-K_C K_P)$ is by definition a_n.

(ii) If $D < D^0$, then the *fifth* term in (3-40) becomes that with the lowest power of z, therefore its coefficient $(K_C K_P)$ is by definition a_n.

(iii) If $D > D^0$, then the *seventh* term in (3-40) becomes that with the lowest power of z, therefore its coefficient $(-K_C K_P)$ is by definition a_n.

For any of the cases, the necessary condition (3-17) states that $|K_C K_P| < 1$. Allowing the statement (F-2) to be true would violate the condition, proving that there are no unstable pole-zero cancellations that could alter the conclusions of testing the roots of the characteristic equation for location relative to the unit circle.

APPENDIX G
REVIEW OF WEAK ACID-STRONG BASE CHEMISTRY

By definition, when a weak acid or base is dissolved in water, its molecules always exist in (at least) two states, protonated and unprotonated. (Molecules that can donate or accept multiple protons have additional, partially protonated states.) The relative abundance of the two states is related through the dissociation constant, K. For a weak acid, it is designated K_a (for a weak base, K_b), and is defined the equation

$$K_a = \frac{[H^+][A^-]}{[HA]} \tag{G-1}$$

where K_a is a constant related to a particular acid, [HA] is that acid, $[A^-]$ is the conjugate base of that acid, and $[H^+]$ are free existing hydrogen ions; all are concentrations measured in moles per liter (mol/L). [For each additional proton a multiprotic acid or base can have, there is similar, additional K value.] The basis for this definition is Le Chatelier's Principle

$$[HA] \Leftrightarrow [H^+] + [A^-] \tag{G-2}$$

which states that a change in the concentration of any of the species will cause a shift in the equilibrium to exactly preserve a constant ratio (K_a). The immediate consequence is that each weak acid or base has the ability to drive the overall pH of the system (since they all contain the term $[H^+]$), and therefore all such equations are coupled. Most importantly, they are also highly non-linear.

APPENDIX H
APPLICATION OF DESCARTES' RULE OF SIGNS

To find the nature of the roots of the polynomial given in main body of the text as (4-24)

$$[H^+]^3 + ([Na^+] + K_a)[H^+]^2 + ([Na^+]K_a - K_a[A] - K_w)[H^+] - K_aK_w = 0$$

Descartes' Rule of Signs dictates examination of the coefficients. Let

$$A = 1 \; A = 1 \tag{H-1}$$

$$B = [Na^+] + K_a \tag{H-2}$$

$$C = [Na^+]K_a - K_a[A] - K_w \tag{H-3}$$

$$D = -K_aK_w \tag{H-4}$$

Due to the fact that concentrations must always be non-negative and dissociation constants are positive, it is concluded that A, B, and D always have the same sign (+, +, and -). Only C can vary, and negative, positive, and zero are all possibilities. This ensures that the polynomial will have one of exactly three forms when only the signs of the coefficients are considered

$$X^3 + X^2 + X - 1 = 0 \tag{H-5}$$

$$X^3 + X^2 - X - 1 = 0 \tag{H-6}$$

$$X^3 + X^2 \quad - 1 = 0 \tag{H-7}$$

In essence, Descartes' Rule of Signs states that there as many positive real roots of a polynomial as there are sign changes of the coefficients (Borowski, 1991). In addition, replacing X with (-X) before counting sign changes indicates the number of negative real roots. The remaining roots must then be complex. Finally, zeros are ignored.

Examining each of the three cases:

Case 1

$$X^3 + X^2 + X - 1 = 0 \tag{H-8}$$

There is one sign change, indicating one positive real root; substituting (-X)

$$-X^3 + X^2 - X - 1 = 0 \tag{H-9}$$

There are now two sign changes, indicating two positive real roots. Furthermore, a cubic polynomial has exactly three roots, meaning there must be exactly one positive real root, two negative real roots, and zero complex roots.

Case 2

$$X^3 + X^2 - X - 1 = 0 \tag{H-10}$$

Again, there is one sign change, indicating one positive real root; substituting (-X)

$$-X^3 + X^2 + X - 1 = 0 \tag{H-11}$$

There are again now two sign changes, indicating two positive real roots. Once more, it is concluded that there must be exactly one positive real root, two negative real roots, and zero complex roots.

Case 3

$$X^3 + X^2 \quad - 1 = 0 \tag{H-12}$$

Again, there is one sign change, indicating one positive real root; substituting (-X)

$$-X^3 + X^2 \quad - 1 = 0 \tag{H-13}$$

There are again now two sign changes, indicating two positive real roots. Once more, it is concluded that there must be exactly one positive real root, two negative real roots, and zero complex roots.

All three possible scenarios result in the same conclusion—there is always exactly one real positive root and two real negative roots for (4-24).

APPENDIX I
DEVELOPMENT OF THE EXHAUSTIVE NUMERICAL SEARCH USED TO OPTIMIZE CONTROL PERFORMANCE

To find the optimal controller gain K_C and integral time constant τ_I for closed-loop performance with respect to the ITAE criterion, an adaptive gridding system is used. The first grid range for the controller gain can be selected arbitrarily, and a decade of potential solutions is used (e.g. 0.001 to 0.009 by steps of 0.001). For the integral time constant, familiarly with the system suggests that the decade of potential solutions from 10 to 100 by steps of 10 should be used for regulation responses and 100 to 1000 by steps of 100 for servo responses should be used.

After the initial run is completed, the controller gain K_C is determined to either be with the bounds or at one of the bounds. If it equal to one of the bounds, the decade is adjusted by one decade in the proper direction to allow the potential solutions proposed in the second run to encompass values beyond the bound equal to the solution found in the first run (*i.e.,* if 0.001 to 0.009 by steps of 0.001 returns a solution of 0.009, then the next run should be from 0.01 to 0.09 by steps of 0.01). This process is repeated until the optimal solution falls within the range of bounds of the latest trial. For example, if the second iteration is from 0.01 to 0.09 by steps of 0.01 and 0.03 yields the lowest ITAE, the first step in the process is complete. In this case, the optimal solution reported $\pm$ the previous step size become the bounds for the second step. For example, a solution of 0.03 in steps of 0.01 will dictate bounds of 0.02 and 0.04 for the second step.

The lone exception to this scenario is when the lowest ITAE is found at a bound of the n-th iteration and subsequently at the adjacent bound of the next iteration (e.g. when a range of 0.001 to 0.009 by steps of 0.001 returns an optimal solution of 0.009 and the next iteration returns an optimal solution of 0.01). If this is the case, the solution is known to fall between one appropriate step to the outside of the two values, and one step outward from each becomes the bounds for the second step (*i.e.,* in the scenario described, the new bounds are 0.008 and 0.02).

With the bounds discovered for the second step, the step size is reduced to one tenth of the previous step size, and the optimization is re-run. For example, with bounds of 0.02 and 0.04, a step size of 0.001 is used. Similarly, if the bounds are determined by the exception given above, the step size will be one tenth of the finer of the two bounds (*i.e.,* in the case of 0.009 (bound at 0.008) and 0.01 (bound at 0.02) previously given, the step size becomes 0.0001).

In this way, the second step will return a number for the controller gain K_C such as 0.23 following the first example. This is said to be accurate to two significant figures as referred to in the main body of the text. In the second example given for the exception, a plausible solution might be 0.0094.

With controller gain K_C identified to two significant figures, the integral time constant of the controller τ_I is examined to confirm that it is with the chosen decade for its possible solutions. If it is, the optimization is complete. If it is not, the value must be 100 (recall that bounds of 10 and 1000 are imposed on the optimization), and the bounds are revised to allow the optimal solution to include more extreme values of τ_I. During this process, familiarity with the behavior of the system dictates that the gain K_C should

be expanded from the optimal solution by five step sizes on either side to ensure that fine changes in the value of controller gain K_C for the optimal solution are recorded. When both parameters fall within the optimization bounds, with the gain K_C established to two figures and the time constant τ_I to one figure, the optimization is complete.

APPENDIX J
MOVING AVERAGE AND EXPONENTIAL FILTERS

Moving Average Filter (MAF)

The MAF calculates the mean of a group of previous data points. It has one parameter, N, which is the number of points that are included

$$y_f(k) = \frac{y(k) + y(k-1) + y(k-2) + \cdots + y(k-(N-1))}{N} \tag{J-1}$$

$$y_f(k) = \frac{1}{N}\sum_{i=1}^{N} y(k-i) \tag{J-2}$$

To reduce the repetitive calculations, a more efficient version can be derived by using the previous filtered value

$$y_f(k-1) = \frac{1}{N}\sum_{i=0}^{N-1} y(k-i-1) \tag{J-3}$$

Subtracting

$$y_f(k) - y_f(k-1) = \frac{1}{N}\left[\sum_{i=0}^{N-1} y(k-i) - \sum_{i=0}^{N-1} y(k-i-1)\right] \tag{J-4}$$

$$y_f(k) - y_f(k-1) = \frac{1}{N}\left[y(k) + \sum_{i=1}^{N-1} y(k-i) - \sum_{i=0}^{N-2} y(k-i-1) - y(k-(N-1)-1)\right] \tag{J-5}$$

Shifting the index of the second summation results in the two summations summing to zero, which yields

$$y_f(k) = y_f(k-1) + \frac{1}{N}\left[y(k) - y(k-N)\right] \qquad \text{(J-6)}$$

Note that the filter must be initialized, since the first (N-1) calculations will not have enough data for every term. In practice, this can be done with any reasonable set of constants, since any error introduced from them is quickly eliminated by the integral action of the controller.

The implication is that it requires a full N samples for a significant change in input to be completely realized. The response for a standard step change is as follows

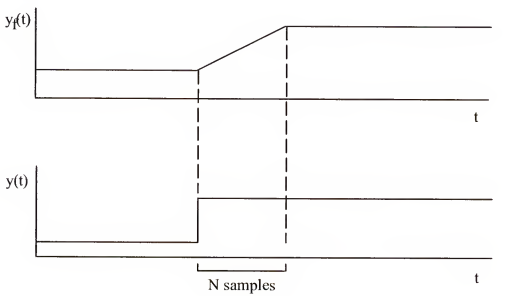

Figure J-1. Illustration of how a step change is observed after passing through a moving average filter.

Therefore, the delay manifests itself as a ramp with duration of N sample intervals.

Exponential Filter (EF)

The EF calculates a weighted average of all previous data. Similarly, it has one parameter, α. It is a recursive relationship, with α being the weight given to the new data point, and $(1-\alpha)$ the weight assigned to the previously calculated value

$$y_f(k) = \alpha y(k) + (1-\alpha) y_f(k-1) \qquad \text{(J-7)}$$

As new samples arrive, previous individual data points are weighted less and less. Theoretically, all old data is part of every new calculation, but becomes insignificant after some time has passed

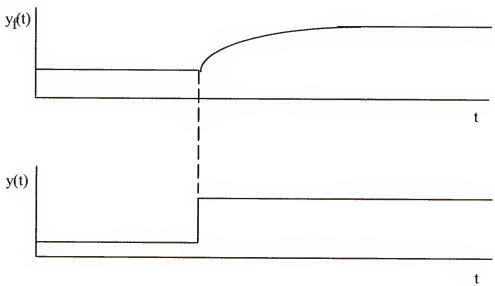

Figure J-2. Illustration of how a step change is observed after passing through an exponential filter.

In contrast to the MAF, there is no initialization required, provided the first sample is simply passed through without being averaged.

As a result of the algorithm, the delay manifests itself in the shape of an exponential function, hence the name.

LIST OF REFERENCES

Adam, E. J., Latchman, H. A., and Crisalle, O.D. (2000) "Robustness of the Smith Predictor with Respect to Uncertainty in the Time-Delay Parameter," *Proceedings of the American Control Conference*, Chicago, IL, pp. 1452-1457, IEEE, Piscataway, NJ.

Barrios, Carlos, Gregg, Terese, Harris, Robert, Mayorga, Kenneth, Ortiz, Mario, and Teague, Nick (2002) "Minimizing Chlorine Loss in the Chlorine Contact Basins at the Kanapaha Water Reclamation Facility," *Final Report for Integrated Product & Process Design (IPPD), University of Florida,* UNPUBLISHED.

Bierck, Barnes R., Blatchley, III, Ernest R., Connell, Gerald F., Cudrak, Audrey A., Devkota, Laxman Mani, Finch, Gordon R., Fleury, Michael, Hart, Frederick L., Hom, Victor, Jeyanayagam, Samuel S., Kinner, Nancy E., and Scheible, Otto K. (1996) *Wastewater Disinfection, Manual of Practice FD-10*, Water Environment Federation, Alexandria, VA.

Boning, D. S., Moyne, W. P., Smith, T. H., Moyne, J., Telfeyan, R., Hurwitz, A., Shellman, S., and Taylor, J. (1996) "Run by Run Control of Chemical Mechanical Polishing," *IEEE Trans. On Components, Packaging, and Manufacturing Technology*, vol. 19, no. 4, pp. 307-314.

Borman, Stu (1992) "Fiber-Optic Sensors: Device Measures pH Inside Single Cells," *Chemical & Engineering News*, vol. 70, no. 44, pg. 4.

Borowski, E. J., and Borwein, J. M. (1991) *The Harper Collins Dictionary of Mathematics*, HarperPerennial, New York, NY.

Card, Jill P., Naimo, Mark, and Ziminsky, William (1998) "Run-to-Run Process Control of a Plasma Etch Process with Neural Network Modeling," *Quality and Reliability Engineering International*, vol. 14, pp. 247-260.

Chang, Sylvia H., Druen, Shannon L., and Garcia-Rubio, Luis H. (1995) "Modeling and Analysis of Fiber Optic Sensors: Effect of the Ionic Strength," *SPIE Proceedings*, vol. 2388, code#2388B-71.

Demir, Feridun (2001) "Modeling of Chlorine Disinfection and Kaolin Dispersion Systems with Control Applications," Doctoral Dissertation, University of Florida, Gainesville, FL.

Florida Department of Environmental Protection (DEP) (1996) "Design and Operating Criteria," *Wastewater and Other Related Rules*, 62-400.440(5)(b).

Foess, Gerald W., Meenahan, James G., and Harju, J. Michael (1976) "Evaluation of Flow Equalization at a Small Wastewater Treatment Plant," *Environmental Protection Agency*, EPA-600/2-76-181.

Fogler, H. Scott (1992) *Elements of Chemical Reaction Engineering,* 2nd Edition, Prentice-Hall, Inc., Englewood Cliffs, NJ.

Garcia-Rubio, L. H., and Clavette, D. K. (1991) "High Resolution Self-Calibrating pH Sensor," *AIChE Annual Meeting*, Symposium on Electrochemical Sensors, Los Angelos, CA.

Geankoplis, Christie J. (1993) *Transport Processes and Unit Operations,* 3rd Edition, Prentice-Hall, Inc., Englewood Cliffs, NJ.

Gillet, D., Bonvin, D., and Crisalle, O. D. (2001) "Run-to-Run Control of DC-Sputtering Processes," *Proceedings of the American Control Conference*, Washington, D.C., pp. 1997-2002, IEEE, Piscataway, NJ.

Gustafsson, Tore K., Skrifvars, Bengt O., Sandstrom, Katarina, and Waller, Kurt V. (1995) "Modeling of pH for Control," *Ind. Eng. Chem. Res.*, vol. 34, no. 3, pp. 820-827.

Gustafsson, Tore K., and Waller, Kurt V. (1983) "Dynamic Modeling and Reaction Invariant Control of pH," *Chemical Engineering Science*, vol. 38, no. 3, pp. 389-398.

Hammer, Mark J., and Hammer, Jr., Mark J. (1996) *Water and Wastewater Technology,* 3rd Edition, Prentice Hall Inc., Englewood Cliffs, NJ.

Janowiak, Michelle L. (2003) "Dynamic Model for the Interpretation of Fiber Optic Sensors: Case Study pH," Doctoral Dissertation, University of South Florida, Tampa, FL.

Jolley, Robert L., Condie, Lyman W., Johnson, J. Donald, Katz, Sidney, Minear, Roger A., Mattice, Jack S., and Jacons, Vivian A., editors (1990) *Water Chlorination Chemistry, Environmental Impact and Health Effects*, vol. 6, Lewis Publishers, Inc., Chelsea, MI.

Kailath, Thomas (1980) *Linear Systems*, Prentice-Hall, Inc., Englewood Cliffs, NJ.

Kosut, Robert L., de Roover, Dick, Emami-Naeini, Abbas, and Ebert, Jon L. (1998) "Run-to-Run Control of Static Systems," *Proceedings of the 37th IEEE Conference on Decision and Control*, pp. 695-700.

Kreyszig, Erwin (1999) *Advanced Engineering Mathematics,* 8th Edition, John Wiley & Sons, New York, NY.

Latchman, H. A., and Crisalle, O. D. (1995). "Exact Robustness Analysis for Highly Structured Frequency-Domain Uncertainties," *Proceedings of the American Control Conference*, Seattle, WA, pp. 3982-3987, IEEE, Piscataway, NJ.

Lencastre, Armando (1987) *Handbook of Hydraulic Engineering*, Ellis Horwood Limited, Chichester, West Sussex, England.

Levine, William S., editor (1996) *The Control Handbook*, CRC Press, Boca Raton, FL.

Mahuli, S. K., Rhinehart, R. R., and Riggs, J. B. (1993) "pH Control Using a Statistical Technique for Continuous On-Line Model Adaptation," *Computers chem. Engng.*, vol. 17, no. 4, pp. 309-317.

Marlin, Thomas E. (2000) *Process Control—Designing Processes and Control Systems for Dynamic Performance*. McGraw-Hill, Boston, MA.

McAvoy, Thomas J. (1972) "Dynamic Models for pH and Other Fast Equilibrium Systems," *Ind. Eng. Chem. Process Des. Develop.*, vol. 11, no. 4, pp. 630-631.

McAvoy, Thomas J., Hsu, Elmer, and Lowenthal, Stuart (1972) "Dynamics of pH in Controlled Stirred Tank Reactor," *Ind. Eng. Chem. Process Des. Develop.*, vol. 11, no. 1, pp. 68-70.

McMillan, G.K. (1991) "Understand Some Basic Truths of pH Measurement," *Chemical Engineering Progress,* vol. 87, no. 10, pp.30-37.

McMillan, G.K. (1994) *pH Measurement and Control,* 2nd Edition, Instrument Society of America, Research Triangle Park, NC.

Metcalf & Eddy, Inc. (1979) *Wastewater Engineering: Treatment Disposal Reuse,* 2nd Edition. McGraw-Hill, New York, NY.

Moore, R.J. (1990) "Good pH Measurements in Bad Process Streams," *Instrumentation & Control Systems*, vol. 63, no. 12, pp.39-43.

Morris, J. C., and Wei, I. W. (1969) "Chlorine Ammonia Breakpoint Reactions: Model Mechanisms and Computer Simulation," *American Chemical Society*, Minneapolis, MN.

Moyne, James, del Castillo, Enrique, and Hurwitz, Arnon Max (2001) *Run-to-Run Control in Semiconductor Processing*. CRC Press, Boca Raton, FL.

Nagaraju, V. D., Murthy, C. T., Ramalakshmi, K., and Srinivasa Roa, P. N. (1997) "Studies on Roasting Coffee Beans in a Spouted Bed," *Journal of Food Engineering*, vol. 31, pp. 263-270.

Narayanan, N. R. L., Krishnaswamy, P. R., and Rangaiah, G. P. (1998) "Use of Alternative Process Variables for Enhancing pH Control Performance," *Chemical Engineering Science*, vol. 53, no. 17, pp. 3041-3049.

Ogunnaike, Babatunde A. and Ray, W. Harmon (1994) *Process Dynamics, Modeling, and Control.* Oxford University Press, New York, NY.

Ongerth, J. E. (1979) "Evaluation of Flow Equalization in Municipal Wastewater Treatment," *Environmental Protection Agency*, EPA-600/2-79-096.

Ozdemir, Murat and Devres, Onur (2000) "Analysis of Color Development During Roasting of Hazelnuts Using Response Surface Technology," *Journal of Food Engineering*, vol. 45, pp. 17-24.

Ozdemir, Murat and Devres, Onur (2000) "Kinetics of Color Changes of Hazelnuts During Roasting," *Journal of Food Engineering*, vol. 44, pp. 31-38.

Rao, B.S., Puschett, J. B., and Matyjaszewski, K. (1991) "Preparation of pH Sensors by Covalent Linkage of Dye Molecules to the Surface of Polystyrene Optical Fibers," *Journal of Applied Polymer Science*, vol. 43, pp. 925-928.

Seborg, D. E., Edgar, T. F., and Mellichamp, D. A. (1989) *Process Dynamics and Control.* John Wiley & Sons, New York, NY.

Seitz, Rudolf W. (1984) "Chemical Sensors Based on Fiber Optics," *Analytical Chemistry*, vol. 56, pp. 16A-34A.

Seitz, Rudolf W. (1988) "Chemical Sensors Based on Immobilized Indicator and Fiber Optics," *CRC Critical Reviews in Analytical Chemistry*, vol. 19, issue 2, pp. 135-173.

Skoog, Douglas A., Holler, F. James, and Nieman, Timothy A. (1998) *Principles of Instrumental Analysis,* 5th Edition, Thomson Learning, Inc., Crawfordsville, MD.

Smith, Robert (1971) "Wastewater Treatment Plant Control," *Environmental Protection Agency*, PB 213 827.

Snoeyink, Vernon L., and Jenkins, David (1980) *Water Chemistry*, John Wiley & Sons, New York, NY.

Sturm, Terry W. (2001) *Open Channel Hydraulics*, McGraw-Hill, New York, NY.

Sung, Su Whan, and Lee, In-Beum (1995) "pH Control Using an Identification Reactor," *Ind. Eng. Chem. Res.*, vol. 34, no. 7, pp. 2418-2426.

Sung, Su Whan, Lee, In-Beum, Choi, Jin Young, and Lee, Jitae (1998) "Adaptive Control for pH systems," *Chemical Engineering Science*, vol. 53, no. 10, pp. 1941-1953.

Waller, Kurt V., and Makila, Pertti M. (1981) "Chemical Reaction Invariants and Their Use in Reactor Modeling, Simulation, and Control," *Ind. Eng. Chem. Process Des. Dev.*, vol. 20, pp.1-11.

Williams, Gaylon L., Rhinehart, R. Russell, and Riggs, James B. (1990) "In-Line Process-Model-Based Control of Wastewater pH Using Dual Base Injection," *Ind. Eng. Chem. Res.*, vol. 29, no. 7, pp. 1254-1259.

Williams, R. R. (1991) "Fundamental Limitations on the Use and Comparison of Signal-to-Noise Ratios," *Analytical Chemistry*, vol. 63, no. 15, pp. 1638-1643.

Zumdahl, Steven S. (1989) *Chemistry*, D. C. Heath and Company, Lexongton, MA.

BIOGRAPHICAL SKETCH

Christopher Meredith was born in Savannah, GA, on November 21, 1973. He graduated with a B.S. in chemical engineering from the Georgia Institute of Technology in September, 1995. Mr. Meredith joined the graduate program at the University of Florida in August of 1997. He received his Ph.D. in chemical engineering in December 2003, along with a minor in electrical and computer engineering.

I certify that I have read this study and that in my opinion it conforms to acceptable standards of scholarly presentation and is fully adequate, in scope and quality, as a dissertation for the degree of Doctor of Philosophy.

Oscar D. Crisalle, Chairman
Associate Professor of Chemical Engineering

I certify that I have read this study and that in my opinion it conforms to acceptable standards of scholarly presentation and is fully adequate, in scope and quality, as a dissertation for the degree of Doctor of Philosophy.

Haniph A. Latchman
Professor of Electrical and Computer Engineering

I certify that I have read this study and that in my opinion it conforms to acceptable standards of scholarly presentation and is fully adequate, in scope and quality, as a dissertation for the degree of Doctor of Philosophy.

Spyros A. Svoronos
Professor of Chemical Engineering

I certify that I have read this study and that in my opinion it conforms to acceptable standards of scholarly presentation and is fully adequate, in scope and quality, as a dissertation for the degree of Doctor of Philosophy.

Jason F. Weaver
Assistant Professor of Chemical Engineering

This dissertation was submitted to the Graduate Faculty of the College of Engineering and to the Graduate School and was accepted as partial fulfillment of the requirements for the degree of Doctor of Philosophy.

December 2003

Pramod Khargonekar
Dean, College of Engineering

Winfred M. Phillips
Dean, Graduate School